Effect of OPTN and OPTN phospho mutants on the innate immune response to Toll-like receptor and NOD Like receptor stimulation

By

Abdulaziz Mohammed Ghannam

A thesis submitted to UCL for the degree of

Doctor of Philosophy

Eastman Dental Institute

Department of Microbial Disease

2022

I, Abdulaziz Mohammed Ghannam, confirm that the work presented in this thesis is my own. Where information has been derived from other sources, I confirm that this has been indicated in the thesis.

ALHAMDULILLAH

Abstract

Inflammatory diseases represent a large section of conditions affecting the oral cavity. Many chronic diseases may last for life, with their causal factors deemed multifactorial or unknown. Optineurin (OPTN) is an adaptor protein with multiple roles in cellular function. One of its primary roles is related to the promotion of proinflammatory cytokines and chemokines expression and secretion. Gene mutations within OPTN have been identified to contribute to multiple inflammatory or autoimmune conditions.

The main aim of this study is to investigate a link between OPTN and NOD2 activation with MDP in the form of a phosphorylation site in OPTN structure. Also, to test the ability of this phosphorylation site to impact NOD2 activation of the NFkB pathway through phosphoproteomics modification in OPTN structure. Finally, measure the significance of this link to inflammation and bacterial response in the form of cytokines release.

During this study, I identified a novel phosphorylation site in OPTN that impacts the NFkB pathway by activating the bacterial receptor NOD2. THP-1, the human monocytic cell line, was genetically modified to express human OPTN tagged with EGFP on its N-terminus (THP-1^{OPTN}). The THP-1^{OPTN} cell line was utilised to study protein localisation intracellularly, immunoprecipitation and phosphoproteomics. I identified a novel Serine 526 (Ser526) phosphorylation site induced after NOD2 stimulation with muramyl dipeptide (MDP). To determine the functional consequence of Ser526, phosphorylation site-directed mutagenesis was used to introduce an amino acid substitution at position 525 in the EGFP-OPTN, resulting in phosphomimetic amino acids. Phospho-dead and phospho-active OPTN constructs were generated by switching Ser526 to Ala526 (S526A) and Glu526 (S526E),

respectively. In addition, stable THP-1 cell lines were produced (THP-1^{S526A} and THP-1^{S526E}), and the impact of these mutations on the immune response downstream of NOD2 and Toll-like receptors (TLR) was investigated.

THP-1^{S526E} cells demonstrated a significant elevation in the induction and secretion of proinflammatory cytokines upon NOD2 stimulation. THP-1^{S526A} ability to secrete cytokines was significantly impeded upon stimulation. The phosphorylation at Ser526 seemed to augment TLR signalling resulting in a significant boost in the induction and release of cytokines.

These studies have identified a novel role for OPTN in the immune response downstream of NOD2. The phosphorylation of Ser526 upon NOD2 activation acts as an immune booster which can cooperate with other receptors, such as TLRs, upon bacterial challenge. Mutations in OPTN and NOD2 are associated with a host of human diseases, and the relevance of this pathway to these conditions warrants further investigation.

Impact Statement

Innate immunity is the body's first defence against infective agents and response to tissue damage. Cells can detect infection and damage by expressing an extensive network of pattern recognition receptors (PRR) and damage associated pattern receptors (DAMP). Upon PRR and DAMP activation, various biological events occur to correct and maintain our health. One of its major events is the initiation of inflammation, where cytokines and chemokines are deployed to exert many changes in response to the foreign invading entity recognised in our system. These cytokines and chemokines play a pivotal role in the inflammatory process and white blood cells recruitment to the site of insult. Our body can control the inflammatory process, as its excessive activation leads to unwanted destruction in our tissue. Underactivation can lead to infection, loss of tissue healing and death. Defective innate immunity can result in the development of autoimmune or autoinflammatory conditions. Such conditions are chronic and life-long, requiring constant follow-up and treatment. This is true in the case of oral diseases causing many clinical presentations that warrant continuous management and follow-up, leading to reduced quality of life and a major financial burden on healthcare providers.

Optineurin (OPTN) is a multifaceted protein that participates in many cellular functions. Mutations in gene encoding OPTN have been shown to be detrimental in developing many conditions affecting our biological systems. An essential aspect of its process is related to cytokines and chemokines signalling cascade, protein trafficking and secretion.

Nucleotide oligomerisation domain 2 (NOD2) is an integral cog in our innate immunity recognising bacterial MDP intracellularly and a principal initiator of the NFkB pathway. A

mutation in this cellular receptor is a disease-causing participating factor ranging from periodontal disease to systemic conditions like Crohn's disease.

My results may establish a newly found link between NOD2 and OPTN in the event that it boosts the immune response to release copious amounts of pro-inflammatory cytokines or significantly dampens the immune response. A previously found phosphorylation site in OPTN structure, but unknown to impact the immunity, is now unveiled as a significant modulator of the innate immune response to bacterial ligands and PRR activation. In our current strategies as medical providers, the management of immune diseases has shifted from the classical usage of corticosteroids because of their adverse side effects to a more targeted approach centred on specific immune pathways related to our patient's condition. This novel link between OPTN and NOD2 may present a possible target to modulate the anti-bacterial and viral immune response. These two molecules have been linked to many chronic diseases, such as Crohn's disease, Amyotrophic lateral sclerosis, Primary open-angle glaucoma, and Paget's disease, among others. Hence, my findings could impact future drug development in many systemic conditions. Ultimately giving us more tools to improve our patient's quality of life.

Acknowledgements

This work was supported by Umm Al-Quran University, Ministry of Education of Saudi Arabia. I want to thank and acknowledge the following people who supported and contributed to this body of work:

- Mrs Loloah Alawi my lovely wife and soulmate for her extreme patience, constant encouragement and support during difficult times of my PhD.
- Dr Mohammed Ghannam and Professor Maha Hejazi, my father and mother, as they are the reason for my accomplishments.
- My brothers and sisters, whom I aspire to be a good role model.
- Professor Andrew M Smith, my supervisor, teacher, and boss, for his unending belief in me, patience and support with everything I needed during my time under his care.
- Professor Folma Buss for her time and guidance.
- Professor Anthony W Segal for wise words during our time in his Lab.
- Dr Julio Martinez-Torres for his valuable insight and technical teaching at the beginning of my PhD.
- Dr Thomas O'Loughlin for his help in Lab knowledge.
- Dr Andre Ribeiro and Erni Marlina, my senior PhD colleagues, taught me a lot at the beginning of my PhD.
- Dr Gregory Sebepos-Rogers, for making me feel at home while away and for his invaluable help in times of need.
- Dr Juliet Foote, Dr Riccardo Wysoczanski, Dr Francesca Semplicci, Dr Mathena Pavan and Mrs Sophia Joyce - Segal Lab members for welcoming me among them.

Abbreviations

AIM2	Absent In Melanoma 2
ALR	AIM2-like receptors
ALS	amyotrophic lateral sclerosis
AXL	Tyro3-Axl-Mer (TAM) receptor tyrosine kinase
CARD	caspase activation and recruitment domain
CTD	C-terminal Domain
CXCL10	C-X-C Motif Chemokine Ligand 10
CXCR3	C-X-C Motif Chemokine Receptor 3
DAMP	Damage-associated molecular patterns
EGFP	Enhanced Green Fluorescent Protein
IAP1	Inhibitor Of Apoptosis Protein 1
IFN α	Interferon Alpha
IFN β	Interferon Beta
IFN γ	Interferon Gamma
IKK	inhibitor of nuclear factor kappa-B kinase
IL	Interleukins (1-10)
IRAK1	Interleukin 1 Receptor Associated Kinase 1
IRF1	Interferon Regulatory Factor 1
IRF3	Interferon Regulatory Factor 3
IRF7	Interferon Regulatory Factor 7
JNK1,	JUN N-Terminal Kinase 1
LAP	LC3 Associated Phagocytosis
LC3	Microtubule-associated proteins 1A/1B light chain 3B
LGP2	Laboratory of Genetics and Physiology 2
LIR	LC3 Interacting Region
MAPK1	Mitogen-Activated Protein Kinase 1
MAVS	Mitochondrial Antiviral-Signaling Protein
MDA-5	melanoma Differentiation Associated protein 5
MDP	Muramyl dipeptide
MyD88	Myeloid differentiation primary response 88
NEMO	NF-kappa-B essential modulator
NLR	Nucleotide oligomerisation domain (NOD)-like receptor
NOD1	Nucleotide-binding oligomerisation domain 1
NOD2	Nucleotide-binding oligomerisation domain 2
OFG	orofacial granulomatosis
OLP	Oral Lichen planus
OPTN	Optineurin
OSCC	Oral Squamous cell carcinoma
PAMP	Pathogen-associated molecular patter
PIK3R2	Phosphoinositide-3-Kinase Regulatory Subunit 2

PINK1	PTEN Induced Kinase 1
PRR	Pattern Recognition Receptors
RANKL	Receptor activator of nuclear factor kappa-B ligand
RIG I	Retinoic acid Inducible Gene I
RIPK1	Receptor-interacting serine/threonine-protein kinase 1
RIPK2	Receptor-interacting serine/threonine-protein kinase 2
RLR	RIG-I-like receptors
SLE	Systemic lupus erythematosus
SNP	Single nucleotide polymorphisms
SQSTM1	Sequestosome 1 gene
TAK	TGF-Beta Activated Kinase 1
TANK	TRAF Family Member Associated NFKB Activator
TBK1	TANK Binding Kinase 1
TIR	toll-interleukin-1 receptor
TLR	Toll-interleukin receptor (1-10)
TNF α	Tumour Necrosis Factor-alpha
TNFR1	Tumour necrosis factor receptor 1
TRAF3	Tumour necrosis factor receptor 3
TRAF6	Tumour necrosis factor receptor 6
TRIF	TIR-domain-containing adapter-inducing interferon-β
UBAN	Ubiquitin binding domain
XIAP	X-Linked Inhibitor of Apoptosis

Table of Contents

Table of Figures

Table of Tables

Chapter 1 Introduction

1. Innate immunity overview

The innate immune system is the first part of the body to recognise invaders such as viruses, bacteria, parasites and toxins, or sense wounds or trauma. Upon recognising these agents or events, the innate immune system activates cells to attack and destroy the outsider or initiate repair while simultaneously informing and modulating the adaptive immune response that follows this first line of defence. Innate immunity depends on a group of proteins like pattern recognition receptors (PRRs) and phagocytes that recognise the conserved characteristics of pathogens and are quickly activated to destroy invaders[1].

Receptors of the innate immune system detect conserved determinants of microbial and viral origin. Activation of these receptors initiates signalling events that culminate in an effective immune response. Recently, the view that innate immune signalling events rely on and operate within a complex cellular infrastructure has become an essential framework for understanding the regulation of innate immunity. This infrastructure's compartmentalisation allows the cell to assign spatial information to microbial detection and regulate immune responses. In addition, several cell biological processes play a role in regulating innate signalling responses; at the same time, innate cellular processes as a defence or promote immunological memory[2,3].

A significant PRR-induced innate immune response component is transcription, which produces pro-inflammatory cytokines and interferons (IFN); These chemical messages are critical for initiating innate and adaptive immune responses. PRR activation also initiates non-transcriptional responses such as the induction of phagocytosis, autophagy, cell death, and cytokine processing[4].

A common theme that has emerged in the study of innate immune receptor signalling is the need for adapter proteins that link receptors to an enzymatic signal. Adapters integrate a signal from more than one receptor and are crucial for detecting numerous ligands. Thus, the adapters perform a function that is more critical than the function of either receptor alone. Each adapter or set of adapters contains domains that allow protein-protein interactions with an upstream receptor and a downstream signalling protein. Although not every innate immune receptor requires adapter proteins for signalling, the cellular biology of several adapters is an area of current research interest[5].

This introduction highlights these aspects of cell biology in pattern-recognition receptor signalling by focusing on respective pathways and their interaction with the adaptor protein optineurin.

1.2 Pattern recognition receptors (PRR)

1.2.1 TLR Toll-like receptors

The Toll-Like Receptors (TLRs) are a family of membrane proteins residing at the cell surface and within intracellular vesicles. They are an integral part of the innate immune system and function as pattern recognition receptors (PRRs) which recognise highly conserved molecules from a host of microbes. In addition to TLRs, mammals also express several other classes of PRRs, including RIG-I-like receptors (RLRs), Nod-like receptors (NLRs) and AIM2-like receptors (ALRs)[4,6].

TLRs expression can be found in innate immune cells like dendritic cells (DCs) and macrophages and in non-immune cells such as fibroblasts and epithelial cells[4,7]. Structurally TLRs consist of an ectodomain with leucine-rich repeats (LRRs), which form the intermediate pathogen-associated molecular patterns (PAMPs) recognition site, a transmembrane domain, and a cytoplasmic Toll/IL-1 receptor (TIR) domain that initiates the intracellular signalling cascade. TLRs interact with their respective PAMPs or damage associated molecules patterns (DAMPs) as a homo- or heterodimer; some TLRs enlist the help of a co-receptor or accessory molecule[8].

Humans express 10 TLRs divided into two subfamilies based on their cellular location. Cell surface TLRs includes TLR1, TLR2, TLR4, TLR5, TLR6, and TLR10, while intracellular TLRs are localized in the endosome and include TLR3, TLR7, TLR8 and TLR9[9].

Cell surface TLR2 forms a heterodimer along with TLR1 or TLR6 and recognises a variety of PAMPs that include lipoproteins, peptidoglycans, lipoteichoic acids, zymosan, mannan, and tGPI-mucin[9]. TLR4 primary function is to recognise bacterial lipopolysaccharide (LPS)[10]. TLR5 respond profoundly to bacterial flagellin[4]. TLR10 collaborates with TLR2 in an anti-inflammatory fashion and causes negative regulation of proinflammatory cytokines, but it can identify ligands from listeria, or TLR10 can also sense influenza A virus infection independently[11,12].

Intracellular TLR3 distinguishes different types of RNA that include viral double-stranded RNA dsRNA, small interfering RNAs, and self-RNAs derived from damaged cells[13]. TLR7 is chiefly expressed in DCs and recognises single-stranded RNA (ssRNA) from viruses, RNA released into endolysosomes after bacterial phagocytosis[14]. In humans, the detection of viral ssRNA through TLR8 is identified, and TLR8 is responsible for detecting host self-ribonucleoprotein complexes[15]. TLR9 recognises bacterial and viral DNA rich in unmethylated CpG-DNA motifs. Also, it recognises hemozoin, an insoluble crystalline by-product generated by Plasmodium falciparum during the detoxification process of host haemoglobin[16].

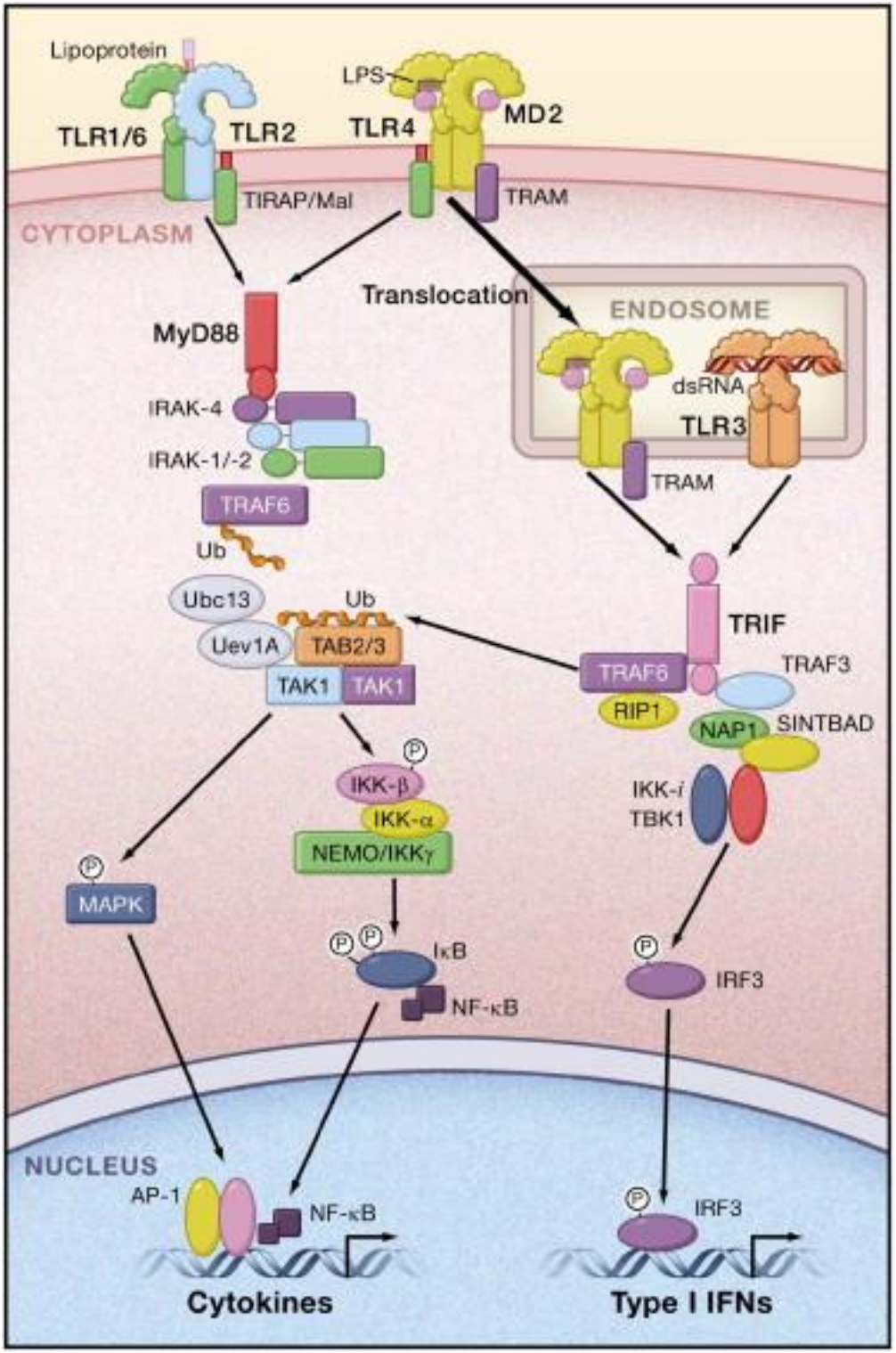

Figure 1. 1 Overview of the TLRs signalling cascade through NFkB and type I IFN activation.

(Image adopted from Global Animal Science Journal-GASJ 1(1):1118-1127, 2013)

All TLRs manufacturing takes place in the Endoplasmic Reticulum (ER), then transported to the Golgi and is recruited to the cell surface or intracellular compartments such as

endosomes. Efficient intracellular localisation of TLRs plays a critical part in ligand recognition and in preventing TLRs from encountering self-nucleic acids, which would lead to causing autoimmunity. In ER, the chaperone protein Gp96 is responsible for the trafficking of TLRs; among other functions, macrophages deficient in Gp96 lacked responsive TLRs 1, 2, 4, 5, 7, and 9[17]. The ER protein PRAT4A or Cnpy3 functions to traffic TLR1, TLR2, and TLR4 from ER to the cell plasma membrane while transporting TLR7 and TLR9 which depend on the same protein to transport it from ER to endolysosomes compartments[18]. The transmembrane protein UNC93B1 controls the trafficking of intracellular TLRs from the ER to endosomes. UNC93B1 associates with TLR3, TLR7 and TLR9 because of direct interaction with their transmembrane domains (TMD) and facilitates translocation of these intracellular TLRs from the ER to the endolysosomes[19].

TLR activation mainly follows one of two pathways: the MyD88- or TIR-domain-containing adapter-inducing interferon-β TRIF-dependent pathway. TLR4 is the only known receptor capable of activating the MyD88 and the TRIF pathways upon LPS stimulation. Downstream signalling pathways induce innate immune responses by producing inflammatory cytokines, type I interferons (IFN), and other mediators[20].

1.2.2 NLR Nod-like receptors

A complex family of cytoplasmic proteins that belong to pattern recognition receptors (PRRs) is Nucleotide binding and oligomerisation domain (NOD) like receptors (NLRs); they are known to play an integral part of innate immunity sensing a wide variety of pathogen associated molecular patterns (PAMPs) and damage associated molecular patterns (DAMPs) related to cellular insult or damage. PAMPs could be bacterial in the form of pore-forming toxins, lethal toxins, flagellin, muramyl dipeptides (MDP), RNA and DNA or viral RNA or M2 viral protein or fungal glucans, hyphae, and others. DAMPs can be intrinsic as ATPs, cholesterol crystals or uric acid, or extrinsic like alum, asbestos, alloy particles or UV radiation[21].

NLRs can be classified as a family of ATPases as they possess motifs that bind ATP and instigate hydrolysis to ADP + Pi. The structural composition of all proteins belonging to this family is similar regarding their main domain having a NACHT named after (NAIP, CIITA, HET-T, TP-2)[22]. Seven motifs are characterised in the NACHT domain, Walker A motif forms an ATP binding pocket, Walker B facilitate ATP hydrolysis, an arginine finger motif, Mg^{2+} binding motif, and 3 other specific motifs[23,24]. Such ATP binding is required for the oligomerisation of NLRs to achieve downstream signalling. On the C-terminal of NLRs, there is a Leucine Rich Repeats (LRR) responsible for the recognition, binding of ligands and activation of NLRs; it is present in all members except NLRP10[25].

NLRs are classified into four different subfamilies based on their N-terminal composition and effector domain that interacts with other proteins. NLRA subfamily consists of one

member and contains an Acidic Transactivator domain (AT) acting on the CIITA gene to induce Major Histocompatibility complex II (MHC II)[26]. NLRB also has one member with baculovirus inhibitor of apoptosis repeats (BIR), NAIP domain signals through TAK-1 to activate JNK1, assemble inflammasome with NLRC4 upon flagellin or T3SS recognition and contributes to pyroptosis[27]. NLRC family members have a caspase activation and recruitment domain (CARD) on its N-terminal. It contains six members: NOD1, NOD2, NLRC3, NLRC4, NLRC5 and NLRX1, although all members should have a CARD domain, NLRC3, NLRC5 and NLRX1 do not contain such domain but are classified as NLRC family members due to their phylogenetic relationship to other members[28]. NLRP family 14 members all display a pyrin domain on their N-terminals and share similar structures except for NLRP1, having an add CARD domain on its C-terminal and NLRP10, which misses an LRR domain on its C-terminal[25].

After activation of NLRs, their various cellular functions can be defined in four main functions: Inflammasome formation, either canonical or non-canonical, signal induction, transcription activation and autophagy. All these functions are essential and closely related to other PRRs like TLRs to facilitate pro-inflammation, antigen presentation, phagocytosis of invading pathogens or pyroptosis[26].

Signal induction of NLRs is mainly attributed to two members of the NLRC family, NOD1, which senses γ-d-glutamyl-meso-diaminopimelic acid (E-DAP) from gram-negative bacteria and NOD2, which senses muramyl dipeptide (MDP) from both gram-positive and negative bacteria[29]. As a member of the NLRC family, the NOD2 protein contains two CARD domains at its N-terminal, which are functionally responsible as effectors mediating homophilic

interaction downstream CARD-containing proteins[30]. After their activation, both interact with receptor interacting protein 2 (RIP2) to initiate NFkB signalling resulting in pro-inflammatory upregulation[31]. In this regard, both NLRP2 and NLRP4 act as a negative regulator of the NFkB pathway through blockage of TRAF6 protein[32,33]. RIPK2 through NOD2 activates MAPK and Activator Protein 1 (AP-1), impacting cell proliferation, differentiation and apoptosis[34,35]. NOD2 activation also activates Caspase 1 through CARD-CARD domain interaction, starting the process of IL-1β production[36].

Autophagy is regulated by NLRs and is predominantly used to dispose of invading pathogens via autophagosome formation and fusion with lysosomes to degrade its content. NOD1 and NOD2 recognise bacterial invasion, recruit ATG16L1 to the plasma membrane at the entry site, and facilitate the recruitment of LC3 to the phagosomal membrane[37]. NOD1 and NOD2 recruitment of ATG16L1 was shown to be independent of RIPK2 activity[37]. Recently, emerging evidence indicates a possible NOD2/RIPK2-dependent autophagy activation process in dendritic cells[38]. Additionally, NOD2-dependent autophagy via RIPK2 is enhanced as RIPK2 activates p38 MAPK and relives repression of autophagy mediated by phosphatase PP2A[39]. NOD2 activation mediates the recruitment of LC3 to vesicles containing internalised bacteria to initiate xenophagy. It is still unclear if such event signals through RIPK2 or direct by NOD2/ATG16L1 interaction[40]. Alternatively, internalised commensal bacteria *Bacteroides fragilis* in outer membrane vesicles (OMV) can trigger NOD2/ATG16L1 LC3-associated phagocytosis (LAP) in dendritic cells in intestinal tissue. LAP activation produces regulatory T-cell differentiation within the intestine and suppresses excessive inflammation[41]. It is still unclear how NOD2-associated LAP functions, but its role in suppressing microbial-induced inflammation at mucosal surfaces, instead of the expected

NOD2 role in pro-inflammatory activation, may be relevant to conditions such as Crohn's disease[40].

1.2.3 RLR RIG-I-like receptors

It is an essential part of innate immunity responsible for detecting viral RNA at the cytoplasmic level, promoting Interferon type I production downstream of its signalling cascade. Three members of this type have been identified as RLR, two of this family are Retinoic acid Inducible Gene I (RIG I) and melanoma Differentiation Associated protein 5 (MDA-5) have both similar structures having a central DExD/Helicase domain and N-terminal CARD domain and a C-terminal Domain (CTD) where helicase and CTD sense viral RNA and N-terminal CARD interacting with Mitochondria and peroxisomes through MAVS adaptor protein. A third member is Laboratory of Genetics and Physiology 2 (LGP2). Structurally it does not have CTD but, instead, has a trans-membrane domain at its C-terminal. It is a specific role that is not fully understood but suggested that it performs a regulatory role in IFN production instead[42].

It is well established that RIG I is activated by sensing negative sense RNA viruses such as ss-RNA of Influenza type A virus (IAV), rhabdovirus, orthomyxoviruses, positive sense RNA like HCV and even ds-DNA viruses like Epstein-Barr virus through its transcriptional RNA generated by polymerase III. RIG I activation by the previously mentioned and other viruses like West Nile Virus (WNV) or short Poly I/C but not self RNA is attributed to its ability to recognise the 5’ triphosphate group in viral RNA where this moiety is not present in human RNA as it is lost during host RNA maturation[43]. Inactivated RIG I, Interferon beta promoter stimulator-1 (IPS-1), also known as MAVS, play an adaptor role when interacting with N-terminal CARD of RIG I to activate MAPK and NF-κB through TRAF3/6, caspase 8/10, RIP 1 and Fas-associated death domain (FADD) resulting in type I interferon production[44]. Such

activation of RIG I is understood to be found at early stages of viral RNA replication and detection where peroxisomes are involved through IRF1 and IRF3, leading to rapid anti-viral response and through IRF3/ IRF7 in mitochondria to initiate IFN type I at later stage[45].

MDA-5 is known to interact with Picornaviruses like Encephalomyocarditis and caliciviruses, a type of virus recognised for their ability to produce long ds-RNA in infected cells. It is also possible to activate MDA-5 by long-stranded poly I/C as well. A similar process follows such activation as RIG I activation to produce an anti-viral response in type I IFN through similar downstream signalling pathways[46].

1.3 The functional role of the adaptor protein Optineurin

1.3.1 NFkB and IRF3 signalling.

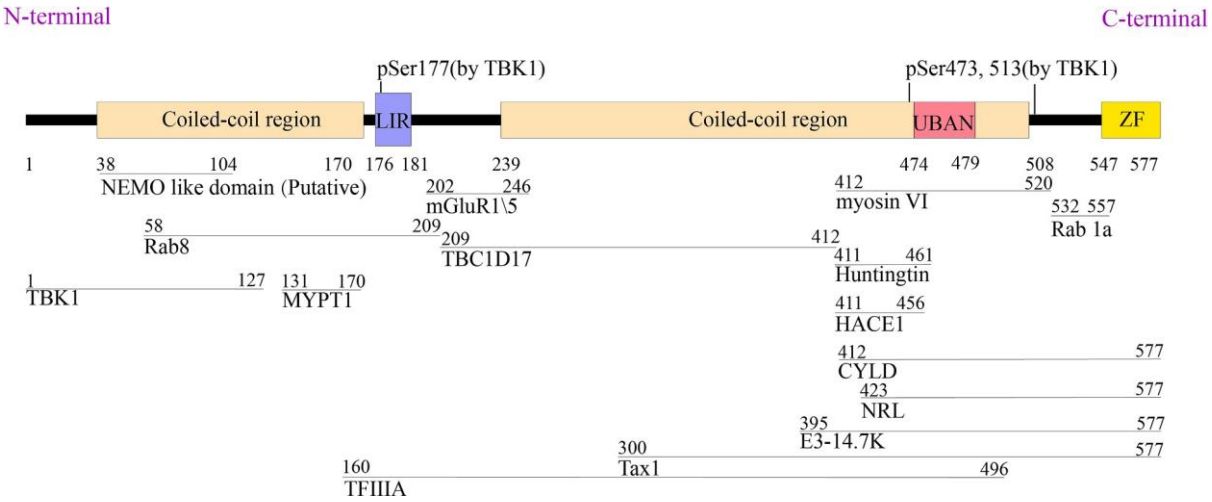

Figure 1. 2 Optineurin structure and domains interaction with other human proteins.

The NEMO-like domain at N-terminus is a putative sequence.TBK-1 phosphorylation site (p Site) is marked at the LIR domain and enhances OPTN to LC3 interaction. In C-terminus, phosphorylation (Ser 473, Ser513) at UBAN, together with the Zinc figure, is associated with poly Ub chain binding among other proteins.

Optineurin can play an inhibitory role in TNF receptor 1 (TNFR1) signalling by competing with NF-κB essential modulator (NEMO) for ubiquitinated RIPK1. NEMO and OPTN contain a ubiquitin-binding (Ub) domain (UBAN) with 53% homology. The substitution of NEMO for OPTN results in a signalling complex that cannot release NF-κB from its inhibitor IkBα and, therefore, switches off the TNFR1 signal[47].

OPTN binding to the deubiquitinase, clyndamitosis (CYLD), also dampens NFkB activation downstream of TNFR1 or TLR signalling pathways. When OPTN bind CYLD, it induces catalytic activity resulting in the cleavage of M1/K63 linked ubiquitin from RIPK1 and inhibition of TNFR signalling [48]. OPTN can also bind to IRAK1 via its UBAN domain, directing

CYLD catalytic activity towards TRAF6, which in turn prevents its poly ubiquitination blocking downstream TLR signalling and NFkB activation[49].

If TNFR signalling complex II is activated via RIP1, Fas-associated death domain protein (FADD) and caspase 8, OPTN can also negatively block such a cascade. By binding to pro-caspase eight at its death domain, OPTN inhibits activation of pro-caspase 8 through TNF-mediated cleavage and minimises the formation of TNFR signalling complex II[50].

On the other hand, OPTN has also been shown to positively enhance NFkB signalling in T cells during a viral infection. OPTN binds to Tax1 binding protein 1 (Tax1BP1), forming a complex that strengthens the association between Tax 1 and NEMO. This, in turn, stimulates the IKKs formation and NFkB activation[51].

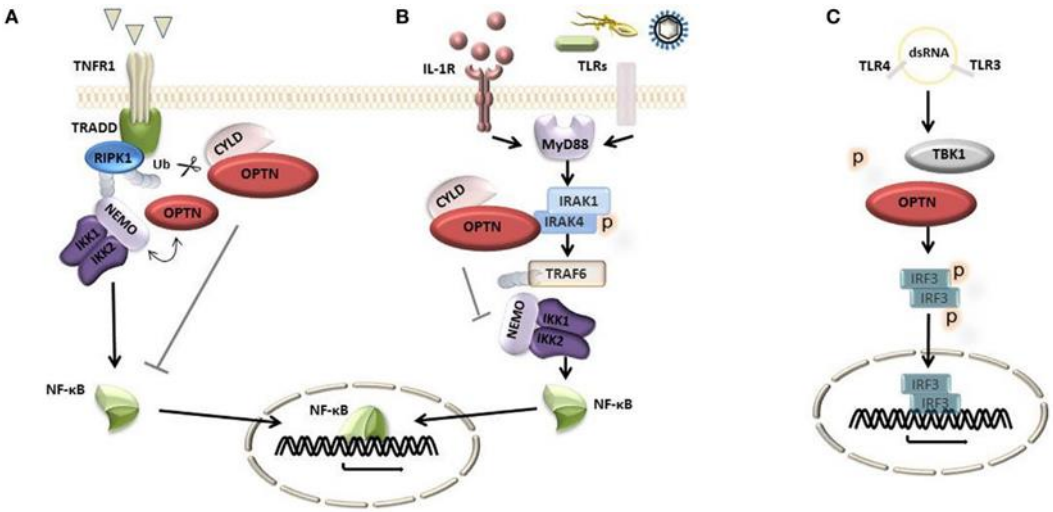

Figure 1. 3 Optinurin intercellular signalling (Image adapted from Solwicka L. et al., 2018).

A) Tumour Necrosis Factor receptor (TNFR1) activation results in OPTN recruitment to the receptor complex. OPTN would compete with nuclear factor NFkB essential modulator (NEMO) for binding

with RIPK1. OPTN attraction of clyndamitosis (CYLD) may cleave off Ub-chain from NEMO and RIPK1, blocking downstream signalling.

B) Activation of IL-1 or TLRs receptors downstream MyD88 would recruit IRAK1 and TRAF6 to activate NFkB, and OPTN/CYLD complex binding to IRAK1 can block TRAF6 binding via TRAF6 auto-ubiquitination, blocking NFkB activation.

C) TLR3/TLR4 activation induces TANK-binding kinase (TBK-1) activation, which binds OPTN at Ser177 to be phosphorylated. This event leads to dimerisation, phosphorylation, and nuclear translocation of IRF3, resulting in Interferon Type I induction.

Bacterial or viral activation of TLRs, NLRs and RIRs results in TBK1 phosphorylation and activation. TBK-1, upon activation, is directed to phosphorylate IRF3 and IRF7, which induces the transcription of type I interferon genes. OPTN can mediate TBK1 activity. Upon PRR activation, TBK1 is recruited to the Golgi apparatus through binding to OPTN and K63 polyubiquitin chains. The formation of the TBK-1/OPTN complex initiates an autophosphorylation of TBK1, resulting in the phosphorylation of IRF3/7 and the induction of type 1 interferons[47]. Alternatively, OPTN binding to TBK1 and TRAF3 prevent IRF3/7 activation and inhibits type 1 interferon production[52].

1.3.2 In vesicle trafficking and cytokine release

OPTN binding to Rab8 and TBC1D17 regulates membrane trafficking and transferrin receptor (TfR) plasma membrane levels. Connecting GTP-bound Rab8 (a Golgi localised GTPase) to TBC1D17 a (GTPase activating protein) through bridging OPTN at the plasma membrane converts membrane-bound Rab8 to a soluble cytoplasmic form through the hydrolysis of the associated GTP to GDP. Removal of Rab8 from the plasma membrane

blocks the recycling of TfR, which subsequently undergoes ubiquitination, binds OPTN via its UBAN site and gets trafficked to the ER. This interaction regulates and reduces the membrane level of TfR[53].

In addition to TfR regulation, OPTN interacts with GTP-Rab8 via myosin IV. This complex plays an essential role in the fusion of secretory vesicles to the plasma membrane. One example is the exocytosis of the Endothelial Growth Factor Receptor (EGFR), which promotes the formation of lamellipodia and cell migration under the stimulation of the epidermal growth factor[54].

OPTN is an essential cargo protein that plays a role in releasing pro-inflammatory cytokines from secreting cells. It has been shown that OPTN is involved in the secretion of cytokines in both humans and mice[55]. Reduced expression of OPTN has been shown to produce a weak pro-inflammatory immune response resulting from diminished secretion of cytokines. This phenomenon was observed in several individuals that had developed CD where monocytes derived macrophage [MDMs] exhibited low OPTN expression[56]. Under normal circumstances, upon stimulation with bacteria or TLR ligands (e.g., LPS and Poly (I: C)) MDMs, would upregulate the expression of OPTN. Initially, OPTN localises to the cytoplasmic compartment and then redistributes to the Golgi complex compartment over a few hours[55]. This increase in expression and relocalisation upon immune stimulation facilitates the pro-inflammatory response. Loss in OPTN expression or mutations within LC3 interacting domain (LIR) or ubiquitin-binding domain (UBAN) domains of OPTN results in defective immunity and alterations in the release of pro-inflammatory cytokines [56,57].

The generation of an $OPTN^{-/-}$ knockout mouse provided further evidence of the role of OPTN in pro-inflammatory cytokine secretion[58]. In particular, bone marrow-derived macrophages [BDBM] from $OPTN^{-/-}$ mice stimulated with E. coli had an impaired ability to release TNF, IL-6, IL-10, and CXCL-1, although, interestingly, autophagy induction seemed to be normal[58]. Several infection and inflammation models were conducted on the $OPTN^{-/-}$ animals. In addition, they demonstrated increased susceptibility to bacterial infection (E. coli, Salmonella and Citrobacter) and the development of chronic intestinal inflammation[59].

1.3.3 Autophagy

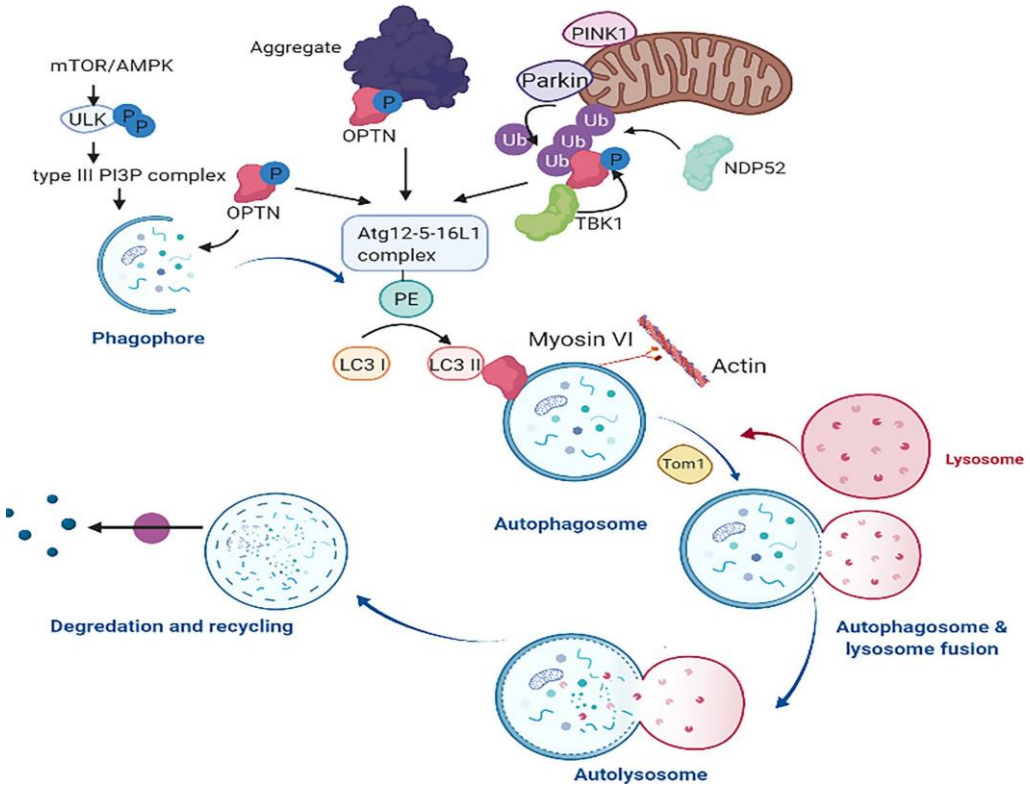

Figure 1. 4 Optinurien role in autophagy and mitophagy.

OPTN is attracted to poly-Ub located on early phagophores, protein aggregates or damaged mitochondria. OPTN is involved in autophagosome formation and then maturation via LIR to LC3 interaction or myosin VI/Tom1 to facilitate autophagosome/lysosome interaction fusion. The PINK1-Parkin complex generates a poly Ub chain on damaged mitochondria to attract and bind OPTN. TBK-1 binding to the Ser177 phosphorylation site boosts OPTN – poly Ub binding (image adapted from Guo et al. [60]).

-Autophagy

Autophagy is a basic degradative process leading to this disintegration of cellular components in lysosomal compartments in multiple fashions (chaperon mediated, micro autophagy, macroautophagy) according to cellular needs. It has been described as involved in cell development, immunity, homeostasis, clearing the cytoplasm of unwanted cytotoxic cytoplasm components and invading pathogens. The autophagy process can be enhanced under stressful conditions, such as cellular starvation, misfolded protein aggregates, damaged organelles and pathogenic invasion[61].

- Role of OPTN during basal and starvation-induced autophagy

OPTN is recognised as an autophagy adapter or receptor through its UBD domain that binds to ubiquitinated cargo and brings it to autophagosomes associated proteins LC3 OPTN LIR domain. On the other hand, not all OPTN involvement with autophagy is ubiquitin dependant[62]. A recent study provided evidence of the relationship between OPTN and tyrosine kinase AXL. In cells lacking PIK3R2 through knockdown of its gene, an enhanced binding between AXL and OPTN with increased phosphorylation of OPTN at the S526 location is observed[63]. OPTN is positively involved in AXL degradation, as overexpression of OPTN results in reduced AXL levels. In a mutated OPTN at S526A residue, S526A OPTN failed to decrease AXL level compared to other known phosphorylation sites[63].

- Role of OPTN in Xenophagy

Autophagy is also involved in removing intracellular pathogens in a process labelled xenophagy. Cytosol or vacuole-contained bacteria is tagged by ubiquitin, resulting in the recruitment of OPTN through its UBAN domain. The bacterial-linked OPTN then couples to LC3 via its LIR domain, which becomes internalised in the developing autophagosome. TBK-1 play a regulatory role in this event by phosphorylating OPTN at Ser 177, increasing its affinity to LC3, and improving bacterial clearance. Other autophagy adapters like p62/SQSTM-1 and NDP52 also play a similar role as OPTN in bacterial clearance, but all have a non-redundant role in xenophagy[64]. OPTN deficiency has been associated with increased susceptibility to intracellular bacterial infection due to a reduced level of xenophagy[62].

-Role of OPTN in mitophagy

Mitophagy is another autophagic process ridding the cell of damaged microconidia via autophagy. Phosphatase and tension homology-induced kinase (PINK-1) is recruited to damaged mitochondria and stably bind to the outer mitochondrial membrane, where it attaches to the E3-ligase parkin. Ubiquitinated proteins located on the outer membrane of mitochondria are recognised by OPTN via the UBD domain, facilitating autophagosome attachment through OPTN LIR domain interaction with LC3. OPTN is an essential component of mitophagy, as any mutation in either UBAN or LIR domains decreases the clearance of damaged mitochondria. In addition, several naturally occurring mutations in OPTN have been associated with defective mitophagy and human disease (see section 1.4.4). In addition, P62/SQSTM-1 mediates mitophagy at different locations on the mitochondrial surface[65].

OPTN also mediates mitophagy after its initiation by DAMPs. Damaged mitochondria stabilise phosphatase and tension homology-induced putative kinase proteins (PINK1) to its outer membrane and recruit E3 ligase Parkin by phosphorylation of Ser65 site in Parking ubiquitin-like domain[66]. After Parking activation, the outer layer of mitochondria is ubiquitination and polyubiquitination chain formation, which attract OPTN via its ubiquitin-binding domain and attach to the PINK1-Parking complex polyubiquitin chain[67]. TBK1 then recruited to OPTN/NDP52 to phosphorylate residues of OPTN at Ser 177, Ser473, and Ser513, which generate a negative charge on the N terminus of OPTN attracting LC3B through its side chain[68]. OPTN/NDP52 complex then recruits ATG12, ULK1, DECP1 and WITI 1 to complete the formation of membrane structure around the damaged mitochondria and move this complex through Myosin to form autophagosomes[69].

1.3.4 In human disease

amyotrophic lateral sclerosis (ALS)

A disease caused by spinal cord motor neuron degeneration leads to the loss of all voluntary movement. Multiple gene mutations like UBQLN2, TDP-43, Fus and SOD1 are implicated in ALS pathogenesis coupled with a mutation in OPTN[70]. It may synergistically boost the chances of ALS development. Familial ALS, which affects 10% of all ALS patients, display OPTN association with SOD1, while sporadic ALS feature pathognomic inclusions of OPTN and TDP-43[71]. It has been reported that OPTN mutations in ALS patients are present in 1% of the total sum of patients. Such mutation can present as ALS-like pathogenesis ranging from elevated inflammation, ER stress and Golgi malformation[72].

OPTN mutation in ALS was first reported in Japanese ALS patients in E478G, Q398X and deletion in Axon 5[72]. Identification of many mutations followed in either axons or introns, including OPTN[73]. Mutation in V295F was reported from a single familial case[74]. A481V and K59N mutations in European patients, T282P, Q314L, K557T and G23X in Italian patients[75,76]. R96L in French cases and Q165X in Danish patients[77]. Q165X and Q454E in Netherlands[78]. In England, E322K mutation has been reported[79]. In Moroccans, a non-sense 691-692ins AG represents almost 6% of all patients and around 0.3% of Ashkenazi Jewish[80]. In all mentioned mutations, OPTN function is compromised and gives a note of OPTN significance in ALS development.

Mechanistically, mutations hinder OPTN's ability to function normally as it alters OPTN structure within the UBAN domain or interferes with TBK1/OPTN interaction. E478G

mutation eliminates ubiquitin binding, resulting in a loss of OPTN binding to mitochondria, protein aggregates and Myosin IV[65]. Such mutation dampens autophagic activity and NFkB activation. In the case of both E478G and Q389X, OPTN loses its ability to bind Myosin IV, leading to an irregular cytoplasmic distribution, abnormal cargo delivery, and Golgi structure[81]. Also, upon immune stimulation of cells expressing the E478G mutant, excessive NFkB activation is observed and subsequent elevation in pro-inflammatory cytokines, including IL-1α, IFNγ and TNF, potentiating elevation in neural cell necroptosis[82].

Primary open-angle glaucoma (POAG)

Primary open-angle glaucoma is an ocular disease characterised by pathological alteration to retinal ganglion cells (RGC) among other ocular cells[83]. In familial POAG patients, there are almost 17% mutations in OPTN gene[84]. Multiple mutations have been identified in OPTN including E50K, R545Q, H486R, T202R, M98K, H26D, A336G, A336T and E322K[84–88]. The presence of multiple mutations and other causative gene mutations dictate the disease subtype and its severity[60].

In the E50K mutation, OPTN levels are reduced, and its localisation is hindered. Also, hyperactivation of TBK-1 occurs, which exacerbates the pathological process[89]. E50K affects OPTN's ability to interact with TBC1D17, which is responsible for the cell's inability to traffic Rab8 recycling Endosomes. In addition, recycling Endosomes is essential for iron metabolism in RGC. By blocking the trafficking of recycling endosomes, E50K reduces the survivability of RGC and induces apoptosis[90].

In R545Q, H26D and H486R mutations, RGC-5 cell apoptosis does not occur at the level of E50K[91]. Also, in M98K mutation, it can be identified in both healthy and POAG patients. M98K can even increase OPTN interaction with Rab8 and, at the same time, increase TBK-1 activation leading to elevated autophagic degradation[92]. In all OPTN mutations that lead to reduced protein levels or functionality, exocytotic impairment of neurotrophic factors occurs in RGC[93].

Paget's disease

Sir James Paget described Paget's disease (PD) in 1877 with the term osteitis deformans[94]. It is estimated to be between 2 to 5% prevalent in populations, especially those of Anglo-Saxon descent. Its primary age of clinical presentation is 55 years old with male predisposition[95]. The aetiology of PD is still unknown, but it is theorised to be multifactorial. Ultra-structures of intranuclear inclusions in osteoclast may point towards a viral infection, while its familial clustering and predisposition to Caucasian implement genetic and environmental factors[94]. It can be localised to one side (monostatic) or affect multiple bones (polyostotic), ranging between 77% to 81%, affecting the sacrum, pelvis, skull, and femur[94].

The pathophysiology of PD is characterised by initial rapid bone resorption followed by bone deposition. Such a process is repeated multiple times resulting in the formation of a mosaic pattern in the lamellar bone[96]. Clinically early stages of PD are asymptomatic. Later stages may show variable pain levels, deformities, and fracture of involved bones—facial deformity resulting from maxillary and mandibular bone involvement[97]. Radiographically, PD lesions display an irregular area of radiopacities, and radiolucencies distinctively appear as

"cotton wool" in radiographs[98]. Orally, PD causes many problematic issues, from loss of lamina dura, pulpal pearls, root resorptions, teeth migration, teeth ankylosis and hypercementosis[99]. Current treatment of PD consists of second and third generations of bisphosphonate, calcitonin bisphosphonate and mithramycin[100].

OPTN mutations relevant to PD have been identified; a single point mutation at the promoter region [rs 3829923] and mutations changing OPTN splicing [rs 2238968] are documented in PD patients[101].

OPTN negatively impacts osteoclastic differentiation on activation in both in vivo and in vitro models; such a role is exerted through (MCSF) and NFkB ligand (RANKL)[102]. upregulation of OPTN interaction with CYLD to block the RANKL pathway resulting in reduced NFkB activation and suppression of osteoclast differentiation. Conversely, in human samples, a mutation in OPTN which lacks methylation site [Rs 1561570], results in enhanced expression of OPTN and activation of NFkB[103,104]. Type one IFN downregulation via mutation in OPTN constraints negative autoregulation on osteoclasts changing the status of osteoclast into hyperactivity, increasing bone resorptions[102].

Upregulation of OPTN through the previous pathways reduced osteoclasts in size and numbers. In defective OPTN mice, increased osteoclastic activity and differentiation are shown to be the case. Another aged mouse model with total deletion of OPTN presents PD-like clinical features[104].

Crohn's disease

Crohn's disease (CD) is a chronic inflammatory digestive system disease that affects the entirety of the digestive tract. However, it is still unclear what causes CD, but current evidence indicates an immune deficiency combined with bacterial and genetic factors[58].

OPTN/TBK1 dimerisation is essential to clear bacterial invasion from the epithelial lining of the digestive tract via autophagy. OPTN/TBK1 are recruited to the site of cytosolic ubiquitin quoted bacteria to initiate autophagic machinery and eliminate such bacterial invasion. Also, OPTN deficiency and its subsequent inhibitory effect on type I IFN production results in a compromised innate immunity to viral infection. It has been documented that in CD patients, about 10% produce macrophages that contain reduced levels of OPTN. This reduction in OPTN results in lower levels of proinflammatory cytokines, TNF and IFNγ delaying neutrophils recruitment and bacterial clearance[56]. This is also supported by the higher mortality level in OPTN-deficient mice challenged with either Citrobacter rodentium, E. coli or Salmonella. In addition, the overactivation of immune response beyond clearance of pathogens and the disturbed role of OPTN in NFκB/ IFN pathways may cause a prolonged state of inflammation propagating the condition.

1.4 Inflammatory and autoimmune conditions of the oral cavity

A plethora of autoimmune conditions present as lesions in the oral cavity and may extend beyond the oral cavity. Many autoimmune conditions present first in oral mucosa but could also appear later during such autoimmune condition developments. Oral lesions involving oral mucosa range from blisters, ulcers, erosions, erythema or desquamative gingivitis (a condition of desquamation, erythema and/or erosion of the gingiva)[105].

Oral autoimmune conditions have a similar clinical presentation and may mimic other conditions of non-auto immune or non-auto inflammatory conditions. Clear, thorough patient history and physical examination combined with histopathological, immunological and lab testing are required for correct diagnosis.

In the following section, a brief discussion of some autoimmune conditions that affect the oral cavity with an emphasis on nucleotide oligomerisation domain 2 (NOD2) and Optineurin (OPTN) involvement in these conditions.

1.4.1 Oral Lichen planus (OLP)

A chronic autoimmune mucocutaneous systemic disease is present mainly in the mucosa of the oral cavity but can involve other sites like skin, genitals, scalp and nails[106]. Extraoral involvement is approximately around 15% in patients with OLP. Most genital lesions in females are estimated to be 25% compared to males genital lesions around 2-4%, other sites involvement is uncommon[107]. It is of immune-mediated origin as $CD8^+$ T-cells trigger apoptosis of oral epithelial cells basal layer, but it is still unclear what antigen is responsible for this autoimmunity[108]. Several predisposing factors have been identified for causing OLP ranging from idiopathic, systemic medication, dental materials (mainly causing an Oral lichenoid reaction), chronic liver disease, hepatitis C virus, stress, genetics, tobacco chewing and Graft-versus host disease[108,109].

OLP can be classified clinically into six different types: 1-reticular, 2- papular, 3- plaque form, 4- atrophic, 5- ulcerative or erosive and 6- a rare type bullous form[110]. The first three types can be asymptomatic or with mild discomfort. In contrast, the other types usually present with moderate to severe discomfort requiring clinical intervention. All types require monitoring for malignancy transformation periodically, as OLP usually persist throughout a patient's lifetime. Clinical diagnosis of OLP depends on the requirement of bilateral symmetrical or semi-symmetrical distribution of lesions, white lacy reticular lesions (known as Wickham stria) in reticular form with the inclusion of erosion, atrophy or bullous subtypes in the same patient presenting with reticular form[111]. It is estimated that the frequency of malignant transformation ranges from 0% to 5%, with a strong association of malignant transformation related to the ulcerative and erythematous form of OLP[112,113].

Histologically to confirm OLP diagnosis, specific criteria should be present (Fig. 1) in the lesion. This common lichenoid reaction features a dense band of mainly lymphocytes infiltration of the subepithelial lamina propria combined that obscure margin of both tissues with a liquefaction degeneration of keratinocyte basal layer and normal maturation of epithelium, previous classification would include Civattete bodies (dead keratinocytes) and hyperkeratosis[111]. Exclusionary criteria from OLP lesions are abnormal cytomorphology, nucleus enlargement, blunt rete ridges and abnormal keratosis. Such lesions are classified as dysplastic in nature and may develop into squamous cell carcinoma[114,115].

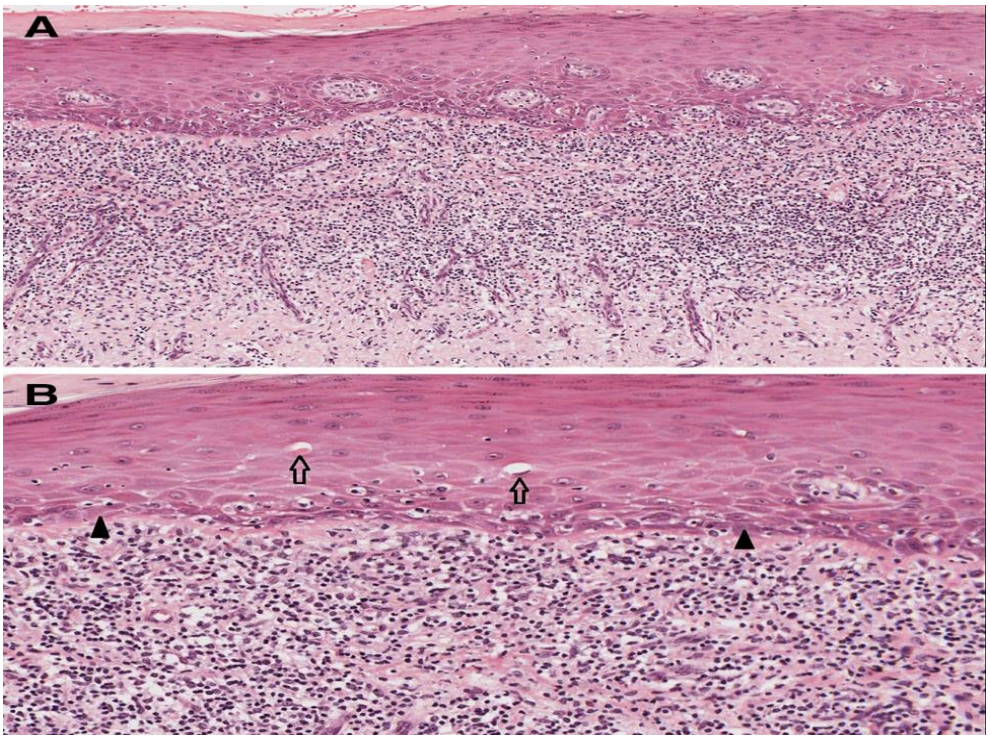

Figure 1. 5 Histopathology of OLP.

a Low power photomicrograph showing parakeratosis, band-like subepithelial chronic inflammatory infiltrate and saw-tooth rete ridges (H & E, original magnification X100). b High-power photomicrograph showing several colloid bodies (arrows) and liquefactive degeneration of basal keratinocytes (arrowheads) (H & E, original magnification X200)[116]

1.4.1.1 A possible link between OLP and oral cancer with TLR3

Previous studies pointed out that among many factors associated with OLP, genetics may play a part in developing OLP in certain families[117]. Genetic alteration is a risk factor in Oral squamous cell carcinoma (OSCC) development and exposure to smoking, alcohol consumption and papillomavirus infections[118]. Another element that counts as a risk factor in head and neck carcinoma is a chronic inflammation which can result from defective signalling of Toll-like receptors (TLRs)[119]. TLR3 is one such TLR expressed in malignant cells in OSCC, breast cancer, and melanoma[120].

Single nucleotide polymorphism (SNPs) in TLRs can be responsible for the change in function and contribute to an imbalance in pro-/anti-inflammatory cytokine and chemokine production, which gives rise to susceptibility to malignancy[121]. TLR3 SNPs rs5743312 and rs3775290, but not rs37755291, are highly implicated in OLP and OSCC development and/or propagation. In OLP, the presence of SNP rs5743312, which change TLR3 wild type from CC to mutant TT, increases the odds ratio (OR) of development as high as 15 folds and can be used as a biomarker of OLP susceptibility[121]. In OSCC, SNP rs5743312 is highly associated with cancer development and was found to be a prognostic tool for the worse malignancy survival in advanced stages[122]. Synonymous SNP rs3775291 in TLR3 changes amino acid from Leu to Phe (L412F). It has links to oral and nasopharyngeal cancers and is associated with increased tumour size in OSCC in Asin and African populations[123,122].

1.4.1.2 OLP associated with an elevation in proinflammatory-cytokines that are upregulated downstream of TLR3.

Keratinocytes from OLP patients cultured under elevated interferon gamma (IFN-γ) or normal OLP keratinocytes produced significantly higher levels of CXCL10 on protein and mRNA levels for an extended time of up to 48 hours. They had significant elevation as early as 3 hours compared to keratinocytes taken from normal healthy individuals under similar conditions. This elevation in CXCL10 in OLP has been confirmed in vivo by using serum samples taken from patients and healthy controls (Figure 1.2). Such an elevation may tip the cytokine balance toward a pro-inflammatory status that promotes the migration of CXCR3-expressing CD4+ lymphocytes into sites of immune activation. In addition, CXCL10 may prove key in propagating OLP pathogenesis with its ability to recruit lymphocytes to produce a band-like infiltration, a diagnostic feature used histologically to help confirm OLP in patients[124].

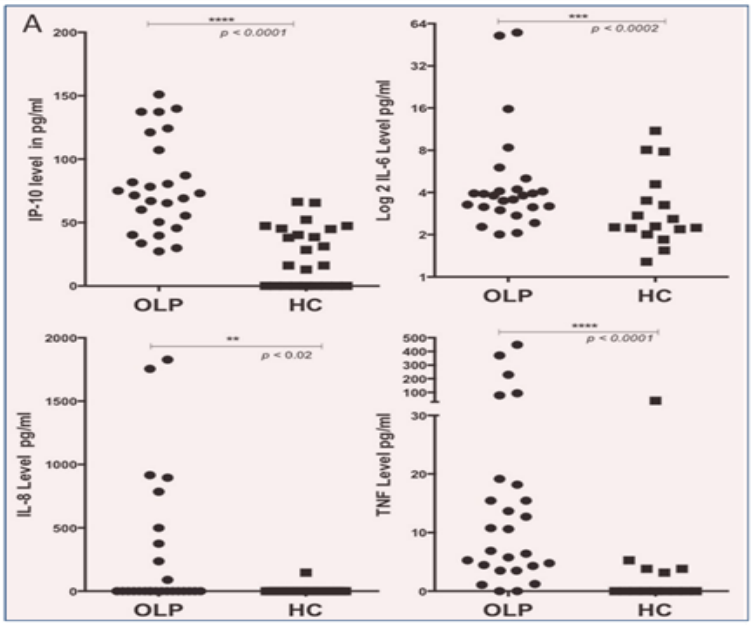

Figure 1. 6 Cytokines profile secretion levels of CXCL10 (IP-10), IL6, CXCL-8, and TNFα in healthy control serum compared to OLP.

N for OLP patients = 26, N for Healthy controls = 16 (Data provided by Dr Erni Marlina[125])

1.4.1.3 NOD2 expression in OLP patients

In a recent study, 20 OLP patients with no other immunological disease and six healthy control volunteers were biopsied at buccal mucosa to evaluate NOD1 and NOD2 expression mRNA via RT-PCR and protein level using immunohistochemistry (IHC). It was found that the NOD2 mRNA level was significantly elevated. Furthermore, NOD2 protein detection using IHC revealed high levels of NOD2 in lymphocytes of sub basial layer (84.2 % of total lymphocytes at sub basial layer) compared to healthy control. The study suggests a vital role of NOD2 in OLP aetiology and a possible therapeutic target[126]. Another study, involving 22 patients of OLP and compared to 15 healthy controls, looked at the Immunity related GTPase M (IRGM) axis role in autophagy related to OLP pathogenesis. Comparison of diseased to healthy controls indicated an elevation of IRGM, LC3B and NOD2 levels in peripheral T cells of OLP patients[127].

1.4.2 Periodontitis

It is an inflammatory condition of teeth supporting structure (alveolar bone, periodontal ligaments, cementum, and gingival mucosa). The inflammatory immune response triggered by microbial elements results in bone loss and, ultimately, tooth loss affecting mastication and quality of life[128]. Periodontitis is associated with numerous systemic diseases, including Diabetes, atherosclerosis of the cardiovascular system and rheumatoid arthritis[129–131]. More than 60% of people aged 65-year-old are thought to be affected by it with varying degrees of severity in the USA[132]. Around 600 bacterial species have been identified in periodontal disease. Among these bacterial species, Porphyromonas gingivalis, Tannerella forsythia, and

Treponema denticola are most relevant for chronic periodontitis. Other lesser impactful bacterial species like Fusobacterium nucleatum, Prevotella, Intermedia, and Prevotella nigrescens are also identified[133,134].

Many studies looked at nucleotide binding oligomerisation domain containing 2 (NOD2) activation in response to bacterial species associated with periodontal disease. It has been established that NOD2 response to P.gingivalis is weaker than other less impactful bacterial species leading to P.gingivalis survival and stagnation at the periodontal pocket[135]. A different study using NOD-/- mice challenged with P.gindivalis in the periodontitis model found that NOD2 activation promoted higher bone resorption through the osteoclastic activity without affecting the osteoclastic differentiation process[136]. Another study examined the impact of NOD2 and RIPK2 knockout mice after injecting gingival tissue with heat-killed Aggregatibacter Actinomycetecomitans. In addition, NOD2 KO mice produced a significantly lower immune response from macrophages and RANKL-induced osteogenesis differentiation leading to high bone resorption and impaired Gram-negative bacterial clearance[137].

1.4.2.1 Aggressive periodontitis (AgP)

AgP is a variant of periodontitis, a rare but severe subtype characterised by rapid alveolar bone loss with no other symptom of inflammation orally with familial predisposition[138]. Such familial hereditary spread led to theorising genetic factors as major causative factors in AgP, with 30% of AgP patients having familial spread patterns35. NOD2 and its variants are

expressed in periodontal ligaments, and oral epithelial cells and previously mentioned studies highlighted NOD2 role in periodontal disease[139].

Recently, NOD2 variants emerged as possible causative for AgP. A study on two families of Asian descent with family members affected with AgP compared against healthy controls from the same family using GWS identified multiple NOD2 variants. In this study, five NOD2 variants were identified (p.A110T) in the CARD domain, (p.R311W, H370Y, R459C) in NBD and (p.A868T) in the LRR domain. NOD2 variant (p.A110T) was predicted to be probably damaging by PloyPhen-2 and SIFT programs, and variant (p.R311W) was predicted to be deleteriously damaging by PROVEAN, PloyPhen-2 and SIFT programs[140]. In another more recent study involving 101 patients (37 patients with familial history and 64 sporadic patients), genetic testing revealed two NOD2 variants (p.R311W) familial group and (p.R471C) in the sporadic group. NOD2 variants (p.R311W) were detected in 6 patients of the familial group, and it was found to be pathogenic by predictive programs. Also, this variant was associated with a more aggressive and earlier onset of AgP. NOD2 variant (p.R472C) was found in 4 patients of the sporadic group, but this was not found to be pathogenic by any predictive program[141]. New evidence immerged linking SQSTM1/p62 mediated autophagic degradation of NOD2 through S-palmitoylation of NOD2. Such degradation is inhibited when NOD2 is palmitoylated by zinc finger DHHC-type palmitoyltransferase 5 (ZDHHC5) and would lead to upregulation of NFkB signalling. Furthermore, NOD2 variant R444C, a disease-associated variant, had increased S-palmitoylation of NOD2, further stabilising NOD2 and retard its degradation. The NOD2 R444C variant is encoded by rs1078327, which has been found in patients of IBD, Blau syndrome (BS), acute myeloid leukaemia or Aggressive periodontitis. It is possible that this

variant impacts the positive upregulation of NFkB signalling and may play a role in the pathogenesis of AgP, among other diseases[142].

1.4.3 Crohn's disease

Inflammatory bowel disease is a condition that consists of two main types Crohn's disease (CD) and ulcerative colitis (UC). Both are chronic. While UC manifestation is limited to colon mucosa, by contrast, CD manifest in any site of the digestive tract, including oral mucosa prompting a rationale for focusing on CD only in this introduction[143].

The aetiology of CD is attributed to multiple factors ranging from genetics, environmental factors, and complex autoimmune-driven reaction. For example, orally affected mucosal lesions can present as inflamed gingiva at the mucogingival line, longitudinal ulceration (snail trail) of buccal mucosa at the buccal vestibule, swollen lips because of non-caseous granulomas may become permanent due to fibrotic deposition, cobblestoning of mucosa as a result of hyperplastic changes, fissured tongue and lips, and mucosal tags and nodules[144]. Other complications can be inferred to CD managing drugs or nutritional deficiency to present with aphthous ulcers, a lichenoid reaction like lesions, EM or SJS, and periodontal disease, among many others[105].

CD diagnosis can be achieved through a history of symptoms and a radiographic and endoscopic examination. Additional basic lab and antibodies tests may help diagnostically[145]. Histological examination of biopsy usually displays non-caseating granulomas along with a chronic inflammatory infiltrate[146].

CD patient management warrants a multidisciplinary treatment plan; orally, they experience odynophagia, dysphagia, painful tongue, taste disturbance, depapillation of the tongue, and xerostomia due to multiple medications and salivary gland involvement[145,146]. CD can present at an early age with predominance toward males. Malignancy may arise from administered therapies[147].

1.4.4 Orofacial Granulomatosis (OFG)

OFG is a rare inflammatory disorder of the mouth and may be associated with CD. It affects the oral cavity and perioral regions. Clinically it presents as swelling of the lips with inflammation affecting gingival tissue, buccal mucosa, and other sites of un-keratinised epithelial mucosa[148]. Histologically, OFG may present as CD of the oral cavity[149]. Patients may suffer from OFG or OFG combined with an intestinal CD or OFG with gastrointestinal granulomas with no intestinal CD, but even OFG alone or CD-only patients may develop CD or OFG (respectively) during the disease with no predicting factor[150]. Although OFG aetiology is still unknown, many theorise it may share genetic factors linking OFG to CD because of their association as conditions[151].

A previous study looking into CD and OFG patients found that four out of 12 patients (total patients included 29) who had CD and OFG combined conditions carried one of NOD2 commonly known variants (p.R702W) mutations. This study only looked for commonly found NOD2 variants (p.R702W, p.G908R, p.L100insC) and omitted other newly discovered variants[152]. Another recent study, which included 201 patients (111 OFG/ 90 OFG + CD),

included common CD NOD2 mutations (p.R702W, p.G908R, p. L100insC) and newly discovered CD-associated NOD2 variants (p.M863V, p.D862S, p.R703C, p.S431L, p.V793M, p.R311W) in their patients. The study concluded the presence of all three common NOD2 variants in 9.9% (11/111) and 23.3% of OFG and OFG+CD patients, respectively. Furthermore, including the other seven rare NOD2 variants, the frequency increased to 13.5% (15/111) and 27% (25/90) of OFG+CD patients, respectively[153].

1.4.5 Systemic lupus erythematosus (SLE)

A chronic multisystem autoimmune condition, antinuclear, is characteristic in this condition as the body losses its ability to tolerate nuclear antigens. Autoantibodies in the form of anti-double stranded DNA (Anti-ds-DNA) and Anti-Sm antibodies are found in more than 95% of all SLE patients. They are a prerequisite as criteria in the diagnosis of such disorder[154,155]. It is connective tissue and blood vessel disease and carries a variable diagnosis with it compared to its cutaneous counterpart, which is more benign[156].

Oral lesions related to SLE are not always symptomatic (up to 50% in all cases) and chronic to have a mean duration of up to 4.2 years, according to one study 54. The typical presentation of the oral picture is multiple asymmetrical red and white lesions appearing as erythematic mucosa or erosions with white papules centrally surrounded with white stria as rim with occasional telangiectasia[157]. Other variations of the oral lesion could appear as ulcers, honeycomb reticular plaques, purpura and petechiae. Sites affected intraorally commonly are buccal mucosa, gingiva, hard palate, and lips. On the lip, it can manifest as discoid lesions at the vermillion border or as cheilitis that spread on the perioral skin[158].

Another oral advice effect of this condition is the involvement of minor salivary glands (up to 30%) and the development of secondary (SS) resulting in xerostomia followed by its consequent candidiasis and angular cheilitis[157].

SLE is equally distributed among males and females, although more prevalent in females at childbearing age. Incidence rates range from 1-10 per 100,000 per year, and its prevalence range from 20-70 cases per 100,000 of a population[159].

Histologically the hallmark of SLE lesion is interface mucositis displaying superficial and deep perivascular lymphocytic inflammation coupled with hyperkeratotic epithelium, thickening of the basement membrane, liquefaction necrosis and atrophic rete pegs[158]. The presence of mucin at the lamina propria is a good differentiator histologically of SLE from OLP[160].DIF shows a linear or granular deposition of IgG, IgM, IgA and C3 at the basement membrane zone. IgM is found to be an immune reactant in SLE[156].

1.4.5.1 NOD2 in SLE

NOD2 may be involved in SLE as it has multiple roles in immune modulation and autophagy[161]. Moreover, NOD2 loci (16q12) have been identified as susceptibility loci in SLE patients[162]. A study genotyping NOD2 in 277 SLE patients and 356 healthy controls identified a single SNP (rs2076756), but it was insignificant compared to healthy controls[163]. Another study looking at 1305 cases of SLE in a pooled analysis concluded that SNP (rs2066845) have a substantial effect on susceptibility risk to SLE (OR 2.01: 95%, %CI 1.01- 4.03)[164]. In a recent study on 110 SLE patients compared to 120 controls, two SNPs of NOD2 were investigated

(rs3135500 and rs3135499) for SLE risk in the Asian population. It was found that both SNPs did not present significant risk toward SLE. Although, (rs3135500) had an association with clinical manifestation in terms of severity of neurological symptoms, skin manifestation, renal involvement, and higher serum concentration of creatinine. Also (rs3135499) had an association with renal involvement and creatinine concentration, and both SNPs were associated with early onset of SLE[165].

1.5 Research hypothesis and aims.

This study aims to investigate a link between NOD2 activation with MDP and OPTN post-translation modification in the form of phosphorylation. In this thesis, two mass spectrometry methods establish a link between two essential proteins to innate immunity. I first create a stable cell line expressing EGFP-OPTN to facilitate the isolation of the OPTN enriched protein. Second, I identified a novel phosphorylation site in the OPTN structure at position S526 after NOD2 activation. I then create two phosphomutant variants of EGFP-OPTN cell lines to investigate the importance of this post-translation modification.

The hypothesis investigates:

- The impact of OPTN post-translational phosphorylation on NOD2 ability to activate the NFkB pathway.
- We aim to quantify the impact of this link on pro-inflammatory release in the event of NOD2 activation when OPTN site S526 is either phospho dead or phospho active.
- This post-translation modification may serve as a therapeutic target to modulate immunity in conditions where OPTN play a significant role in its pathogenesis.

Chapter 2 Materials and methods

2.1 Cell culture

2.1.1 THP-1 cells

The THP-1 cell line (ATCC® TIB-202™), a cell line derived from the peripheral blood of a 1-year-old male patient with acute monocytic leukaemia, is a monocyte-derived and spontaneously immortalised cell line. THP1 cells were cultured and maintained in a complete RPMI/THP-1 culture medium. Cells were grown in flasks at a concentration of 2-4x10^5 cells/mL prior to being stimulated. THP-1 cells were maintained by adding or replacing fresh complete RPMI and split 3x times weekly. The THP-1 cells were kept no longer than two months before being replaced from liquid nitrogen stocks.

2.1.1.1 THP1 culture media

The THP-1 culture medium contained RPMI 1640 Medium, GlutaMAX™, plus 10% foetal bovine serum (Sigma F9665), 100 U/mL of Penicillin and 100 µg/mL Streptomycin (Gibco 15140-122), 20 mM HEPES solution (Sigma H0887), and 20 nM 2-mercaptoethanol (Gibco 31350) referred to medium with supplements as complete RPMI.

2.2 Reagents for biological assays

2.2.1 Heat-killed bacteria

2.2.1.1 Luria-Bertani (LB) broth and agar plates

20 g of LB Broth powder (L3022 Sigma) was added to 800 mL of dH2O, mixed with a magnetic stirrer and made up to 1000 mL, then autoclaved and plated. LB broth was made up as above without the agar.

2.2.1.2 Heat-killed *Escherichia coli* (HkEc) stock

The fully antibiotic sensitive clinical isolate, *E. coli* NCTC 10418, was cultured by adding one µL of glycerol stock into 10 mL LB broth (Sigma L3022) and incubated at 37 °C, 250 rpm in an Innova™ 4000 incubator shaker (New Brunswick Scientific) overnight. *E. coli* was centrifuged at 3000 *g* for 20 minutes, room temperature, in a Heraeus Multifuge X1R (Thermo Scientific), washed once with 20 mL PBS, and resuspended in 1 mL PBS. The killing of *E. coli* was carried out by incubating 1 mL of bacteria in PBS at 60 °C for 1 hour in a Grant GD100 circulating immersion bath. The killing of *E. coli* was checked by plating 80 µL of HkEc onto LB agar plates with no antibiotics and incubating at 37°C for 48 hours. The absence of any colonies after 48 hours was deemed to verify the successful killing of *E. coli*.

HkEc solution was counted at 1:20 dilution using a Cecil BioQuest™ CE2502 spectrophotometer. As previously established in our laboratory, the E. coli optical density at 600 nm (OD600) of 1x108 bacteria/mL in PBS is 0.365. The concentration of *E. coli* in PBS was adjusted to $1x10^{10}$ bacteria/mL and stored in 1 ml aliquots at -20 °C.

2.2.2 Mixed biological reagents

The list of reagents containing the description of each item, catalogue number, supplier, and usual working concentration can be found in Table 2. If, in any case, the experiment required the use of a different concentration, this information will be available in the results description. The working concentration was established based on usual concentrations found in the literature and/or titrated and toxicity determined by MTT assay (see section 2.4.1).

Item description	Catalogue #	Supplier	Work Conc.
Pam3Cys-Ser-(Lys)4, trihydrochloride	ALX-165-066	Alexis Biochemicals	10 µg/mL
LPS from Salmonella abortus equi S-form	ALX-581- 009	Alexis Biochemicals	100 ng/mL
Poly IC (HMW)	tlrl-pic	Invivogen	500 ng/ml
Muramyldipeptide (L-D isoform, active) (MDP)	tlrl-mdp	Invivogen	5 µg/ml
BX795(TBK1/IKKε inhibitor)	702675-74-9	Cambridge Bioscience	10 µM/ml
Phorbol 12-myristate 13-acetate (PMA)	P8139	Sigma- Aldrich	140 nM/ml
Polybrene	TR-1003-G	Millipore	4 µg/ml
G418 (Geneticin)	ant-gn-1	Invivogen	10 µg/ml
Doxycycline hydrochloride	D3447-500MG	Sigma	300 ng/ml

Abbreviations: Catalog #, catalogue number; Work conc, working concentration

Table 2. 1 List of mixed biological reagents containing the description, catalogue number, supplier, and usual working concentration.

2.3 Cell stimulation

2.3.1 PMA-induced differentiation of THP-1 cells to a macrophage-like phenotype.

THP-1 cells were incubated with 140 nM PMA in complete RPMI for 72h at 37 ^{o}C 5% CO_2. Supernatant containing PMA is removed after 72h. The cells were then washed twice with sterile PBS (Gibco). Fresh complete RPMI is supplemented for 4 days to enable M1 Macrophages to develop and rest.

2.3.2 Stimulation of cells

Cells were stimulated with HkEc with a multiplicity of infection (MoI) 10:1 (bacteria/cell) established after titration. The TLR ligands LPS (TLR4) smooth (100 ng/mL), 500 ng/mL Poly IC HMW (TLR3), and 10 µg/mL PAM3CSK4 (TLR1/2) were used for the immunological challenge of specific TLRs.

The list of all the biological reagents with their working concentration and time required for preincubation is described in Table 2.1. Any alteration in concentrations used in the described experiments will be documented in the results section.

2.4 Cell viability assays

2.4.1 MTT cell viability assay

2.4.1.1 MTT (3-[4,5-dimethylthiazol-2-yl]-2,5-diphenyl tetrazolium bromide)

A 0.5% solution of MTT (3-[4,5-dimethylthiazol-2-yl]-2,5-diphenyl tetrazolium bromide) was made by dissolving 500 mg of MTT (Sigma M2128) in 100 mL of PBS and stored at 4 °C in the dark.

2.4.1.2 MTT lysis solution

One litre of lysis solution was prepared using 900 mL of isopropanol, 47 mL of dH2O, 50 mL of 10% sodium dodecyl sulfate (SDS) and 3 mL of concentrated HCl were added together, which was kept at room temperature.

2.4.1.3 MTT assay

Cells were cultured in 96-wells plate within 100 µL of the medium under different conditions and time frames depending on the experimental protocol. The viability of the cells at the end of the protocol was determined by adding 30% of total volume of 0.5% MTT (30 µL) and incubated for at least 4 hours at 37^0C 5% CO_2. After MTT incubation, the plate was centrifuged at 8000 rpm for 5 minutes. The supernatant was removed with a multi-channel pipette and 100 µL of MTT lysis solution was added to the cells and pipetted multiple times until all formazan crystals were dissolved. Results were read on a FLUOstar Omega microplate reader (BMG LABTECH) at 563 nm.

2.4.2 CCK-8 cell viability assay.

The Cell Counting Kit-8 (B34306 Biotool) ready-to-use solution was added to each well to a concentration of 10% v/v and kept in a humidified tissue culture incubator at 37 °C, 5% CO2 for 1 hour. Results were read on a FLUOstar Omega microplate reader at 450 nm.

2.4.3 AlamarBlue viability assay

AlamarBlue kit (BUF012B BioRad) ready-to-use solution was added to each well to a concentration of 10% v/v and kept in a humidified tissue culture incubator at 37 °C, 5% CO2 for 1 to 3 days. Cells were read for absorbance on a FLUOstar Omega microplate reader at 570nm and 600nm wavelengths.

2.5 Cytokine assay

2.5.1 Enzyme-linked immunosorbent assay (ELISA) assay

Cytokine levels from supernatant or total cell lysate (see section 2.7.1.1) from cultured THP-1/M1 Macrophage cells under several conditions were collected and stored at -80°C prior to use. After removal of supernatants for storage, cell viability was assessed using the MTT assay (2.4.1). Total cell lysates were standardised prior to test using the Pierce™ BCA Protein Assay Kit (23225 Thermo Fisher Scientific) and stored at -80°C. Samples were diluted with reagent diluent for ELISA assay. According to manufacturers' instructions, the ELISA assays were carried out using Duo-Set ELISA kits and read on a FLUOstar Omega or CLARIOstar microplate reader (BMG LABTECH). Microplate readers were set to 450 nm and 570 nm, the last used for wavelength correction, for ELISA kits supplied by R&D Systems. The wavelength correction was done using MARS Data Analysis Software by subtracting readings at 570 nm from the readings at 450 nm for (Table 2).

Kit	Catalogue #	Manufacturer	Dilution
Human IL-8/CXCL8 DuoSet ELISA	DY208	R&D Systems	1:20
Human TNF-alpha DuoSet ELISA	DY210	R&D Systems	1:10
Human IL-6 DuoSet ELISA	DY206	R&D Systems	1:10
Human IP-10 DuoSet ELISA	DY266	R&D Systems	1:25

Abbreviations: Catalog #, catalogue number

Table 2. 2 Description of ELISA kits used, catalogue number, supplier, and supernatant dilutions.

2.6 Gene expression

2.6.1 RNA purification

Total RNA was extracted and purified from THP-1 cells after several treatments. Cells were harvested, and the supernatant was removed (or collected), and 350 µL of RLT lysis buffer (Qiagen) with 1% 2- mercaptoethanol (M3148 Sigma) was added and stored at -80 oC prior to extraction. RNA was extracted using the RNeasy Mini Kit columns with RNase-free DNase treatment (Qiagen) and processed following manufacturer's instructions with RNase-free DNase treatment (Qiagen) step. The concentration of total RNA in RNase-free H_2O (Qiagen) was measured with a NanoDrop ND-1000 spectrophotometer (Thermo Scientific) and/or Qubit 2.0 Fluorometer (Invitrogen). Additionally, OD_{260}/OD_{280} and OD_{260}/OD_{230} were measured, which assessed protein and solvent contamination.

2.6.2 Complementary DNA (cDNA) synthesis

Total RNA was converted to cDNA using the Moloney Murine Leukemia Virus Reverse Transcriptase (M-MLV RT) kit (M1705 Promega). 500 ng of total RNA diluted in 15 µL of RNase-free water was added to 1 µL of oligodT primer (Sigma) and incubated for 10 minutes at 70 °C for primer annealing and then placed on ice for 5 minutes. After that, a master mix containing 1 µL of M-MLV Reverse Transcriptase, 5 µL of 5X Reaction Buffer, 1 µL Recombinant RNasin® Ribonuclease Inhibitor (Promega), and 2 µL of dNTP Mix (NU-0010-10

Eurogentec) was added to each RNA sample making a total volume of 25 µL. Samples were incubated at 40 °C for 10 minutes for DNA polymerisation and heated at 70 °C for 5 minutes for enzyme deactivation on a DNA Engine Tetrad 2® Peltier Thermal Cycler (Bio-Rad). Samples were made up to 100 µL with RNase-free water and stored at -20 °C.

2.6.3 Semi-quantitative PCR

cDNA originated as previously described were amplified by PCR with primers created using Primer3 (Table 4). Stock primers at 100 µM were diluted to 5 µM i.e., 50 µL per 1 mL of RNase-free water for and stored at -20 °C. The PCR reaction was made up of 12.5 µl of HotStarTaq Master Mix (1000 U), 1 µL forward primer, 1 µL reverse primer, 2 µL cDNA and8.5 µL RNase-free water, to a total volume of 25 µl. The final concentration in each reaction volume was 1.25 U HotStar Taq DNA polymerase, 1X PCR buffer containing 0.75 mM MgCl2, 100 µM of each dNTP, 0.25 µM of each primer and ~10 ng of RNA equivalent. The RT-PCR was activated at 95 °C for 15 minutes, denatured at 95 °C for 30 s, annealed at 60 °C for 45 s, extended at 72 °C for 60 s, for a total of 35 cycles, then extended for a final time at 72 °C for 10 minutes before being cooled to 4 °C on a DNA Engine Tetrad 2® Peltier Thermal Cycler (Bio-Rad). The annealing temperature of 60 °C was chosen after a temperature gradient was run for the primer pair.

After the PCR, 5 µL of 6X Orange Loading Dye (R0631 Thermo Fisher Scientific) and loaded on 1% agarose gel containing 0.01% ethidium bromide. The gels were cast on

horizontal electrophoresis and ran at 100V for 25 minutes. Images were captured using Thermo Scientific MYECL Imager.

Table 2. 3 List of primers used for PCR/qRT-PCR.

GENE	Forward primer	Reverse primer	Target exons	Tm
IL6	5’-CACTGGCAGAAAACAACCTG-3’	5’-TGTACTCATCTGCACAGCTCT-3’	3-4	63°C
CXCL10 (IP10)	5’-AGTGGCATTCAAGGAGTACC-3’	5’-TGATGGCCTTCGATTCTGGA-3’	1-3	63°C
IFNb1	5’-ACGCCGCATTGACCATCTAT-3’	5’-GCTCATGAGTTTTCCCCTGG-3’	1-2	63°C
IL1B	5’-ACTGAAAGCTCTCCACCTCC-3’	5’-CTCTCCAGCTGTAGAGTGGG-3’	4-6	64°C
CXCL-8	5’-CAGTTTTGCCAAGGAGTGCT-3’	5’-CCAGTTTTCCTTGGGGTCCA-3’	2-3	63°C
TNF	5’-GGACCTCTCTCTAATCAGCCC-3’	5’-TGGTTATCTCTCAGCTCCACG-3’	2-4	62°C
PPIA	5’-GTGTTCTTCGACATTGCCGT-3’	5’-CCATTATGGCGTGTGAAGTCA-3’	1-3	62°C

2.6.4 Quantitative reverse transcription PCR (qRT-PCR)

cDNA originated as previously described were amplified using primer pairs from Table 3. qRT-PCR was performed using the QuantiFast SYBR® Green PCR kit (Qiagen), in duplicate on a Mastercycler® ep *realplex* (Eppendorf). Stock primers at 100 µM were diluted to 5 µM i.e., 50 µl per 1 mL of RNase-free water for qRT-PCR and stored at -20 °C. The qRT-PCR reaction was made up of 12.5 µl 2x QuantiFast SYBR Green PCR Master Mix, 0.5 µl forward primer, 0.5 µl reverse primer, 2 µl cDNA and 9.5 µl RNase-free water, to a total volume of 25 µl. The final concentration in the reaction volume was 1x QuantiFast SYBR Green PCR Master Mix, 0.1 µM of each primer and ~10 ng of RNA equivalent per reaction. The PCR mix was activated at 95 °C for 15 minutes, denatured at 95 °C for 15 s and annealed/extended at 60 °C for 60 s, for a total of 40 cycles, then a melting curve was performed. The annealing temperature of 60 °C was chosen after a temperature gradient was run for each primer pair.

Normalised mean gene expression values ± SD were determined from duplicate cycle threshold (Ct) values for each gene and the housekeeping gene peptidylprolyl isomerase A (*PPIA*). Relative transcript levels were determined by the $2^{-\Delta\Delta Ct}$ method.

2.6.5 DNA sequencing

DNA samples (plasmid or cDNA) were sequenced using Eurofin Mix2seq kit. A 100 ng of each DNA samples (1 µL volume) was added with 5 µM sequencing Primer (1 µL volume) and RNase-Free water (8 µL volume) into the sequencing tube. Mixture was pipetted 3 times to ensure homogeneously formed samples. Sequencing tube is sealed with a cap pad and sent for overnight sequencing.

2.6.6 Transient Transfection

Using Clontech Xfect™ Transfection Reagent (Takara, Cat# 631318). The original EGFP OPTN pLXIN plasmid was used for transient transfection reaction, 5 µg plasmid DNA in total, THP-1 cells were plated in a 6 well tissue culture plate (VWR, Cat# 736-0019) at 2 X 10^5 cells in 1 ml of RPMI 1640 without phenol red (Thermo Fisher, Cat# 11835063) supplemented with 1 % HEPES (Sigma, Cat# H0887), 250 µl 2-Mercaptoethanol (Thermofisher, Cat# 31350010), 10% FBS from (Sigma, Cat# F9665), 5% penicillin/streptomycin (Life Technologies, Cat# 15140-122). The transfection reaction protocol and the parameter are shown below:

	EGFP OPTN pLXIN
DNA	4.2 µl @1211.6 ng/ µl
X buffer	95.8 µl
X polymer	1.5 µl

1. Add 5µg DNA to Xfect buffer to a final volume of 100 µl in 1 ml Eppendorf tube, vortexing for 5 seconds at high speed.
2. Add 1.5 µl to the diluted DNA-Buffer and mix by vortexing for 10 seconds at high speed.
3. Incubate the mixture at room temp for 15 min. to allow nanoparticles complex to form.
4. Spin the mixture for 5 seconds to collect the content to the bottom of the tube.

5. Add 100 µl of the mixture to cells in 6 well plate and gently rock the plate to allow of added mixture to spread evenly.
6. Incubate for 24 hours at 37 °C and 5% CO_2 to allow cells to take up plasmids and for optimum expression of transfected protein.
7. Next day, supplement each well with another 1ml of RPMI 1640 medium to allow for further cell culture propagation.
8. Visualisation of florescent EGFP is observed from THP-1 Cells.

2.6.7 Heat shock transformation (transformation of competent cells')

The circularised DNA was used to heat shock transform Stellar™ Competent E. coli (Cat. #636766) following the protocol below:

1. Thaw Stellar Competent Cells in an ice bath just before use.

2. After thawing, mix gently to ensure even distribution, and then move 50 µl of competent cells into a 1-ml round bottom tube (falcon tube). No vortex.

3. Add no more than 2 µl of ligation solution for transformation.

4. Place tubes on ice for 30 min.

5. Heat shock the cells for exactly 45 sec at 42°C.

6. Place tubes on ice for 1–2 min.

7. Add 448 µl SOC medium to bring the final volume to 500 µl, and SOC medium should be warmed to 37°C before use.

8. Incubate by shaking (225 rpm) in Eppendorf ThermoMixer® for 1 hr at 37°C.

9. Add 150 µl of 500 µl bacterial solution to an LB Agar plate supplemented with Ampicillin at a concentration of 100 µg/ml and keep for 15 min to dry near flame then covered with lid and moved to a bacterial incubator for 24 hours at 37 °C.

2.6.8 Retroviral particles production

Our plasmids contain an MMLV expression vector, and we included pVSV-G as an envelope to HEK 293 GP-2 to manufacture viruses containing the intended DNA code for EGFP OPTN. Enveloped plasmid pVSV-G is provided from Takara in a Retro-X Universal vector Set (Cat# 631457). Plasmid is then Heat shock transformed into Stellar competent cells and grown in bacterial culture, made into glycerol stocks, and Maxi prepped to give a plasmid stock stored at -80^{o}C. HEK-293 GP-2 cells were grown in a 20 cm dish (SLS, Cat#CC7862-3394) at 30-40 % confluency in 10 ml of DMEM, High glucose, no phenol red from Gibco (Cat# 21063045) supplemented with 10% FBS from Sigma (Cat# F9665), 5% penicillin/streptomycin from Life Technologies (Cat# 15140-122) at cultured at 37 °C and 5% CO_2. To co-transfect both EGFP OPTN and pVSV-G plasmids, Xfect™ Transfection Reagent was used. For each plasmid, 30 µg DNA was used, combined 30 µg DNA of envelop plasmid in a separate reaction. The protocol is the same as described in section 2.6.6, and the ratios are specified according to the table in the next page.

	EGFP OPTN pLXIN	pVSV-G
DNA	24.8 µl @1211.6 ng/µl	34 µl @885.1 ng/µl
X buffer	575.2 µl	566 µl
X polymer	9 µl	9 µl

Transient transfection of EGFP OPTN and envelop plasmid pVGV-G into HEK-293 GP-2 cells.

After the transfection, the HEK-293 GP-2 cells are moved to an incubator set at 32 °C and 5% CO_2 and kept for 48 hours, after which supernatant is collected. The supernatant is then centrifuged for 20 minutes at 1000 x G, 4 °C to pellet any debris and finally filtered through a 0.2 µm cellulose acetate filter (VWR, Cat# 514-0061), aliquoted and stored at -80 °C.

One aliquot of viral supernatant was utilised to verify the presence of the OPTN construct in the viral particles in each preparation. Viral RNA was purified using Qiagen QIAamp viral RNA Mini Kit (Cat# 52904), converted to cDNA using HotStar Taq Master Mix from Qiagen (Cat# 203445) and Anchored Oligo(dT)20 Primers from Thermo (Cat# 1257011) to sequence and confirm the integrity of EGFP OPTN code before THP-1 cells transduction with viral medium.

2.7 Immunoblot

2.7.1 Cell lysate preparation

2.7.1.1 Whole cell lysate preparation

THP1 cells were plated in a 24-well plate with a cell count of 2 x 10^6 cells under several treatments. At the planned stimulation time, cells were scraped with sterile 24 cm cell scrapers (SLS 99002T) and transferred to an Eppendorf tube and centrifuged with a Beckman Coulter Microfuge 22R for 1 minute at 2500 rpm. The supernatant was discharged (or collected and stored at -80 ^oC) and the cell pellet was resuspended and washed with 1 mL of ice-cold PBS and centrifuged again using the same settings. The PBS was removed by aspiration and cells were lysed in 250 µL of ice-cold radioimmunoprecipitation assay (RIPA) buffer containing protease inhibitor cocktail (Roche 11697498001) and PhosSTOP™ (4906845001 Sigma) and vortexed (Table 5).

The cell lysate was then sonicated using a MSE Soniprep 150 (MSE) for three 10 seconds bursts with an amplitude of 7 microns intercalated with periods of 10 s on ice for disrupting cellular membranes, releasing the cells contents and shearing of DNA. After the sonication, the lysates were centrifuged for 10 minutes at 4 ^oC and ≥ 10,000 rpm.

Reagent/Manufacturer	Stock	Final concentration
Trizma® base (T1503 SIGMA)	1 M	50mM
Sodium chloride (S3014 SIGMA	5 M	150mM
Sodium-deoxycholate (D6750 SIGMA)	5%	0.50%
EDTA solution (03690 SIGMA)	500 mM	1mM
EGTA (E3889 SIGMA)	500 mM	0.5mM
IGEPAL® CA-630 (I8896 SIGMA)	100%	1%
SDS (L3771 SIGMA)	10%	0.10%
PBS (P4417 Sigma)	10X	1X

Table 2. 4 Cell lysate buffers for immunoblot.

2.7.2 Sample preparation

The protein concentration of each sample was measured using the Pierce™ BCA Protein Assay Kit (23225 Thermo Fisher Scientific) according to the manufacturer's instructions and read on a CLARIOstar or FLUOstar Omega microplate reader (BMG LABTECH) at 562 nm. Samples were then standardised with appropriate amounts of cell lysate and lysis buffer. One volume of sample buffer mix made of 3 volumes of 4X NuPAGE® LDS Sample Buffer (NP0007 Thermo Fisher Scientific) and 1 volume of 2-mercaptoethanol (Gibco 31350) was added to 2 volumes of standardised lysis buffer and then boiled at 95 oC for 5 mins and stored at-20 °C.

2.7.3 SDS-PAGE gels

Sodium dodecyl sulfate-polyacrylamide gel electrophoresis (SDS- PAGE) gels were cast using the Mini-PROTEAN® System (Bio-Rad) with 30% w/v Acrylamide/ProtoFLOWGel (SLS H16996), 1.5 M Tris-HCl pH 8.8 (resolving gel), 1 M Tris-HCl pH 6.8 (stacking gel), dH2O, 10% SDS (Sigma L3771), freshly made 10% ammonium persulphate (Sigma A7460) and TEMED (Sigma T9281) (added in the order listed with TEMED last).

10% SDS-PAGE gels were used and loaded onto 15-well SDS- PAGE gels and run in ~700 ml of 1X transfer buffer without methanol (Table 5) at 100 V (constant voltage) for 40 minutes.

Alternatively, precast Novex 4-12% Bis-Tris Midi Protein Gels (WG1403 Thermo Fisher Scientific) were used on XCell4 SureLock Midi-Cell Chambers and run in ~1000 mL of 1X NuPAGE MOPS SDS Running Buffer (NP0001 Thermo Fisher Scientific) at 120 V for 2 hours.

10X Tris-buffered saline (TBS) pH 7.4		
Reagent	Stock	Final concentration
Trizma® base	24.2 g	20 mM
NaCl	80.06 g	137 mM
dH2O		800 mL
HCl (H1758 SIGMA)	5 M	pH to 7.4
dH2O		Top up to 1 L
10X Transfer buffer		
Reagent	Stock	Final concentration
Glycine (G8898 SIGMA)	144 g	191 mM
Trizma® base	30.2 g	25 mM
dH2O		Top up to 1 L
10X Running buffer		
Reagent	Stock	Final concentration

Glycine	144 g	191 mM
Trizma® base	30.2 g	25 mM
SDS	10%	0.1%
dH2O		Top up to 1 L

Table 2. 5 Buffers for SDS-PAGE gels.

2.7.4 Protein transfer to membrane

Proteins were transferred using a wet transfer system to methanol- activated Immobilon-P PVDF Membranes (IPVH00010 Millipore). 400 mL of 1X transfer buffer containing 20% methanol on a Novex™ Bolt™ Vertical Mini Blot Module (B1000 Invitrogen™) and Invitrogen™ Mini Gel Tank (A25977 Invitrogen™) at 20V.

The SDS-PAGE gel was removed from its mould in the transfer buffer, the stacking gel was gently cut off with spatulas and the gel was placed on top of the bottom layer formed by a sponge and a piece of blotting paper. The PVDF membrane was placed then on the top of the gel and a roller was used to remove all the trapped bubbles. The membrane was topped by another layer of blotting paper and a sponge. The Mini Blot Module was then closed and mounted in the tank and the chamber was filled with transfer buffer and ran at 20 V for 60 minutes.

2.7.5 Antibody staining

Membranes were blocked with 5% BSA (A2153 Sigma) in TBS-Tween for 1 hour (Table 4). Membranes were probed with primary antibody overnight at 4 ^{o}C (Table 5) then washed 3 times for 5 minutes with TBS-Tween. Membranes were probed with secondary antibody for 1 hour at room temperature then washed 3 times for 5 minutes with TBS-Tween. Bound antibody was detected using Luminata Crescendo Western HRP substrate (WBLUR0500 Merck) and exposed to Hyperfilm ECL (Amersham) in a film cassette and scanned in with an Epson Perfection V700 Photo or image captured using Thermo Scientific MYECL Imager. Band intensity was quantified and normalised to actin using Image StudioTM Lite software (LI-COR).

Antibodies	**MW (kDa)**	**Manufacturer**	**Catalogue #**	**WB Conc**	**Species**
α-Tubulin	50	Thermo	MA1-19162	1 µg/mL	Mouse
Vinculin	117	Milipore	MAB3574	1:1000	Mouse
P38	40	Cell Signalling	9218	1:1000	Rabbit
pTBK1/NAK	84	Cell Signalling	5483	1:1000	Rabbit
TBK1/NAK (D1B4)	84	Cell Signalling	3504	1:1000	Rabbit
p-P38 (Thr180/Tyr182)	43	Cell Signalling	4511	1:1000	Rabbit
OPTN	72	Cambridge Bioscience	HPA003360	1:1000	Rabbit

EGFP	27	Abcam	ab6556	1:1000	Rabbit
IKK gamma/NEMO	47	Abcam	ab63551	1:1000	Rabbit

List of secondary antibodies used for western blotting.

Antibodies	**Manufacturer**	**Catalogue #**	**WB Conc**
Goat Anti-Rabbit	Dako	P044801-2	1:2500
ECL Anti-mouse IgG	Amersham	NA931	1:2500

Table 2. 6 List of antibodies used for western blotting.

2.8 Confocal microscopy

22mm Coverslips from Merck (cat. # C9802) Wash in 100% methanol in the tissue culture hood, then left to dry by placing on the tissue culture plate before final wash with PBS from Gibco (cat. #10010023). Coverslips placed in each well, and add THP-1 cells ($1x10^5$ cells per well in a 6 well plate) in 1mL cell suspension of complete RPMI. Supplement RPMI medium with 140 nm/mL PMA to activate THP-1 into Macrophages then leave for 72 Hours incubated in a humidified tissue culture incubator at 37 °C, 5% CO_2. After 72 hours remove PMA containing medium and wash cells with PBS then add fresh complete medium and allow cells to rest for 4 days, incubated in a humidified tissue culture incubator at 37 °C, 5% CO_2. After 4 days Wash off any dead cells with PBS (Gibco, 10010023).

Macrophages derived from THP-1 stimulated with 100 ng/mL sLPS or 5 µg/mL MDP compared with non-stimulated conditions. After 24 hours, stimuli or non-stimuli containing medium is removed and cells are washed with PBS twice.

Fix cells in each well with 1 ml of cyto fix/perm from BD (Cat. # 554723) for 20 mins at room temp. Wash 2x 1mL PBS. Add 300 µL 0.01% Triton X-100 from Sigma (Cat. #K10700601) in PBS for 5 mins at room temp. Wash 1x 1mL PBS, then add 0.1 mg/mL of human IgG from CSL (cat. # 1765) in 0.1% BSA/PBS for 1 hour at room temperature. Wash 1x with 1 ml PBS then add 200 µl primary antibody in 0.1% BSA in PBS for 90 mins at room temperature. Wash 3x 1 ml PBS. Add 200 µl secondary antibody in 0.1%BSA in PBS for 1 hour at room temp. Secondary antibodies should be chosen based on the species of the primary antibody used and the fluorochrome. Wash 2x 1 ml PBS. Wash 3x 1 ml water and leave the water on for 5 mins before removing the coverslip from the well to remove all the salts, which will crystallise when the coverslips dry. Remove the coverslips, add 22 ul ProLong Glass Antifade Mountant from Thermo (cat. # P36980) and mounted on Superfrost Plus Microscope slides from Thermo (cat. #10417002). Slides were kept in semi-humid containers to dry for 24 hours before microscopy imaging.

Slides were imaged with a Zeiss 710 confocal microscope using a 63× oil immersion. DAPI fluorescence was excited at 350 nm and emission at 470 nm. EGFP profiles were excited at 488 nm and emission at 509 nm. Secondary antibodies used stained in the red channel were excited at 556 nm and emission at 570 nm.

Antibodies	Manufacturer	Catalogue #	Working Conc	Species
TBK-1	Cell Signalling	3504	1:500	Rabbit
pTBK-1	Cell Signalling	5483	1:500	Rabbit
RIPK-2	INSIGHT	PA1861	1:500	Rabbit
Goat anti-rabbit Alexa Fluor™ 546	Thermo	A-11035	1:1000	Goat

Table 2. 7 list of antibodies used to stain cells for imaging.

2.9 Mass spectrometry

For liquid chromatography-tandem mass spectrometry (LC-MS/MS) analysis, whole protein lysates were analysed under reducing conditions and samples were labelled using the TMTsixplex™ Isobaric Label Reagent Set (90061 Thermo Fisher Scientific).

2.10 fluorescence assisted cell sorting (FACS).

Positive EGFP-expressing cells were sorted using a BD FACSAria™ III Sorter by Mr James Evans (Division of Medicine, UCL). Cells were sorted based on viability (size and DAPI) and expression of EGFP to isolate single cell clones (figure 4.11). Single cells were then expanded by growing at 37 ^{o}C 5 % CO_2 for 1-2 weeks.

Needed materials:

- 1% FBS in PBS
- 5 ml round bottom tubes with cell-strainer cap
- 5 ml round bottom tubes (semi-clear 12x75mm)
- 1.5ML EPPENDORF TUBES from Starlabs (Cat# S1615-5510)
- cRPMI 1640 with selection AB (10 µg/ml G418)
- Icebox
- 96 well plate with U-shaped bottom X4
- Blue live/ dead kit (light sensitive read @ 450/50 nm) from ThermoFisher (Cat# L23105)

1. Remove cells from the incubator into regular cell culture hood.
2. Add 200ul of cRPMI 1640 plus selection AB in 96 well plate and incubate @ 37 ^{0}C.
3. Add 2.5 ml of cRPMI 1640 to the clear 5 ml round bottom ones and move it to be at RT for collection of remaining EGFP expressing cells.
4. Remove supernatant and plate for 6 well plate add 1 X 10^{6} cells/ well, spin down re-suspend in 1 ml (1% FBS in PBS).
5. If cell counting is done, wash once with PBS after resuspension of cells, spin down @ 1000 G for 3 min, then resuspend using 1% FBS in PBS @ 1 million cells in 1 ml.
6. Add 1 µl (per 1 ml sample) of LIVE/DEAD™ Fixable Blue Dead Cell Stain Kit for UV excitation kit and MIX THE content with a side-to-side movement.
7. Incubate in the dark for 20-30 min.
8. Take the 1.5ml Eppendorf and spin it down, remove supernatant, and resuspend in 1ML 1% FBS in PBS x three times to remove the live/dead blue excess.

9. Use cell sorting tubes {label the tubes} (with blue caps, 5 ml round bottom tubes with cell-strainer cap). Add the 1 ml mix of cells + blue live/dead dye through the cap strainer.
10. Keep the tube cap open when forcing the cells through it (it will be less than 1 ml inside the tubes).
11. Keep samples on ice and vortex for 1-2 sec just before the sort is done.
12. FACS sorting was done by Mr Jamie Evans (Figure 4.11)

    Move sorted cells in 96 well plates in a 37oC and 5% CO_2 cell incubator for propagation, after a week or 1.5 weeks, check the wells. Transfer at least 6 different clones into a 6-well plate for further propagation. Expand a clone for each cell line and prepare cell lysates and mRNA from 10^6 cells to check for EGFP OPTN expression and DNA sequencing.

Chapter 3. Identification of a novel association between OPTN and NOD2, resulting in Ser526 phosphorylation upon MDP stimulation.

3.1 Introduction

This chapter describes generating a stable THP-1 cell line expressing EGFP-OPTN (THP-1^{OPTN}) and phosphoproteomic analysis of OPTN after NOD2 and TLR4 activation.

It has been well documented that the THP-1 cell line as monocytic cells is difficult to transiently transfect by nonviral methods[166]. This is due to their suspension culture, ability to rapidly clear any transient gene overexpression, loss of viability, extremely low transfection efficiency and/or unintentional activation and differentiation to macrophages[167]. Additionally, there is strong evidence of the ability of genetic modification using viruses on the THP-1 cell line with a high percentage of success combined with the elimination of variable gene expression and reduced laboratory work[167].

OPTN, as an adaptor protein, plays multiple roles dependant on cellular needs and cell type. In human monocytes/macrophages, OPTN is involved in vesicular trafficking and pro-inflammatory cytokines release. It has been shown previously that under-expression of OPTN in monocyte-derived macrophages generated from CD patients resulted in diminished pro-inflammatory secretion compared to healthy controls[58]. Reduced cytokine secretion contributes to the attenuated acute inflammatory response previously identified in CD, leading to delayed bacterial clearance and the formation of chronic granulomatous inflammation. A detailed understanding of the mechanisms associated with OPTN and its anti-bacterial immune function is still unavailable. It was

therefore decided to generate a stable EGFP-OPTN reporter human monocytic cell line to help elucidate the role of OPTN in bacterial immunity.

3.1.1 NOD2 and TLRs stimulation activates OPTN gene expression and increases intracellular protein expression.

NOD2 responds to bacterial peptidoglycan by stimulating pro-inflammatory cytokines release. In healthy individuals, upon bacterial invasion, NOD2 activation initiates NFkB signalling resulting in the upregulation of pro-inflammatory cytokines and a host of other genes. In CD patients, NOD2 polymorphisms contribute to hindered pro-inflammatory release, which may cause innate immunity failure to respond to bacterial invasion[57]. NOD2 activation through binding its ligand MDP results in the upregulation of OPTN both transcriptionally and at the protein level (Figure 3.1). In addition, stimulation of TLR2 (Pam_3), TLR4 (LPS) and whole heat-killed E. coli (HkEc) can also upregulate OPTN (Figure 3.1). This upregulation is indicative of OPTN's role in immune activation leading to initiation of pro-inflammatory release or OPTN recruitment for its role in autophagy[55].

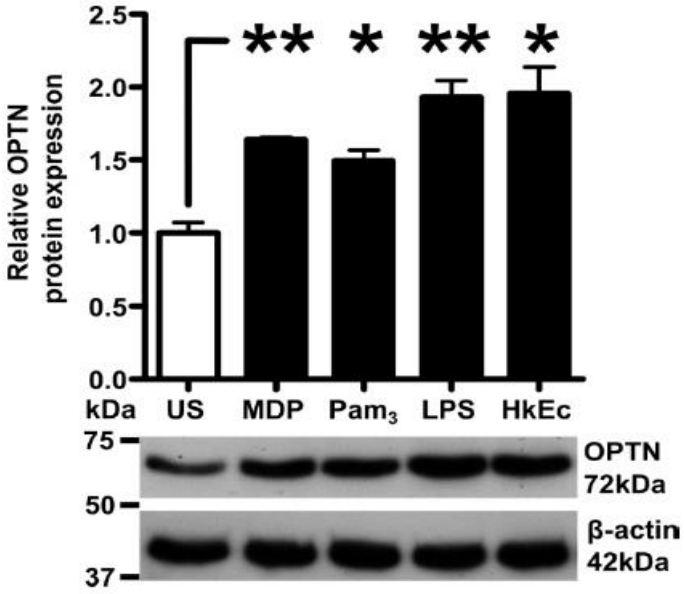

Figure 3. 1 OPTN expression levels in THP-1 cells downstream of NOD2 (MDP), TLR2 (Pam_3), TLR4 (LPS) and whole bacteria (HkEc) stimulation.

Immune activation for 24 hours with bacteria and bacterial ligands resulted in upregulation in OPTN protein. *p<0.05 & **p<0.01. Data were taken from JI 2011 186(7):4027.

3.2 Results

3.2.1 Initial verification of the EGFP-OPTN plasmid

The original EGFP-OPTN pLIXN vector (total size 8,626 bp) was obtained from Prof. Folma Buss, University of Cambridge University (Figure 3.2). Sanger sequencing confirmed the sequence (see methodology 2.6.5) using the primers listed in Table 3.1. Plasmid functionality was tested through transient transfection into the THP-1 cell line (section 2.6.6).

Transfected cells were incubated at 37°C 5% CO_2 for 24 hours and then visualised on a fluorescent Axio vert—A1 microscope (Zeiss, Germany) to confirm EGFP OPTN expression (Figure 3.3). In addition, cell lysates were prepared using RIPA lysis buffer (Cat# 89900) and protein lysate was quantified using BSA assay and normalised to 10 mg/ml. EGFP-OPTN transfected THP-1 lysates were run on a 10% SDS-PAGE gel, transferred to PVDF (methodology see 2.7) and probed with anti-OPTN and anti_GFP antibodies (Figure 3.4) to confirm expression and correct molecular weight of EGFP OPTN protein.

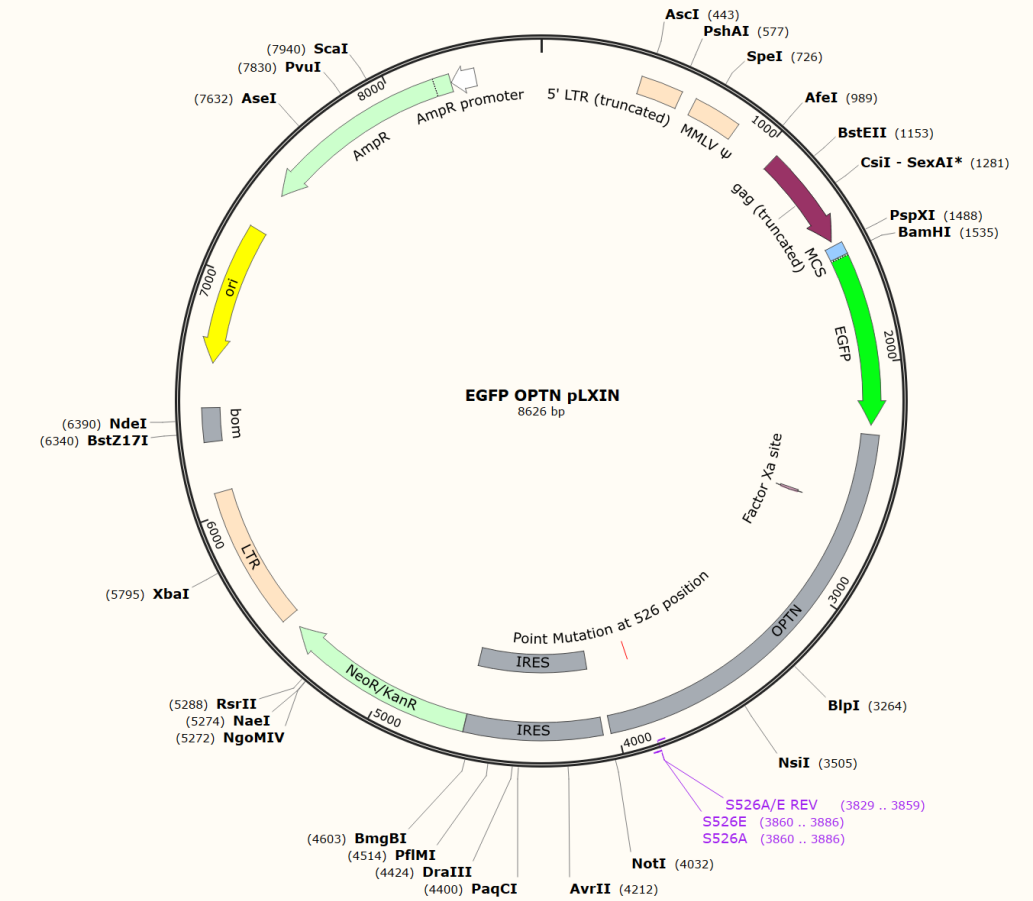

Figure 3. 2 Map for plasmid EGFP OPTN pLXIN.

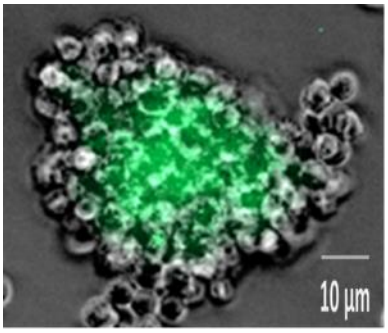

Figure 3. 3 Images of THP-1 Cell lines expressing EGFP OPTN under inverted microscopy X10 magnification, Original EGFP OPTN pLIXN.

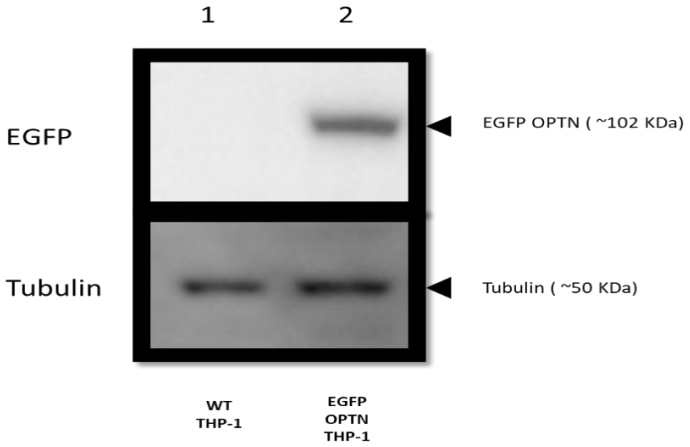

Figure 3. 4 Immunoblot showing EGFP OPTN at 102 kDa expression vs WT THP-1 cell lines.

Primers were designed with Clontech online Primer design tool and ordered from Merck.

OPTN SEQ F	5’-TGAAAGAGCAGCGAGAGAGA
OPTN SEQ R	5’-CTTGGGGCAGGAATGAATCG

Table 3. 1 Primer designs for OPTN sequencing.

3.2.2 Production of intact retroviral particles that encode EGFP-OPTN

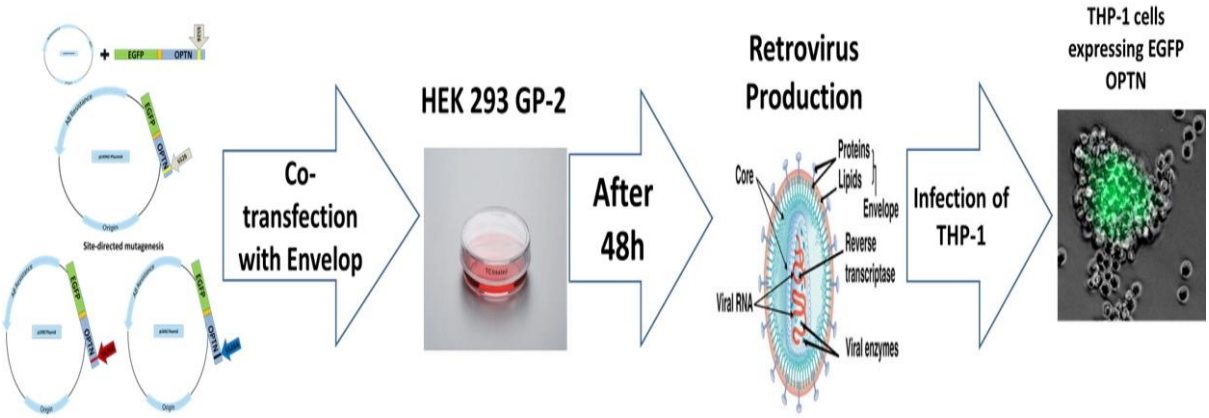

Figure 3. 5 Generalised flow chart of stable cell lines generation.

Using both a pLXIN containing EGFP OPTN construct and an envelope plasmid to transiently transfect the packaging cell line HEK-293 GP2 results in retroviral production. The mature retrovirus containing the pLXIN-EGFP-OPTN construct is released into the supernatant. The viral-containing supernatant is then used to infect THP-1 cells, resulting in the generation of a stable cell line expressing EGFP OPTN or one of its mutant variants.

To produce the virus encoding EGFP OPTN, we used Takara HEK 293 GP-2 packaging cell line (Takara, Cat# 631,458), which contains the viral genes *gag* and *pol* essential for retroviral production. This cell line only requires the supplement of the viral envelop gene (env) to be co-transfected to produce viruses. We used an MMLV expression vector in our plasmids and added pVSV-G as an envelope to make viruses with EGFP OPTN DNA code in HEK 293 GP-2 cells. We got the enveloped plasmid pVSV-G from Takara in a Retro-X Universal vector Set (see section 2.6.7).

cDNA synthesised from viral RNA is then sequenced using OPTN CON F/R primers according to the same protocol used for sequencing of Mix2Seq Kit (Section 3.2.1).

3.2.3 Generation and verification of the stable THP-1 $^{EGFP\ OPTN}$ cell line

WT THP-1 cells were grown in RPMI 1640 supplemented with 10%FBS, 2% HEPES and 50 mM 2Mercaptoethanol in a T25 flask at $1X10^5$ cells/ml in 10 ml. The THP-1 were transferred to a 15 ml falcon tube, and 1 ml of viral supernatant was added, plus 4 µg/ml Polybrene from Millipore (Cat# TR-1003-G). The mixture was then centrifuged at 500 g for 90min at room temp. After centrifugation, the resuspend cell pellet and viral supernatant was added to a T25 flask and incubated at 32°C 5% CO_2 for 24 hours. After 24h incubation, the viral supernatant was replaced with RPMI 1640 supplemented with 10% FBS, 2% HEPES, 50 mM 2Mercaptoethanol and 10µg/ml G418 from Invevogen (Cat# ant-ge-1) as a selection AB. Cell media was replenished every 72h for up to 2 weeks. Cells are monitored over the two-week period for signs of EGFP expression using a fluorescent microscope and for viability. Look at section 2.10 for the FACS protocol.

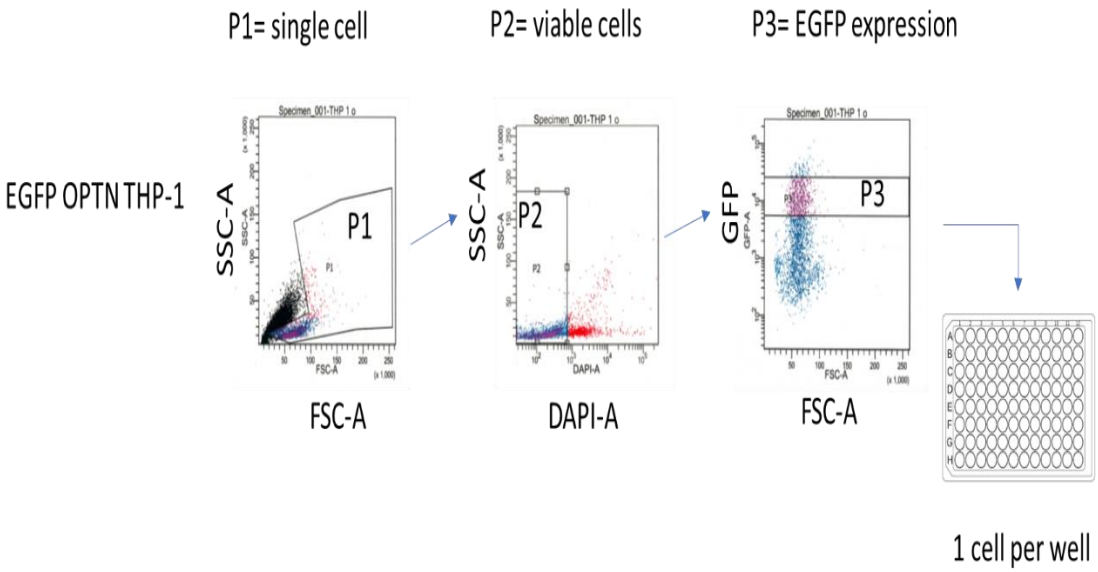

Figure 3. 6 FACS sorting of EGFP expressing THP-1 cells. FACS gating strategy used to isolate viable EGFP positive cells.

Cell lysates extracted from WT THP-1 and THP $^{EGFP\ OPTN}$ cells were probed by western blotting for GFP and OPTN. Cells (10^6 cells) were lysed in RIPA buffer and run on SDS-PAGE NuPAGE™ 4-12% Bis-Tris Protein Gels, 1.0 mm, 15-well from Thermo (Cat# NP0323BOX). Each sample had 15 µg total protein loaded and blotted against anti-OPTN (Sigma (Cat# HPA003360) at 1:2500 and secondary Anti-Rabbit-HRP (Dako (Cat# P044801-2) at 1:10000. Anti-tubulin at 1:10000 dilution was used as a loading control. Bands at 102 KDa represent EGFP OPTN, seen with both the anti-GFP and anti-OPTN antibodies, confirming the expression of the virally transfected protein constructs (Figure 3.6). As expected, the WT THP-1 cells expressed only the native 72 kDa OPTN, and the loading controls demonstrated even loading between samples.

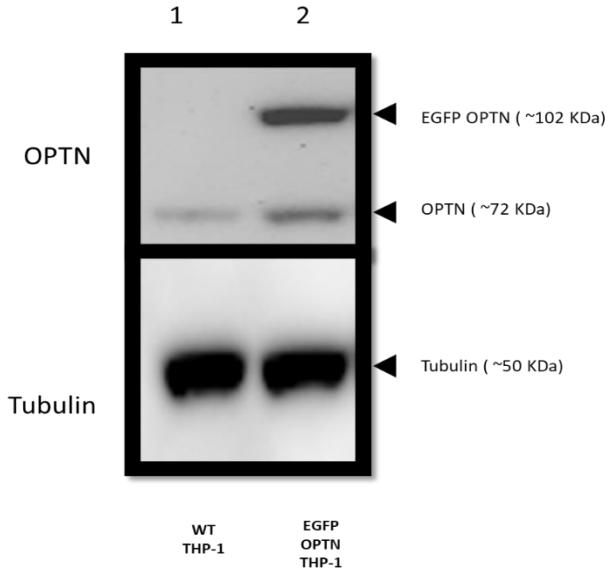

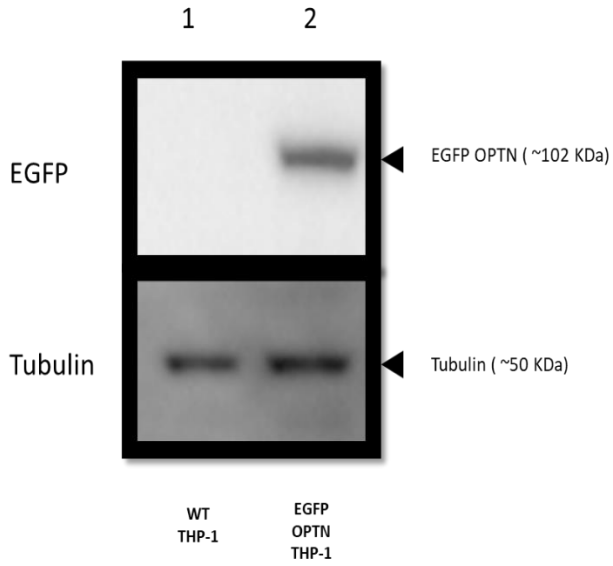

Figure 3. 7 Immunoblot of 1) WT THP-1, 2) THP-1 $^{EGFP\ OPTN}$ whole cell protein lysates against anti-GFP, anti-OPTN and anti- tubulin.

3.2.4 EGFP OPTN Immunoprecipitation and Mass spectrometry results.

EGFP OPTN protein was isolated using a high-affinity single-domain antibody (sdAb) that is covalently immobilised agarose beads (nano-beads) from NanoTag biotechnology (Cat# N0310) from whole THP-1 $^{EGFP\ OPTN}$ lysate. Cell lysates were generated in either an unstimulated state or after 24 hours of TLR4 (500 ng/mL LPS) or NOD2 (10 µg/mL) activation with their specific ligands. RIPA buffer was used as lysis and washing buffer for nano-beads, and Tris-buffered saline was also used in the last washing step. The native cell lysate was clarified by centrifuging at 10000 g for 10 min. The clear lysate was carefully removed into 1 mL Eppendorf tube, and 50 µL collected as input fraction. 20 µl of Beads were washed with

1 mL of RIPA buffer twice before usage. Then the wash buffer was removed, and clarified lysate was added to beads and incubated for one hour at 4 °C with head-over-tail rotation. Beads were then sedimented by centrifuging at 1000 g for 1 minute, and 50 µL collected from lysate as a non-bound fraction remaining lysate was discarded. Beads were then washed twice with RIPA buffer and a final wash with TBS. Each washing step required the sedimentation of beads by centrifuging at 1000 g for 1 minute. The final bound fraction of lysate per sample is made with 50 µL of 2x SDS sample buffer—verification of successful pull-down made with Immunoblot against EGFP antibodies (Figure 3.8).

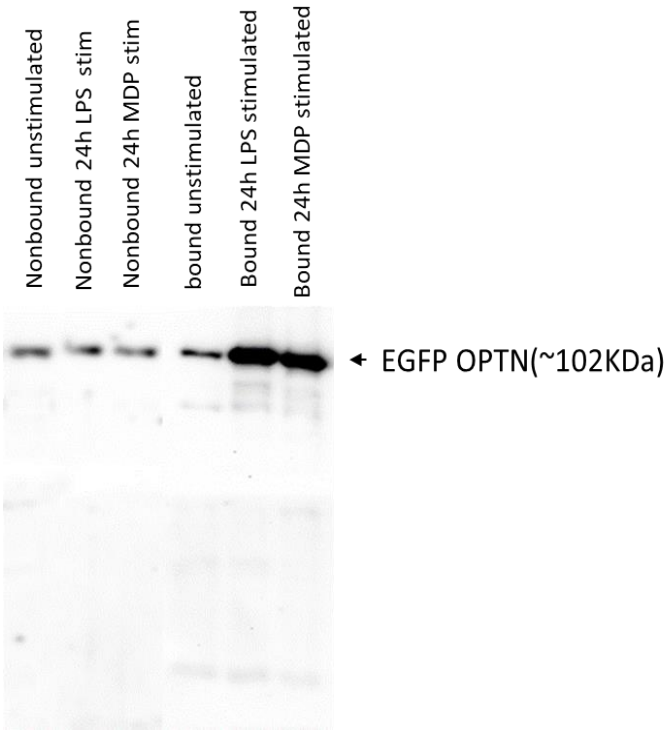

Figure 3. 8 Immunoblot of THP-1 $^{EGFP\ OPTN}$ cell lysate against EGFP antibody.

Comparison between non-bound and bound fractions. Lanes 1) Non-Bound fraction unstimulated THP-1 $^{EGFP\ OPTN}$, 2) Non-Bound fraction of 24 hours LPS stimulated THP-1 $^{EGFP\ OPTN}$, 3) Non-bound fraction of 24 hours MDP stimulated THP-1 $^{EGFP\ OPTN}$, 4) Bound fraction of unstimulated THP-1 $^{EGFP\ OPTN}$, 5) bound fraction of 24 hours LPS stimulated THP-1 $^{EGFP\ OPTN}$, 6) bound fraction of 24 hours MDP stimulated THP-1 $^{EGFP\ OPTN}$

For Mass, spectrometry samples were run on a 10% SDS-PAGE gel, stained with Coomassie blue from Thermo (Cat# 24594) for 2 hours, and then washed in distilled water H_2O for 3 hours to eliminate background staining (Figure 3.9).

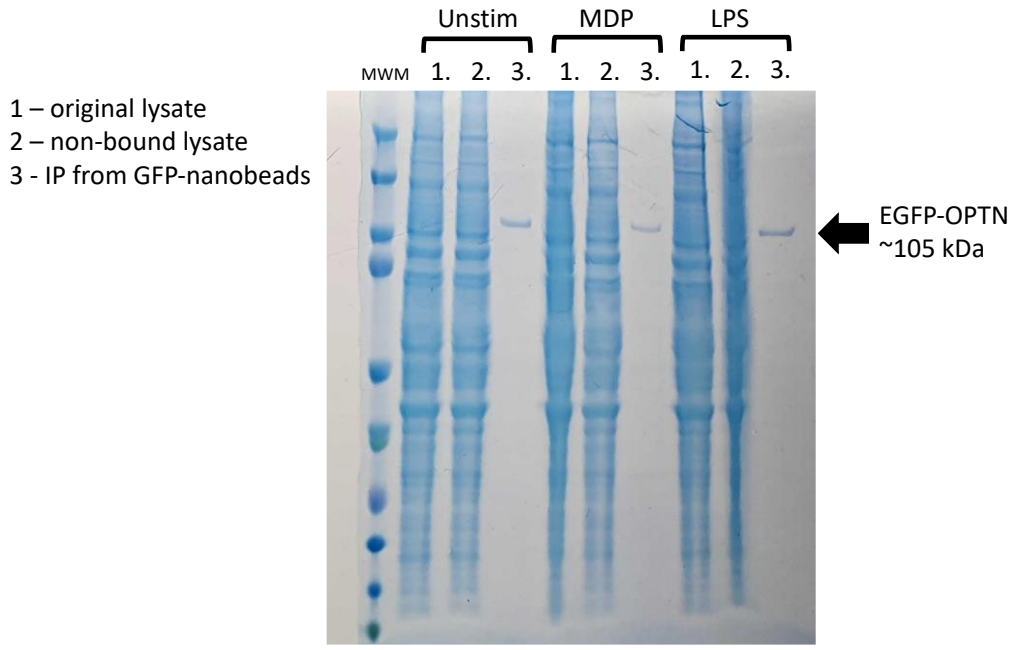

Figure 3. 9 SDS-PAGE gel stained with Coomassie Blue with all fractions run for confirmation of successful EGFP OPTN separation from the complete lysate.

On another SDS-PAGE gel, only bound fractions were run with spacing to eliminate cross-contamination from other wells. Shotgun Mass Spectrometry (see section 2.9) was performed to Identify different phosphorylation sites and attached proteins across all samples. Our results of mass spectrometry proteomics of phosphorylated peptides (see

table 3.3) revealed a novel phosphorylation site at position Ser526 downstream of NOD2 stimulation. Position Ser198 showed phosphorylation regardless of the stimulatory condition of cells.

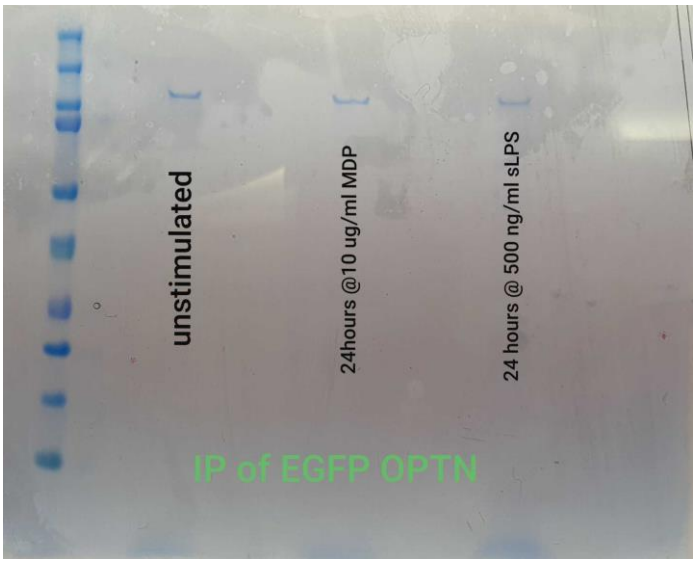

Figure 3. 10 SDS-PAGE gel stained with Coomassie blue stain containing EGFP OPTN only obtained from bound fraction of different stimulatory conditions of THP-1 $^{EGFP\ OPTN}$.

Stimuli	Mr(except)	Mr(calc)	ppm	Miss	Score	Expect	Rank	Phospho site	Peptide
Unstim	1200.5649	1200.5652	-0.26	1	29	0.45	1	Ser198	K.EIKHSPGPTR.T + Phospho_STY (STY)
LPS	1200.5658	1200.5652	0.46	1	26	0.74	1	Ser198	K.EIKHSPGPTR.T + Phospho_STY (STY)
MDP	1200.5648	1200.5652	-0.36	1	25	0.99	1	Ser198	K.EIKHSPGPTR.T + Phospho_STY (STY)
	2010.8884	2010.8909	-1.23	1	76	1.9e-05	1	Ser526	R.HGARTSDSDQQAYLVQR.G + Phospho_STY (STY)

Table 3. 2 Identification of EGFP OPTN phosphopeptides under different conditions using Shot gun Proteomics.

3.2.5 Verification of OPTN phosphorylation downstream NOD2 activation

Identifying a NOD2 inducible phosphorylation site on OPTN was a novel finding to our knowledge. The phosphorylation site Ser526 is listed on Uniprot (https://www.uniprot.org/uniprotkb/Q96CV9/entry), but no information is available on this site. To verify this phosphorylation event downstream of NOD2, I worked with Dr Julio Martinez-Torres, a postdoc in the lab. WT THP-1 cells were genetically modified by Dr Martinez-Torres using CRISPR-based gene editing to knockout NOD2 and create a THP-1$^{NOD2-/-}$ cell line. The loss in NOD2 expression was confirmed through the inability to upregulate TNFα at both protein and mRNA levels upon MDP stimulation (see figure 3.11).

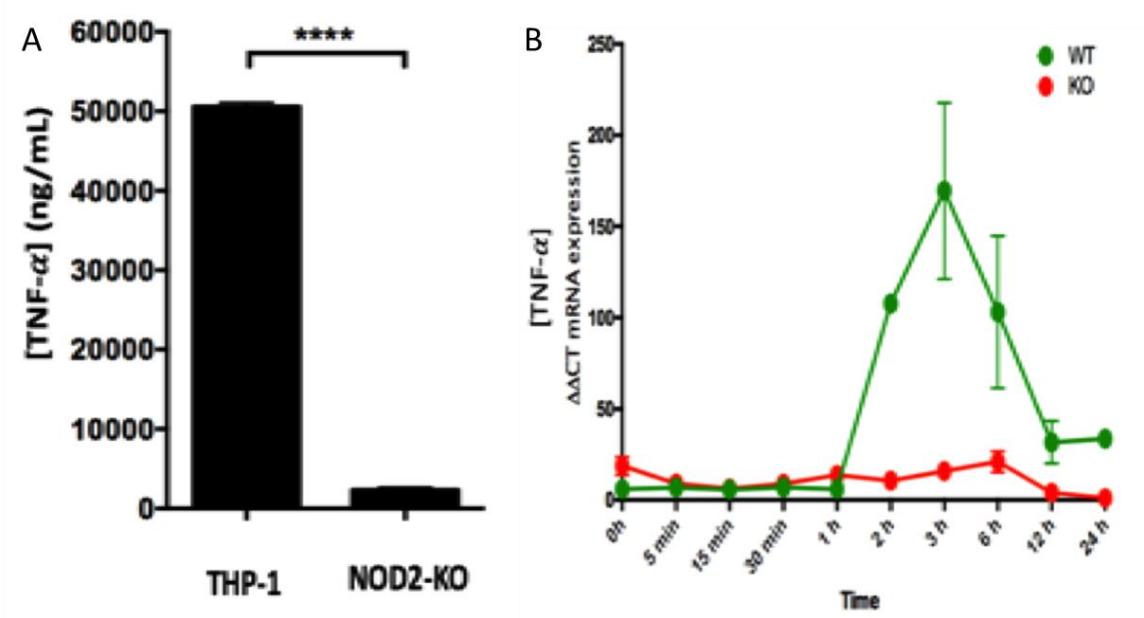

Figure 3. 11 Effective CRISPER based gene editing of NOD2 in THP-1.

A) ELISA analysis of TNF-α after MDP stimulation in THP-1 and THP-1 $^{NOD2-/-}$ cells. Cells were stimulated with MDP (10µg/mL), and levels of TNF- α in the supernatant were measured 24h later. N=3 and ****p<0.0001. B) Time course of gene expression after MDP stimulation in WT THP-1(Green) and THP-1 $^{NOD2-/-}$ (Red). mRNA levels were measured using RT-qPCR where n=3.

To identify phosphorylated proteins downstream of NOD2, we used L-D-MDP (active isomer) or L-L-MDP (inactive isomer) in combination with WT THP-1 and THP-1$^{NOD2-/-}$ cell lines (see Figure 3.12) after stimulation cells were lysed and underwent in solution tryptic digestion. After tryptic digestion, phosphoproteins were isolated using titanium dioxide (Pierce™ TiO2 Phosphopeptide Enrichment Spin Tips). In addition, eluted phosphopeptides were subjected to shotgun proteomics. The above experiments were performed by Dr Martinez-Torres.

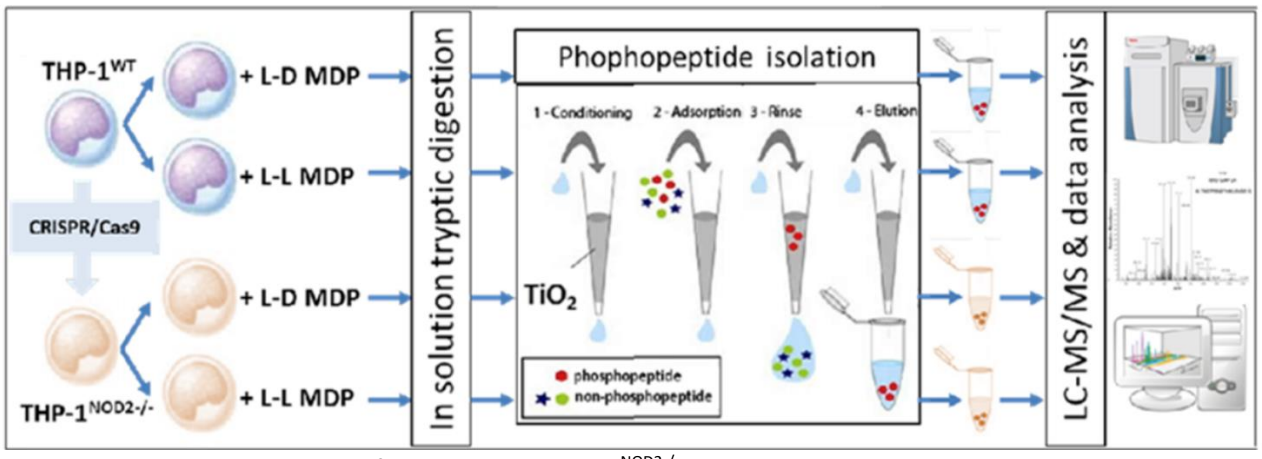

Figure 3. 12 Experimental design of WT THP-1 and THP-1 $^{NOD2-/-}$ stimulation and phosphopeptide isolation using L-D-MDP or L-L-MDP.

Phosphoproteomics results identified OPTN phosphorylation at Ser526 in WT THP-1 stimulated with L-D-MDP only, while Ser198 was present in L-L-MDP stimulated WT THP-1 (see table 3.4). These findings confirmed that OPTN is a downstream phosphorylation target in the NOD2 pathway. However, in THP-1 $^{NOD2-/-,}$ such phosphorylation was not observed at Ser526 in both versions of MDP. This indicates that Ser526 OPTN phosphorylation downstream of NOD2 is specific.

OPTN Peptide	P-value	Location in OPTN
*HGART**S**DSDQQAYLVQR*	*3.61E-06*	*Serine 526*
*EIKH**S**PGPTR*	*0.0193*	*Serine 198*

Table 3. 3 Mass spectrometry results of NOD2 downstream target OPTN phosphorylation.

OPTN Phosphopeptides identified in WT THP-1 treated with L-D MDP compared to L-L MDP and THP-1 NOD2-/- treated with L-D and L-L MDP. Significance p<0.01

3.3 Conclusion from phosphorylation work on OPTN

Our laboratory produced two different experimental designs testing OPTN's relation to NOD2 and verified this link connecting NOD2 activation and OPTN Ser526 phosphorylation. The lack of Ser177, 473 and 513 in THP-1 cells stimulated with MDP, or LPS could be because these are all TBK-1 target sites, and it has been shown that TBK1-mediated phosphorylation of OPTN is locally restricted to mitochondria[168]. Evidence of identified phosphorylation sites (Figure 3.13) in OPTN details discussed in Table 3.5, function or kinase related to Ser526 in literature, is still unclear. Although we established the connection between NOD2 and OPTN, it is still unclear what kinase is involved in OPTN phosphorylation. Evidence indicating upregulation of the OPTN gene but not the closely related p62/NDP52 genes upon MDP activation of NOD2 in myeloid cells of Crohn's patients seems to suggest a specific link between OPTN and NOD2[169]. It is possible that S526 has a regulatory effect on the UBAN domain of OPTN. In the dephosphorylation state, it can bind to a ubiquitinated target (RIPK2) and, through CYLD, de-ubiquitinate RIPK2, switching off the TNFR1 signalling.

Once phosphorylated after NOD2 activation, the OPTN UBAN site is blocked, and therefore, RIPK2 stays ubiquitinated and active. It is reported that an X-linked Inhibitor of Apoptosis (XIAP) is required to ubiquitinate RIPK2 downstream NOD2 activation, while cellular Inhibitors of Apoptosis (cIAP1/2) are dispensable for such activation[170].

A recent study investigating the regulation of AXL receptor kinase (AXL) by p85β, the regulatory subunit of phosphatidylinositol 3-kinase (PI3K), resulted in identifying the OPTN S526 phosphorylation site[63]. The authors reported that increased expression of OPTN resulted in a decrease in the protein levels of AXL, which occurred via autophagic degradation. Upon p85β activation, OPTN was phosphorylated at S526, resulting in enhanced binding to AXL and subsequent degradation. The expression of the phosphor-dead $OPTN^{S526A}$ failed to associate with AXL or reduce the protein level. A similar effect was also noted for $OPTN^{S473A}$ but not the other two known OPTN phosphosites, S177A or S512A. The results demonstrate that phosphorylation at S526 does have a biological function, but the kinase responsible and the relevance outside of the ovarian cancer cell lines used in this study is unclear. Interestingly, S473, which also demonstrated an effect on AXL levels, is known to promote OPTN ubiquitin binding and could suggest that S526 acts similarly.

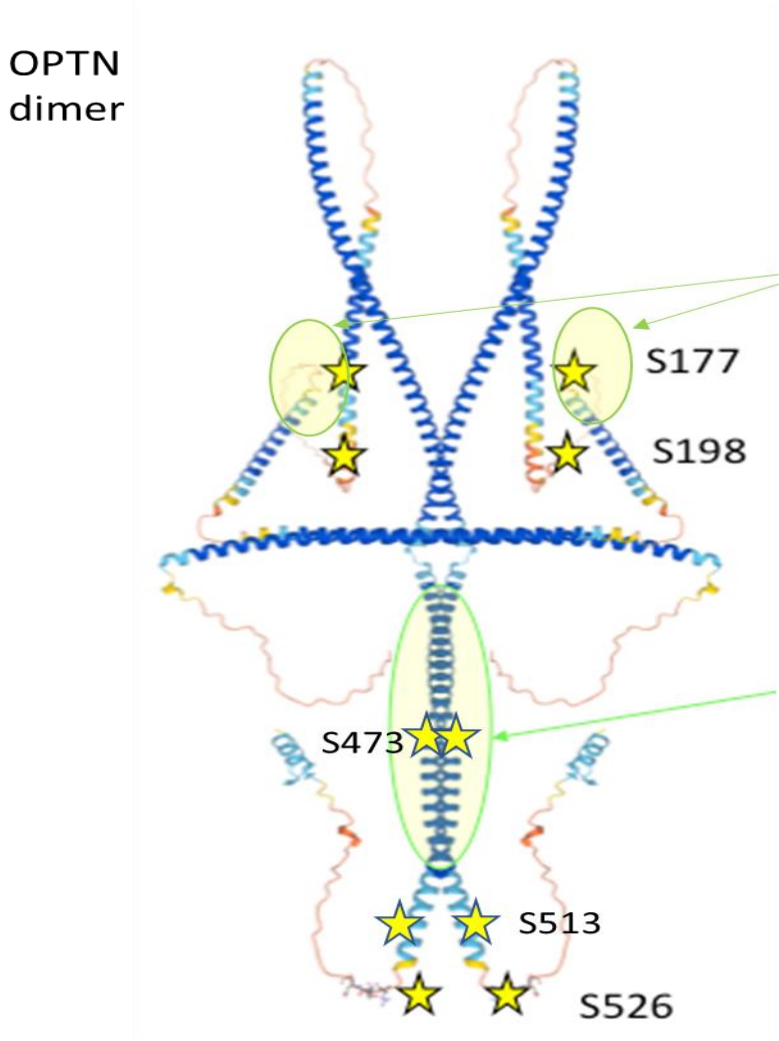

Figure 3. 13 Structural model of OPTN dimer with phosphorylation sites highlighted.

Phospho site	Kinase	Function	Ref
Ser 177	TBK-1	Strengthens the association between OPTN and LC3 during xenophagy for the eradication of intracellular bacteria	J Biol Chem. 2011 Oct 14;286(41):35663. *Science* (2011) 333(6039):228
Ser 198	TBK-1	Involved in OPTN clearance of mitophagy in ALS, mutant SOD1 sequester OPTN mitophagosomes formation	Int. J. Mol. Sci. 2020, 21, 7525. https://doi.org/10.3390/ijms21207525
Ser 473	TBK-1	Phosphorylation increased binding and promiscuous interactions with multiple Lys-linked ubiquitin chain types.	Proc Natl Acad Sci U S A. 2016 Apr 12; 113(15): 4039
Ser 513	TBK-1	It occurs on the mitochondria and participates in mitophagy	J Biol Chem. 2011 Oct 14;286(41):35663.
Ser 526	?	?	

Table 3. 4 OPTN phosphorylation sites, Kinase involved and identified functions.

Chapter 4. Generation of EGFP OPTN Ser526 phospho mutants and stable THP-1 cell lines.

4.1 Introduction

OPTN undergoes several post-translational modifications that have implications on its cellular function (see Figure 1.4/1.5. /1.6). Phosphorylation has been shown to occur downstream of TBK1 at three sites on OPTN Ser177, Ser473 and Ser513[171]. The novel NOD2 inducible phospho-site S526, identified in chapter 3, is located in a region on OPTN where neural retina-specific leucine zipper protein (NRL) and two viral proteins Tax1 and E3-14.7K have been predicted to interact (Figure 1.4). NRL expression is restricted to the retina and not expressed in THP-1 cells. Tax1 is a transcriptional transactivator of virus replication and induces the expression of various cellular genes via the activation of the NF-κB and CREB/ATF pathways[172]. The adenovirus E3-14.7K protein is recruited to TNF-receptor 1 and inhibits STAT1 function by preventing phosphorylation and nuclear translocation[173]. The functional consequence of Ser526 phosphorylation and impact on the NOD2 immune response has not been previously investigated. In order to address these questions, site directed mutagenesis was used to generate two OPTN mutants and retrovirally transform THP-1 cells to produce stable cell lines. Ser 526 was mutated to either alanine (S526A) or glutamic acid (S526E), which results in a phospho-dead or phospho-active OPTN at amino acid position 526, respectively.

Substitution of serine to glutamic acid results in the insertion of a negatively charged amino acid that mimics a phosphorylated serine residue (Figure 4.1). Conversely,

switching serine to alanine, a hydrophobic amino acid, blocks the ability to phosphorylate the site.

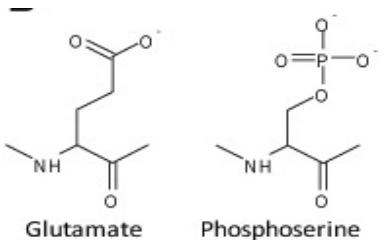

Figure 4. 1 Phosphomimetic substitution: Glutamic acid compared to phospho-serine.

This chapter describes the site-directed mutagenesis process of the pLXIN-EGFP-OPTN construct and retroviral transduction of the THP-1 cell line to generate stable cell lines expressing Ser526 phospho-dead and -active OPTN mutants. It has been well documented that the monocytic THP-1 cell line is difficult to transiently transfect by nonviral methods[166]. This is predominately due to their extremely low transfection efficiency and unintentional activation upon transfection, which initiates the monocyte to macrophage terminal differentiation[167]. In addition, there is strong evidence supporting the use of viruses to introduce stable genetic modifications in THP-1 cells, with a reportedly high percentage of success[167].

4.2 Methodology and results

4.2.1 Generation of the EGFP-OPTN^{S526A} and EGFP-OPTN^{S526E} plasmids

Point mutagenesis was performed on the original EGFP-OPTN plasmid (Figure 3.2) using Thermo scientific Phusion Site-Directed Mutagenesis Kit (Cat. F-541) (Figure 4.3). Both sets of primers were designed according to the kit's specifications. The forward primers included the desired mutation, resulting in the S – A and S – E conversion at amino acid position 526 in OPTN (Figure 4.4). In addition the primers were phosphorylated at the 5' end (Table 4.1) in order to protect the PCR product from DpnI digestion, which is used to destroy template plasmid DNA. Initially, a temperature gradient PCR was performed to identify the optimal annealing temperature (Tm) for both sets of primers. The Tm for primers of S526A had 68.1 ^{0}C /Primers of S526E had 62.3 ^{0}C, and the PCR components and final protocol for a 50 µl reaction are listed in Table 4.2.

Primers were designed with Clontech online Primer design tool and ordered from Merck.

OPTN SEQ F	5’-TGAAAGAGCAGCGAGAGAGA
OPTN SEQ R	5’-CTTGGGGCAGGAATGAATCG
OPTN CON F	5’- TTAACGTCGACCTCGAGC
OPTN CON R	5’- GGCCAGTAACGTTAGGGG
S526A	5’-[PHOS]GGGGCGAGAACAGCTGACTCTGACCAG
S526E	5’-[PHOS]GGGGCGAGAACAGAGGACTCTGACCAG
S526A/E REV	5’-[PHOS]ATGACGACTCTGCATCTCCATCAAGGACTGC

Table 4. 1 Primer designs for OPTN sequencing, point mutagenesis and sequence confirmation after mutation introduction.

Volume	Component
1µl	EGFP OPTN pLXIN DNA template (@60ng/ µl)
2µl	Forward primer
2µl	Reverse primer
10µl	5X Phusion HF Buffer
1µl	10mM dNTPs
34µl	H_2O
50 µl	Total volume

Table 4. 2 for PCR reaction of site directed mutagenesis on EGFP OPTN pLIXN for a 50 µl volume.

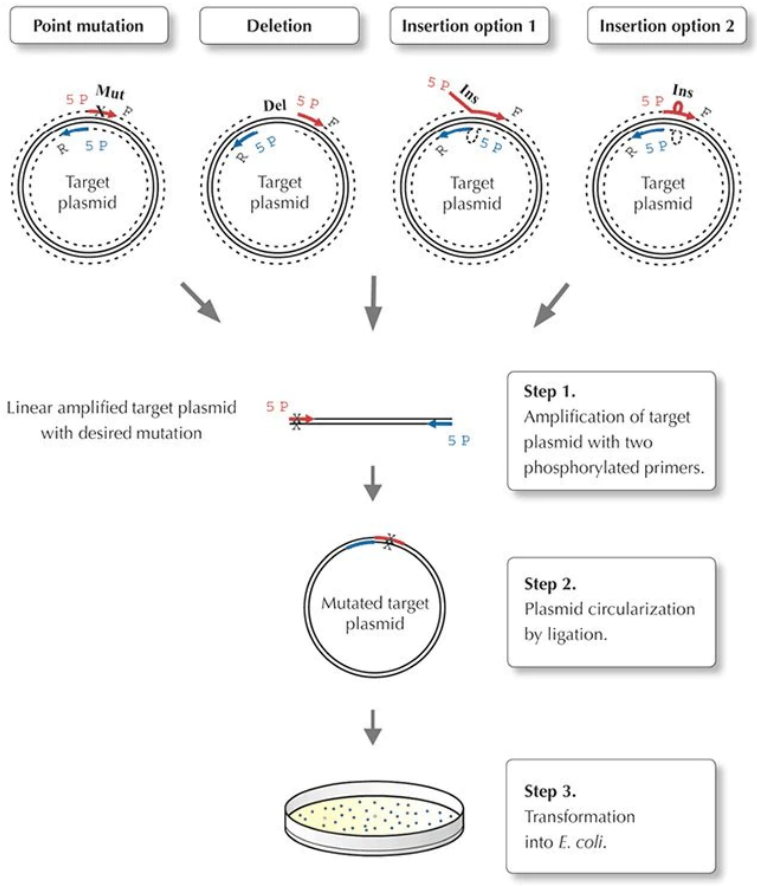

Figure 4. 2 Folw chart diagram for Phusion Site-Directed Mutagenesis Kit.

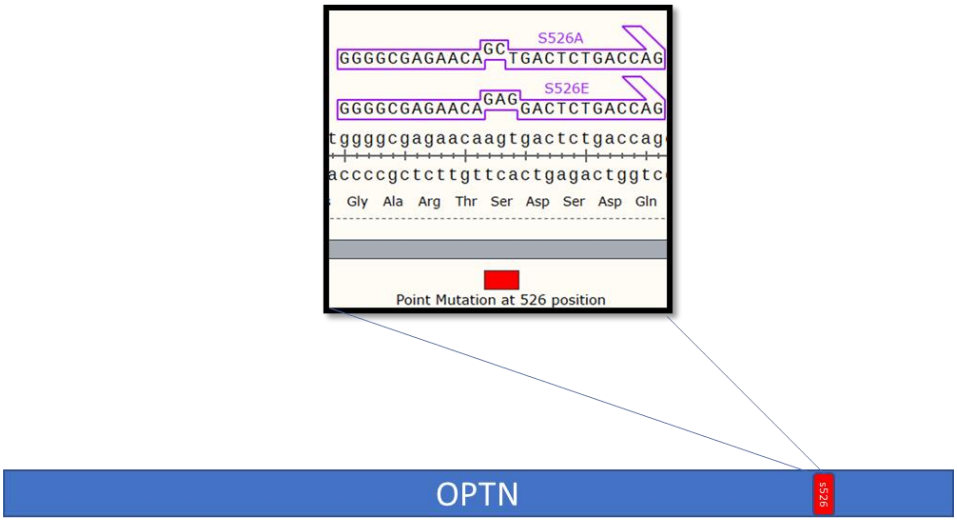

.

Figure 4. 3 Sequence of WT OPTN and position of Ser526 with primers designed for the point mutations serine to alanine (S526A) and Serine to glutamic acid (S526E).

The PCR reaction was run in Bio-Rad thermal Cycler T100 following the conditions listed in tables 4.3 and 4.4 for both S526A OPTN and S526E, OPTN respectively.

Cycle step	Temp.	Time	Number of cycles
Initial Denaturation	98 ^{0}C	30 s	1
Denaturation Annealing Extension	98 ^{0}C 68.1 ^{0}C 72 ^{0}C	10 s 30 s 4.5 min	25
Final extension	72 ^{0}C 4 ^{0}C	10 min Hold	1

Table 4. 3 PCR reaction setting for S526A site directed mutagenesis of EGFP OPTN pLXIN.

Cycle step	Temp.	Time	Number of cycles
Initial Denaturation	98 ^{0}C	30 s	1
Denaturation Annealing Extension	98 ^{0}C 62.3 ^{0}C 72 ^{0}C	10 s 30 s 4.5 min	25
Final extension	72 ^{0}C 4 ^{0}C	10 min Hold	1

Table 4. 4 PCR reaction setting for S526E site directed mutagenesis of EGFP OPTN pLXIN.

After the PCR reaction, products were run on 1% Agarose gel with TAE buffer supplemented with 10 µl of ethidium bromide at 70 V for 30 mintues. Samples were supplemented with 1 µl Quick-Load purple, no SDS (NEW ENGLAND BioLabs (NEB)) for every 5 µl. PCR products plus the original DNA template at 200 ng /µl were run on the gel. As expected, the two PCR products were equal in size to the original DNA template (8626 bp). The original construct was run without being opened by restriction digest. Therefore it produced multiple bands on the gel corresponding to open circle and supercoiled configurations that run higher and lower than the true size of agarose gels respectively (figure 4.4).

Although PCR yield was minimal, DpnI digest was performed to eliminate parental plasmid DNA. DpnI digestion was done by adding 1 µl of FastDigest DpnI enzyme to PCR product at 37 ^{0}C for 15 minutes with no inactivation after digestion.

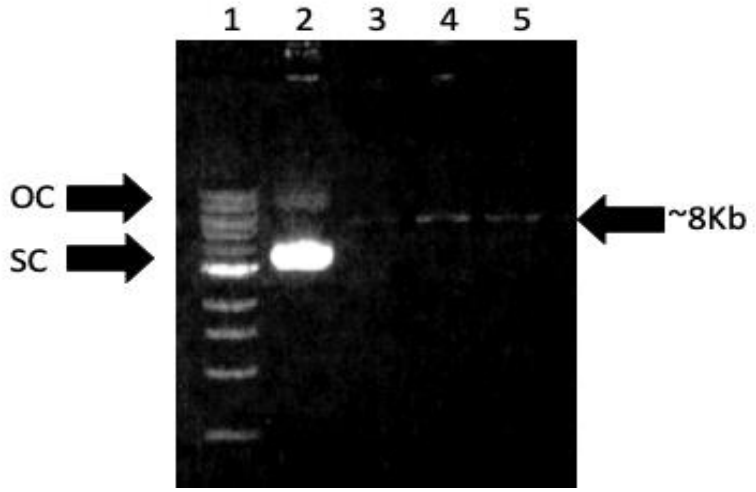

Figure 4. 4 1% Agarose gel image of Site Directed Mutagenesis PCR product run against the NEB 1 Kb Ladder

Lane 1	Lane 2	Lane 3	Lane 4	Lane 5
NEB 1 Kb Ladder	EGFP OPTN pLXIN Uncut	Blank	S526A PCR product (5 µl of total Vol.)	S526E PCR product (5 µl of total Vol.)

and original EGFP OPTN pLXIN DNA. OC = open circular construct, SC = supercoiled construct

After DpnI Digest, PCR samples were quantified using a NanoDrop 1000 Spectrophotometer (Thermo Scientific). This resulted in the generation of 316.7 ng/µl and 288.2 ng/µl of the S526A and S526E mutant PCR products. The linear PCR products were then circularised using T4 DNA Ligase.

Each PCR product after DpnI digestion was diluted with DNase-free H_2O to a final concentration of 20 ng/µl. The PCR products were then ligated in a reaction volume of 10 µl according to table 4.5. Ligation reactions were incubated at 25 ^{0}C for 5 minutes in Thermal Cycler and then chilled on ice for a minute. The newly synthesised plasmid is then heat shock transformed into competent cells (section 2.6.7).

Volume	Component
1 µl	PCR Product (20 ng/µl)
2 µl	5X Rapid Ligation Buffer
6 µl	RNase free H_2O
1 µl	T4 DNA Ligase

Table 4. 5 T4 Ligation reaction of linearised PCR products.

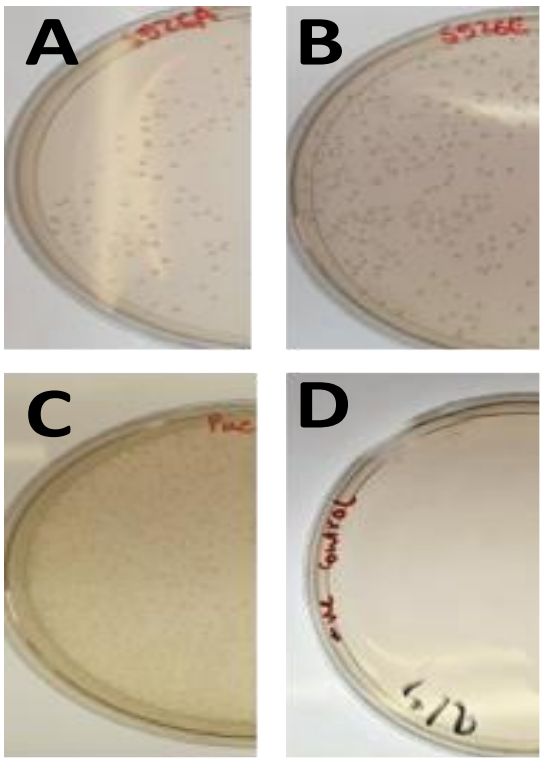

Figure 4. 5 Images of LB Agar - Amp plates after 24 hours incubation at 37 ^{o}C.

A) S526A EGFP-OPTN, B) S526E EGFP-OPTN, C) Puc-19, positive control, D) Negative control

Five bacterial colonies were picked from both S526A and S526E OPTN plates (figure 4.5) and grown in 5 ml of Luria Broth (LB) medium supplemented with 100 µg/ml Ampicillin in 15 ml falcon tube incubated in a bacterial incubator at 37 °C and shaken at 225 RPM for 18 hours. Next day, 0.5 ml of bacterial culture growth was used to make glycerol stock by adding 0.5 ml of glycerol to make an 80% (W/V) glycerol solution. Glycerol stocks were stored in a – 80 °C freezer. The remaining 4.5 ml was used to extract plasmid DNA using Monarch® Plasmid Miniprep Kit (T010L). All samples yielded plasmid DNA which was quantified using a NanoDrop 1000 Spectrophotometer. To confirm the inclusion of S526A/S526E EGFP OPTN at the intended location with the preservation of restriction sites

(BamHI/NotI) and the integrity of the sequence of DNA, a confirmation PCR using OPTN-specific primers, a double digest restriction enzyme and DNA sequencing were used.

After testing all samples for DNA integrity, a single clone from the S526A and S526E was picked to confirm the correct insertion of the point mutations. High fidelity (HF®) restriction Enzymes BamHI HF®(Cat# R3136S) and NotI HF®(Cat#R3189S) were used in a double digest restriction assay. A total of 1 µg DNA of each S526A/S526E EGFP OPTN plasmids were combined with 20 units of each restriction enzyme and incubated for 15 minutes at 37 °C. Each restriction enzyme was used in a single digest enzyme reaction with each plasmid as a control. A double-digested fragment of 2490 bp was expected from both plasmids. To visualise the fragment and determine their size a 1% agarose gel was run (figure 4.6).

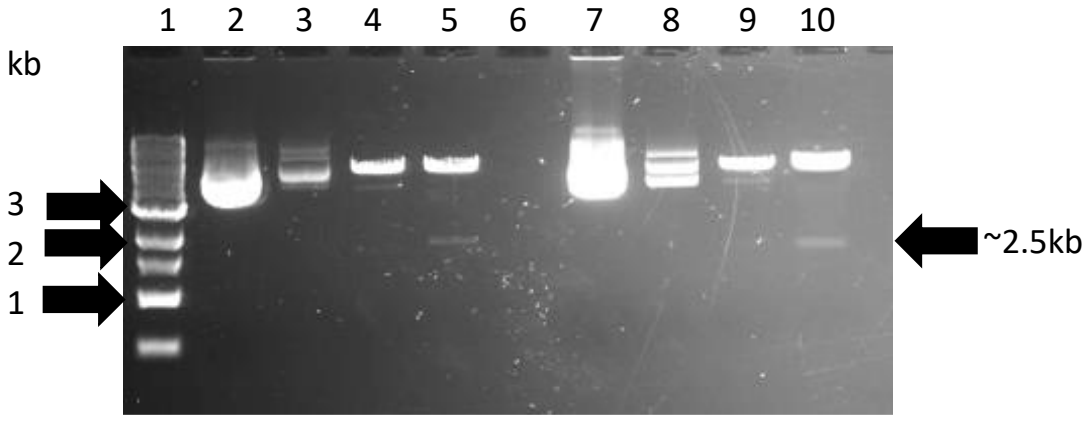

1	2	3	4	5	6	7	8	9	10
Ladder	S526A uncut	S526A BamHI	S526A NotI	S526A D.D		S526E Uncut	S526E BamHI	S526E NotI	S526E D.D

Figure 4. 6 1% Agarose gel run with plasmids DNA of S526A/S526E EGFP OPTN pLIXN either uncut or single digest or double digest according.

S526A/S526E EGFP OPTN pLIXN plasmids were sent for sequence validation using Mix2Seq Kit from Eurofins company. Each sample was sent in a separate tube and contained 1 µl of plasmid DNA (100 ng/µl), plus 1 µl of OPTN CON F or R primer at 10 µM and 15 µl RNase Free H_2O to a total volume of 17 µl. Sequence validation revealed that both samples showed an intact plasmid sequence with the desired point mutation at 526 positions (Figure 4.7).

	Alignment of sequencing results with original *EGFP-OPTN plasmid*	Chromatogram image
Sample S526A EGFP OPTN as seq 2 (EF01197705) alignment against original EGFP OPTN as seq 1	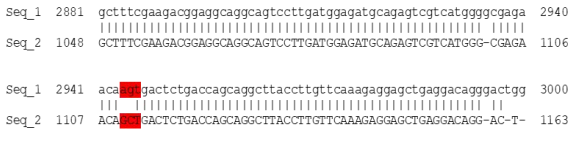	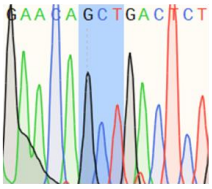
Sample S526E EGFP OPTN as seq 1 (EF01197707) alignment against original EGFP OPTN as seq 2	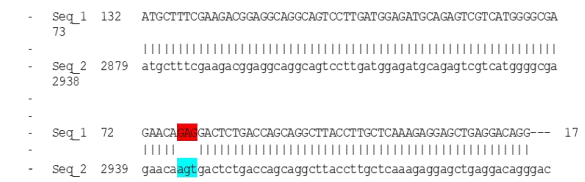	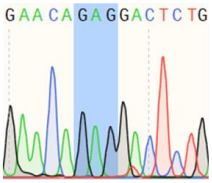

Figure 4. 7 Sequencing results of EGFP-OPTN^{S526A} and EGFP-OPTN^{S526E} plasmids aligned against the original EGFP-OPTN plasmid.

Large-scale plasmid production was performed upon confirmation of successful site directed mutagenesis. Using the previously prepared glycerol stocks, a 200 ml bacterial culture in LB medium supplemented with 100 µg/ml Ampicillin. The bacteria were grown overnight at 37 ^{o}C and 200 rpm. Bacteria were pelleted at 6000 g at 15 ^{o}C and transfection-grade plasmids were purified using Qiagen HiSpeed Maxi Kit (Cat# 12663) following the manufacturer's protocol. After extraction, plasmid concentration and purity were assessed using Nanodrop. S526A EGFP OPTN- pLXIN

had 851.8 ng/µl, and S526E EGFP OPTN- pLXIN had 757.9 ng/µl of high-purity DNA plasmid ready for transfection.

4.2.2 Verification of the expression of EGFP-OPTN^{S526A} and EGFP-OPTN^{S526E} in THP-1 cells

A transient expression of EGFP-OPTN^{S526A} and EGFP-OPTN^{S526E} pLXIN plasmids in THP-1 cells was initially performed to test for recombinant protein expression and EGFP signal. The Xfect™ Transfection Reagent was chosen to transfect the THP-1 cells as this was shown to work with the original EGFP OPTN pLXIN plasmid (Chapter 3.2.1). In this experiment, the EGFP OPTN pLXIN plasmid was used as a positive control. Each transfection reaction had 5 µg plasmid DNA in total. THP-1 cells were plated in a 6-well tissue culture plate (VWR) at 2 X 10^5 cells in 1 ml of RPMI 1640 without phenol red (Thermo Fisher, Cat# 11835063) supplemented with 1 % HEPES (Sigma, Cat# H0887), 250 µl 2-Mercaptoethanol (Thermofisher, Cat# 31350010), 10% FBS from (Sigma, Cat# F9665), 5% penicillin/streptomycin (Life Technologies, Cat# 15140-122). The transfection protocol is the same as in Section 2.6.6; reaction rations are described in Table 4.7.

	EGFP-OPTN pLXIN	EGFP-OPTN^{S526A} pLIXN	EGFP-OPTN^{S526E} pLXIN
DNA	4.2 µl @1211.6 ng/ µl	5.9 µl @851.8 ng/µl	6.6ul@757.9 ng/µl
X buffer	95.8 µl	94.1 µl	93.4 µl
X polymer	1.5 µl	1.5 µl	1.5 µl

Table 4. 6 Transient Transfection reaction rations for plasmids transfected into WT THP-1.

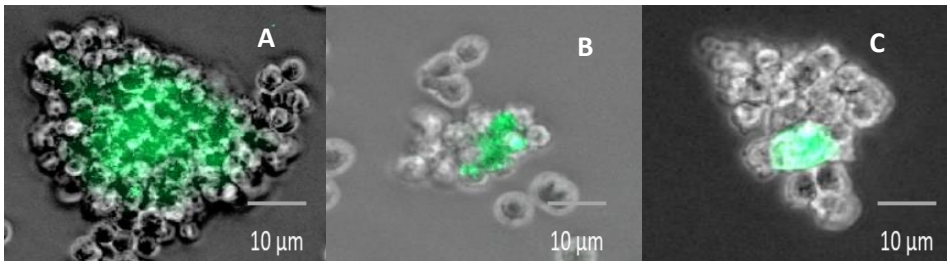

Figure 4. 8 Overlaid phase and EGFP (green) images of THP-1 Cell lines transiently expressing.

A) Original EGFP OPTN pLIXN, B) EGFP-OPTN^{S526A}, C) EGFP-OPTN^{S526E} (x20 magnification).

4.2.3 Production of intact retroviral particles that express EGFP-OPTN^{S526A} and EGFP-OPTN^{S526E}

To produce a retrovirus' that contained EGFP-OPTN^{S526A} and EGFP-OPTN^{S526E} we used Takara HEK 293 GP-2 packaging cell line (Takara, Cat# 631458). The HEK 293 GP-2 packaging cells contain the viral genes *gag* and *pol* that are essential for retroviral production. This cell line only requires the supplement of the viral envelop gene (env), which needs to deliver by transfection to produce intact viruses. We used a pVSV-G containing plasmid (Takara, Retro-X Universal vector Set (Cat# 631457)) as a viral envelope. We transfected HEK 293 GP-2 in combination with our pLXIN plasmids to manufacture viruses containing coding DNA for EGFP-OPTN^{S526A} or EGFP-OPTN^{S526E}. HEK-293 GP-2 cells were grown in a 20 cm dish (SLS, Cat#CC7862-3394) at 30-40 confluency in 10 ml of DMEM, High glucose, no phenol red from Gibco (Cat# 21063045) supplemented with 10% FBS from Sigma (Cat# F9665), 5% penicillin/streptomycin from Life Technologies (Cat# 15140-122) at cultured at 37 °C and 5% CO_2. To co-transfect either EGFP OPTN or the variants with the pVSV-G plasmids, Xfect™ Transfection Reagent was used (Table 4.8). For each plasmid, 30 µg

DNA was used combined with 30 µg DNA of envelop plasmid in a separate reaction in a 1:1 ratio. The protocol is the same as described in section 3.2.1, and the ratios are specified according to the table below:

	EGFP OPTN pLXIN	S526A EGFP OPTN pLIXN	S526E EGFP OPTN pLXIN	pVSV-G
DNA	24.8 µl @1211.6 ng/µl	35 µl @851.8 ng/µl	40 µl@757.9 ng/µl	34 µl @885.1 ng/µl
X buffer	575.2 µl	565 µl	560 µl	566 µl
X polymer	9 µl	9 µl	9 µl	9 µl

Table 4. 7 Co-transfection of pLXIN plasmids with envelop plasmid into HEK-293 GP-2 to produce viral particles.

After the transfection, the HEK-293 GP-2 cells are moved to an incubator set at 32 °C and 5% CO_2 and kept for 48 hours, after which supernatant is collected. The supernatant is centrifuged for 20 minutes at 1000 g, 4 °C to pellet any debris and finally filtered through a 0.2 µm cellulose acetate filter (VWR, Cat# 514-0061), aliquoted and stored at -80 °C. One aliquot of viral supernatant was utilised to verify the presence of the OPTN construct in the viral particles for each preparation. Viral RNA was purified using Qiagen QIAamp viral RNA Mini Kit (Cat# 52904), converted to cDNA using HotStar Taq Master Mix from Qiagen (Cat# 203445) and Anchored Oligo(dT)20 Primers from Thermo (Cat# 1257011). The cDNA was sequenced using OPTN CON F/R primers (see Section 2.6.2) and used to confirm the integrity of EGFP OPTN and variants before THP-1 cell transduction with viral medium (figure 4.9).

	Alignment of sequencing results with original *EGFP-OPTN plasmid*	Chromatogram image
Samples EF01197729 contained cDNA of S526A and OPTN CON R primer confirmed intact DNA code of S526A EGFP OPTN.		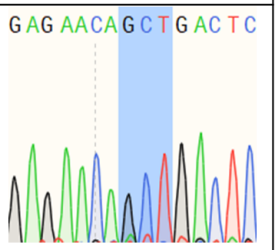
Sample EF01197721 contained cDNA of S526E and OPTN CON R primer confirming intact DNA code of S526E EGFP OPTN.		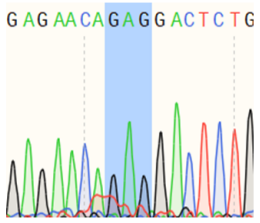

Figure 4. 9 Sequencing results of *EGFP-OPTN*^{S526A} *and EGFP-OPTN*^{S526E} cDNA synthesised from viral RNA aligned against *EGFP-OPTN plasmid* DNA.

4.2.4 Production of stable EGFP-OPTN^{S526A} and EGFP-OPTN^{S526E} expressing THP-1 cell lines.

WT THP-1 cells were grown in RPMI 1640 supplemented with 10%FBS, 2% HEPES and 50 mM 2Mercaptoethanol in a T25 flask at 1X10^5 cells/ml in 10 ml. The THP-1 were transferred to a 15 ml falcon tube, 1 ml of viral supernatant was added, and 4µg/ml Polybrene from Millipore (Cat# TR-1003-G). The mixture was then centrifuged at 500 g for 90min at room temp. After centrifugation, the resuspend cell pellet and viral supernatant was added to a T25 flask and incubated at 37°C 5% CO_2 for 24 hours. After 24h incubation, the viral supernatant was replaced with RPMI 1640 supplemented with 10% FBS, 2% HEPES, 50 mM 2Mercaptoethanol and 10µg/ml G418 from InvivoGen (Cat# ant-ge-1) as a selection AB. Cell media was

replenished every 72h for up to 2 weeks. Cells are monitored over the two-week period for signs of EGFP expression using a fluorescent microscope and for viability. Positive EGFP expressing cells were sorted using a BD FACSAria™ III Sorter by Mr James Evans (Division of Medicine, UCL). Cells were sorted based on viability (size and DAPI) and expression of EGFP to isolate single cell clones (figure 4.10). Single cells were then expanded by growing at 37 ºC 5 % CO_2 for 1-2 weeks.

The protocol for cell sorting is the same as in section 2.10.

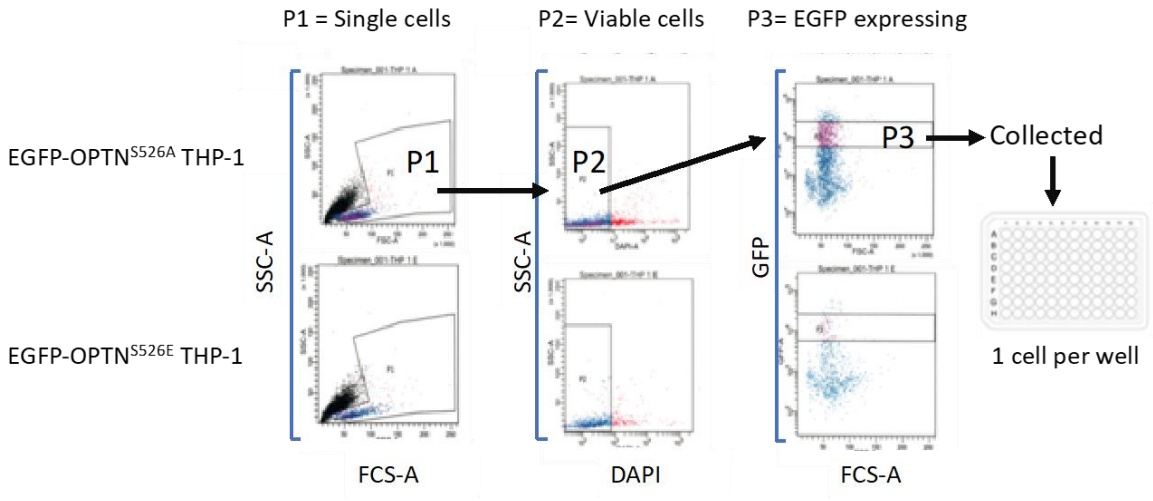

Figure 4. 10 FACS sorting of EGFP expressing THP-1 cells. FACS gating strategy used to isolate viable EGFP positive cells.

Clones chosen to be investigated for correct sequence had their RNA extracted using RNeasy plus mini kit from Qiagen (Cat# 74134). RNA was converted to cDNA (section 2.6.2) and sent to be sequenced using a Mix2Seq kit (section 2.6.5). Analysis of the sequencing results confirmed the preservation of the OPTN mutants in both EGFP-OPTN^{S526A} and EGFP-OPTN^{S526E} clones (figure 4.11).

	Alignment of sequencing results with original *EGFP-OPTN plasmid*	Chromatogram image
Samples EF01197731 contained cDNA of S526A and OPTN CON R primer confirmed intact DNA code of S526A EGFP OPTN.	OPTN1 3720 agcaactggcattgcagctggcagttctgctgaaagagaatgatgctttcgaagacggag 3779 731 1208 AGCAACTGGCATTGCAGCTGGCAGTTCTGCTGAAAGAGAATGATGCTTTCGAAGACGGAG 1267 OPTN1 3780 gcaggcagtccttgatggagatgcagagtcgtcatggggcgagaacaagtgactctgacc 3839 731 1268 GCAGGCAGTCCTTGATGGAGATGCAGAGTCGTCATGGGGCGAGAACAGCTGACTCTGACC 1327	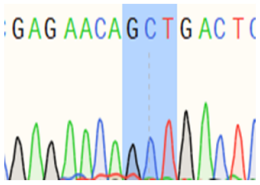
Sample EF01197725 contained cDNA of S526E and OPTN CON R primer confirming intact DNA code of S526E EGFP OPTN.	EGFP 2280 aaggagcaactggcattgcagctggcagttctgctgaaagagaatgatgctttcgaagac 725 51 ---------CTGGCATTGCAGCTGGCAGTTCTGCTGAAAGAGAATGATGCTTTCGAAGAC EGFP 2340 ggaggcaggcagtccttgatggagatgcagagtcgtcatggggcgagaacaagtgactct 725 111 GGAGGCAGGCAGTCCTTGATGGAGATGCAGAGTCGTCATGGGGCGAGAACAGAGGACTCT EGFP 2400 gaccagcaggcttaccttgttcaaagaggagctgaggacagggactggcggcaacagcgg 725 171 GACCAGCAGGCTTACCTTGTTCAAAGAGGAGCTGAGGACAGGGACTGGCGGCAACAGCGG	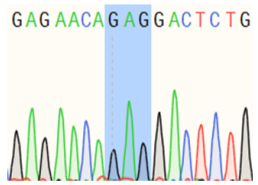

Figure 4. 11 DNA Sequencing results for the FACS sorted clones for *EGFP-OPTN*^{S526A} *and EGFP-OPTN*^{S526E}.

WB for GFP and OPTN has performed cell lysates extracted from EGFP-OPTN^{S526A} and EGFP-OPTN^{S526E} clones. Cells were lysed in RIPA buffer and run on SDS-PAGE NuPAGE™ 4-12% Bis-Tris Protein Gels, 1.0 mm, 15-well from Thermo (Cat# NP0323BOX). Each sample had 15 µg total protein loaded and blotted against anti-OPTN (Sigma (Cat# HPA003360)) at 1:2500 and secondary Anti-Rabbit-HRP (Dako (Cat# P044801-2) at 1:10000. Anti-tubulin at 1:10000 dilution was used as a loading control. Bands at 102 KDa represent EGFP OPTN, and its variants were seen in all three clones with both the anti-GFP and anti-OPTN antibodies, confirming the expression of the virally transfected protein constructs (Figure 4.12). As expected, the WT THP-1 cells expressed only the native 72 kDa OPTN, and the loading controls demonstrated even loading between samples.

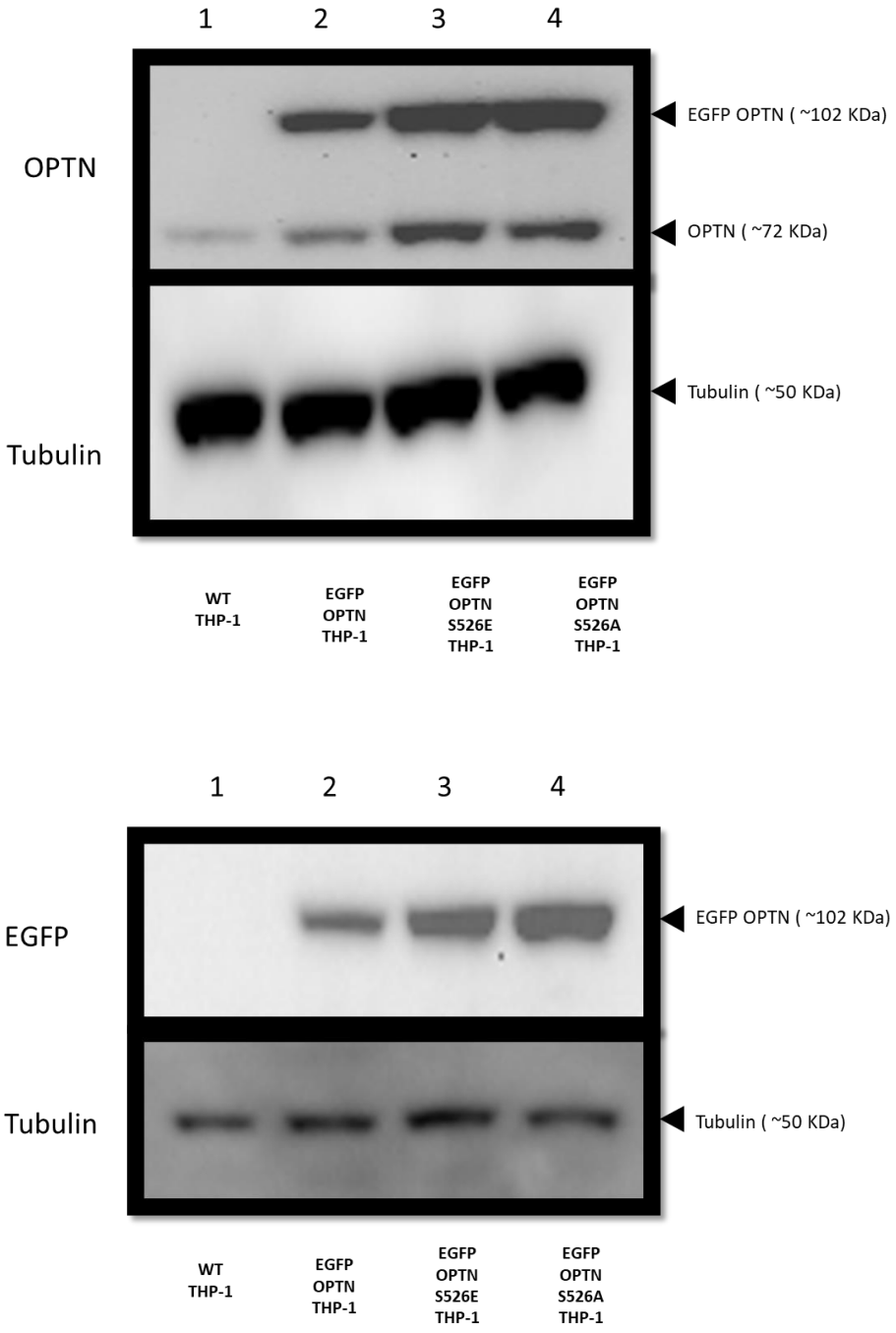

Figure 4. 12 immunoblot of (1) WT THP-1, (2) EGFP OPTN THP-1, (3) EGFP-OPTN^{S526A} THP-1 and (4) EGFP-OPTN^{S526E} THP-1 whole cell protein lysates against anti-GFP, anti-OPTN and anti- tubulin.

4.3 Conclusion

Successfully generated two THP-1 clones expressing EGFP-OPTN^{S526A} and EGFP-OPTN^{S526E}. The expression was verified by DNA sequencing, microscopy, FACS analysis and WB. The proteins folded correctly, as demonstrated by the green fluorescence, and stayed intact within the THP-1 cells, as demonstrated by WB and the single 102 kDa band. Further analysis of biological differences of clones will be tested in chapter 5 to highlight the point mutation effect on cellular functionality and the impact of Ser526 phosphorylation in OPTN and its mutated counterparts on cytokines secretion downstream NOD2 and TLR4.

Chapter 5. Functional Analysis of the novel Ser526 phosphorylation site on OPTN

5.1 Introduction

Phosphorylation of OPTN on Ser177 has previously been shown to boost poly-Ub binding and enhance IFN-β production upon TLR3 and TLR4 stimulation and also plays a crucial role in autophagosome formation[171,174]. The effects of NOD2-mediated phosphorylation of OPTN at Ser526 are currently unknown and have not been previously reported in the literature. The consequences of NOD2 stimulation on the immune response in THP-1 cells expressing either the phospho-active (EGFP-OPTN^{S526E}) or the phosphor-dead (EGFP-OPTN^{S526A}) OPTN mutants will be determined and compared against the THP-1 cells expressing WT OPTN.

5.2 Characterization of pro-inflammatory cytokine dynamics in THP1 upon MDP and/or sLPS stimulation.

Early inflammation mechanisms involve the immediate release of pro-inflammatory cytokines after recognising antigenic stimuli, and macrophages are often one of the first cells to respond to these stimuli. Pro-inflammatory cytokines are essential for coordinating the immune response resulting in the capture and removal of harmful stimuli[175]. Previous studies have demonstrated that NOD2 is capable of initiating an immune response. Still, it can also synergise with other antigenic receptors to boost the production of cytokines and enhance the immune response[176].

To characterise cytokine secretion profiles to sLPS and/or MDP response, a time course was carried out to investigate the cytokine secretion and gene induction of the main proinflammatory cytokines produced by THP1 cells. The protein levels of IL-6, CXCL-8, CXCL-10, and IL1β, TNFα and IFNβ were quantified by ELISA (Figure 5.1) and mRNA gene induction by qRT-PCR (Figure 5.2 and 5.3).

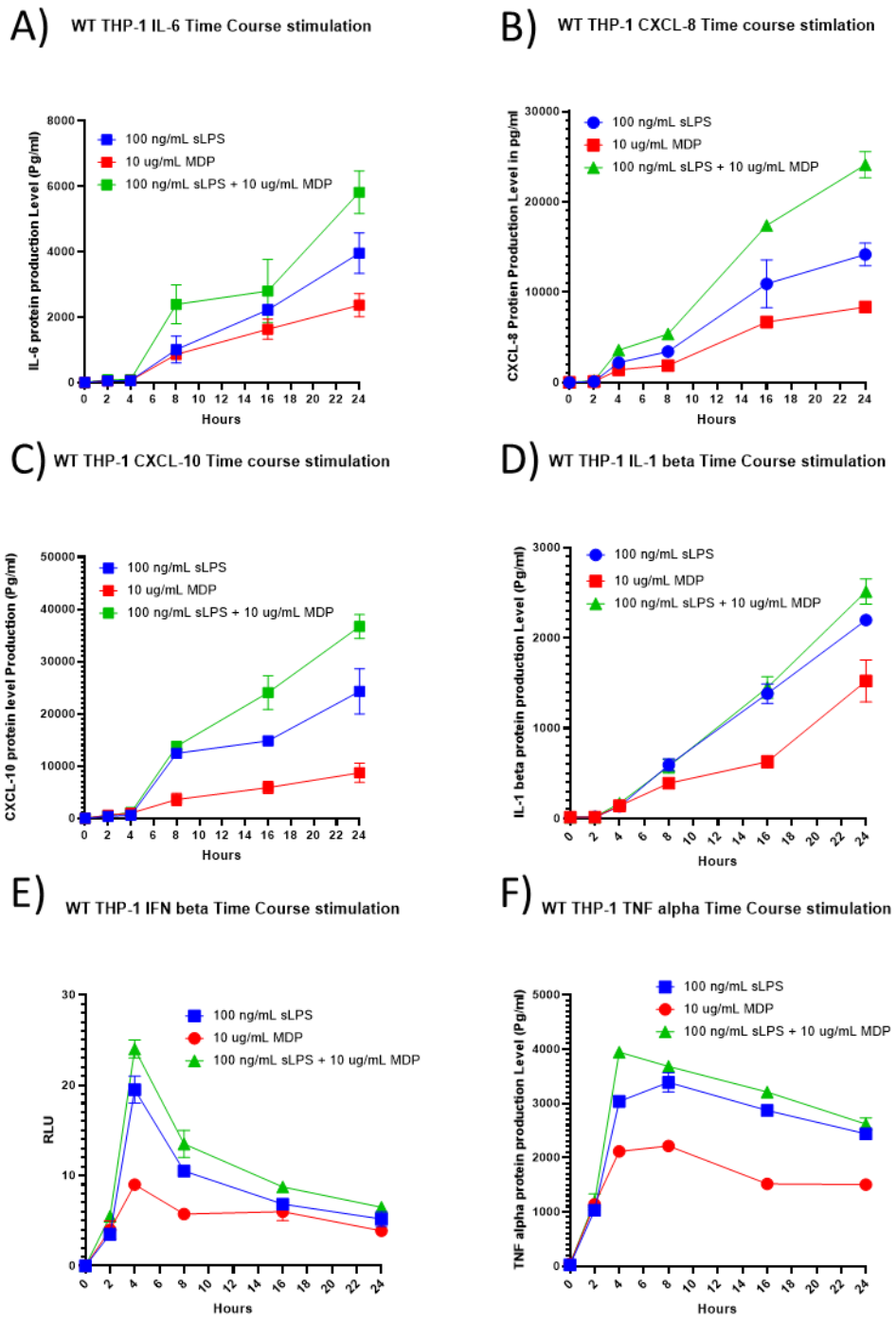

Figure 5. 1 Time course stimulation of WT THP-1 cells with 100 ng/mL sLPS or 10 µg/mL MDP or a combination of both stimuli.

(A) IL-6, (B) CXCL8, (C) CXCL10, (D) IL-1β, (E) IFN-β and (F) TNF-α were all elevated with sLPS stimulation at a higher level compared with MDP stimulation. A combined stimulation activating TLR4 and NOD2 identified a synergistic effect with releasing higher levels of pro inflammatory cytokines.

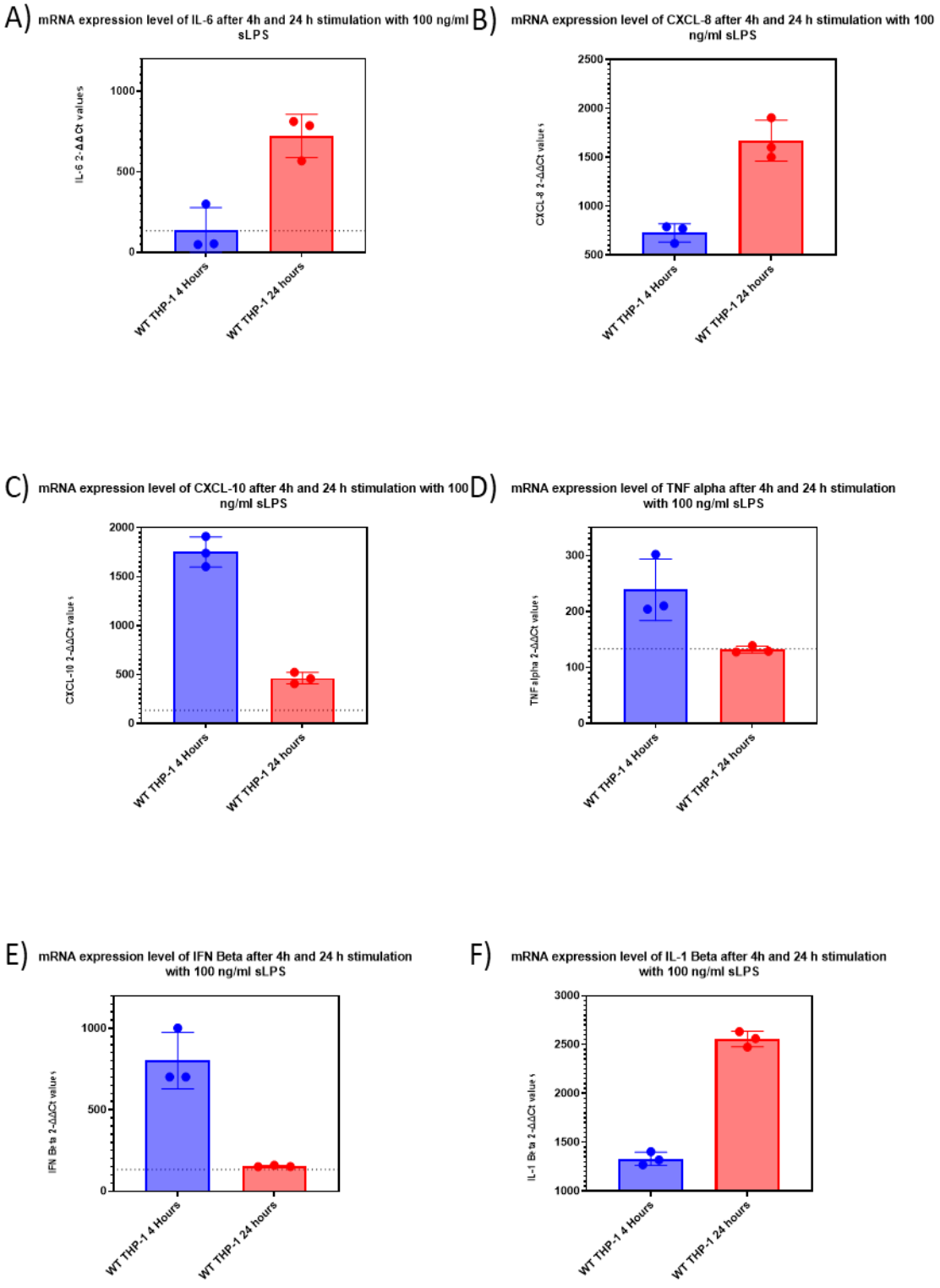

Figure 5. 2 mRNA expression levels of pro inflammatory cytokines and IFN β, downstream TLR4 activation at 4 and 24 hours.

(A) IL-6 (p≤** sig), (B) CXCL8 (p≤** sig), (C) CXCL10 (p≤***), (D) TNF-α (p≤* sig), (E) IFN-β (p≤** sig) and (F) IL-1β (p≤****), Results shown are mean ± SD, n= 3 and 3 independent experiments for mRNA expression (two-tailed, unpaired t-test).

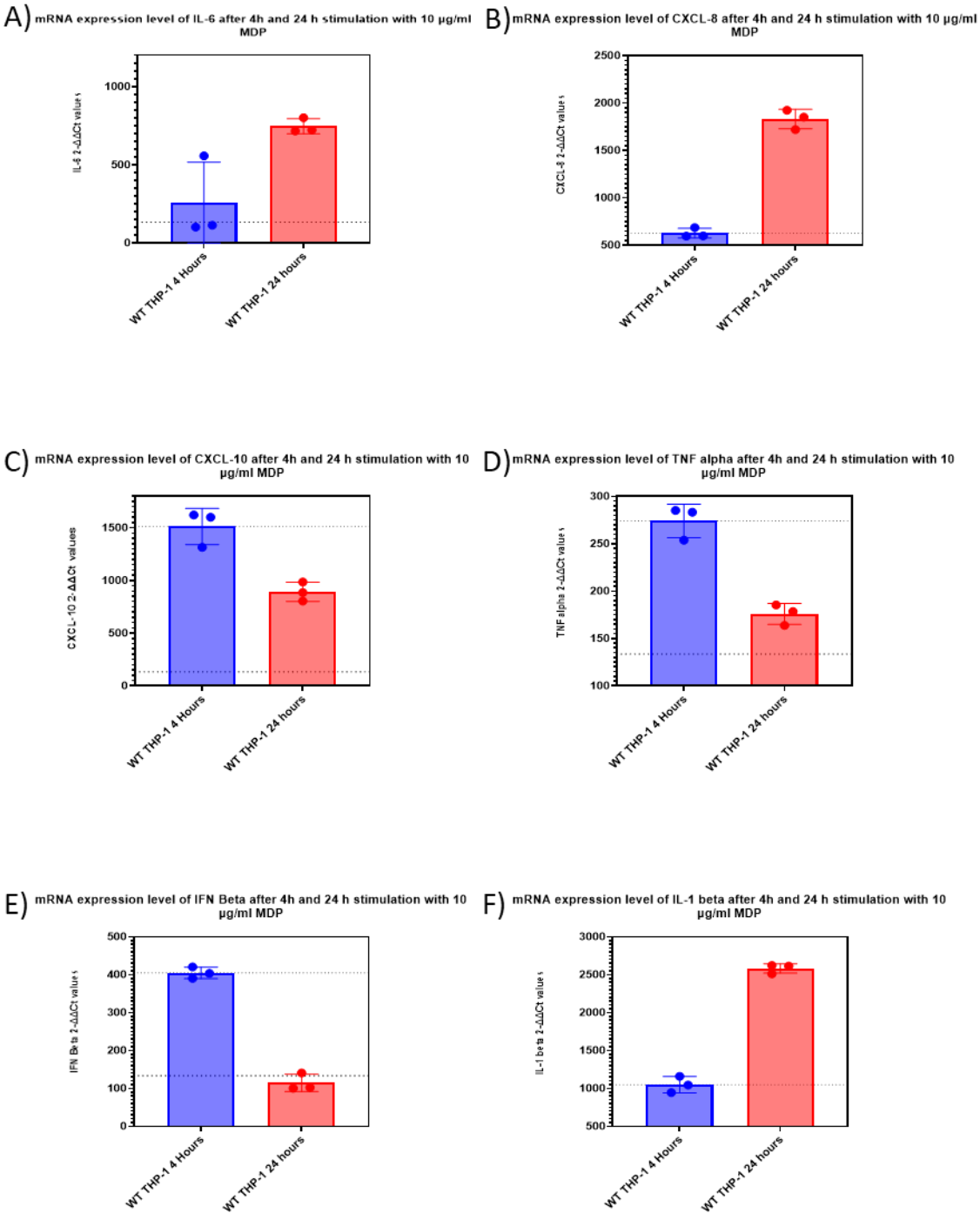

Figure 5. 3 mRNA expression levels of pro inflammatory cytokines and IFN β, downstream NOD2 activation at 4 and 24 hours.

A) IL-6 (p≤* sig), (B) CXCL8 (p≤**** sig), (C) CXCL10 (p≤**), (D) TNF-α (p≤** sig), (E) IFN-β (p≤**** sig) and (F) IL-1β (p≤****), Results shown are mean ± SD, n= 3 and 3 independent experiments for mRNA expression (two-tailed, unpaired t-test).

From our initial stimulation on WT THP-1, results point to sLPS's higher ability to induce pro inflammatory cytokines and IFNβ on proteins and gene levels than MDP stimulation. MDP stimulation managed to induce good levels of expression on both levels of proteins and gene induction. The combination of both sLPS and MDP to activate TLR4 and NOD2 results suggest a synergy in stimulation with activation of both signalling cascades, giving the highest levels of secretion and gene induction of all tested cytokines and chemokines. Also, 24 hours of stimulation is the best time to observe the highest secretion of IL-6, CXCL-8, CXCL-10 and IL-1 β. In the case of TNFα, 4-6 hours time point seems to capture the highest protein and gene levels. IFNβ displayed a quick induction as it had its highest levels at 4 hours post-stimulation. From these baseline profiles, we tested our THP-1 cell lines expressing either EGFP OPTN or its Phospho mutants at 24 hours for IL-6, CXCL-8 and CXCL-10. For TNFα, a 6-hour time point was used, and for IFNβ, a 4-hour time point was chosen as the best time to look at protein and mRNA levels.

5.3 The impact of the Phospho mutants on NOD2 and TLR4 induced pro-inflammatory chemokine and cytokine release.

The secretion levels of CXCL-8 and CXCL-10 were assessed in EGFP OPTN THP-1 and Phospho mutants downstream of TLR4 and NOD2 over 24 hours (Figure 5.4). While EGFP OPTN THP-1 cells showed similar secretion profiles to WT THP-1, the EGFP OPTN ^{S526E} cell line displayed a higher release level over the 24 hours. In contrast, the EGFP OPTN ^{S526A} mutation displayed a diminished secretion of both chemokines compared to WT THP-1 and EGFP OPTN-expressing cells. The results identify the potential importance of the S526 phosphorylation site downstream of NOD2 and TLR4. Over the initial 4 hours after NOD2 or TLR4 activation, the release of CXCL-8 and CXCL-10 was similar in all cell lines. An elevation in CXCL-8 and CXCL-10 secretion became apparent from 8 hours onwards in the cells expressing the phospho-active OPTN. Cells expressing the phospho-dead OPTN produced practically no CXCL-8 or CXCL-10 upon NOD2 or TLR4 activation.

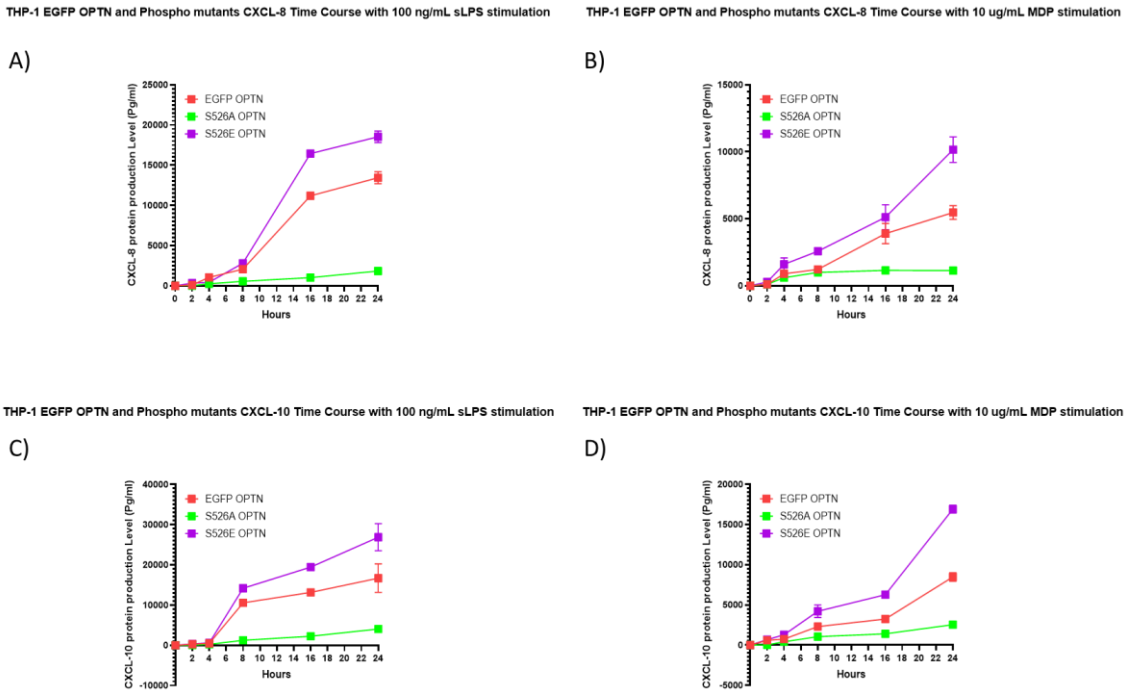

Figure 5. 4 Time course stimulation of EGFP OPTN and its Phospho mutants with sLPS and MDP, CXCL-8 and CXCL-10 are measured using ELISA to quantify production levels of proteins.

Looking at 24 hours after stimulation of EGFP OPTN and EGFP OPTN phospho mutants, the levels of CXCL-8, CXCL-10 and the pro-inflammatory cytokine IL-6 (which are known NFkB-related cytokines) were significantly altered (Figure 5.5). EGFP OPTN ^{S526E} demonstrated a significant elevation in the secretion of all three compared with EGFP OPTN and EGFP OPTN ^{S526A}. EGFP-OPTN^{S526A} released significantly lower CXCL-8, CXCL-10 and IL-6 levels than EGFP-OPTN THP-1 and EGFP-OPTN^{S526E}. Almost identical results were obtained after NOD2 or TLR4 stimulation, suggesting that the impact of the OPTN phosphorylation site S526 occurs downstream of the two receptors at a point where the signalling pathways may converge.

The influence of the Ser526 phosphorylation was also evident at 4 hours post NOD2 or TLR4 stimulation, as illustrated by the release of IFN-β (Figure 5.6 A and B). Expression of EGFP-OPTN^{S526E} resulted in an elevation in the levels of IFN-β, whereas EGFP-OPTN^{S526A} cells released less than WT cells. The alteration in IFN-β secretion due to the OPTN phosphorylation status was also evident downstream of two other TLRs, TLR3 and TLR2, after 4 hours of stimulation with Poly(I: C) and Pam3 respectively (Figure 5.6 C and D). These results implicate the role of the S526 position in OPTN downstream of a host of innate immune receptors and highlight a potential common regulatory mechanism in THP-1 cells.

It is worth pointing out that both phosphoproteomics mutations to OPTN at position S526 altered the NFkB signalling. Although all stable cell lines (WT EGFP OPTN, EGFP OPTN S526A and EGFP OPTN S526E) maintained their native WT OPTN. The excessive upregulation of OPTN protein did alter their baseline response. In the WT EGFP OPTN, upregulating OPTN enhanced its negative regulator effect on pro-inflammatory cytokines level as a reduction that is not significant but observable. In the case of the phosphomutants cell lines, their native WT OPTN protein did not manage to correct the effect of mutated OPTN. Instead, it seems that the dimerisation of phosphomutants with native WT OPTN resulted in mutant OPTN overtaking WT OPTN and dominantly displaying its effect.

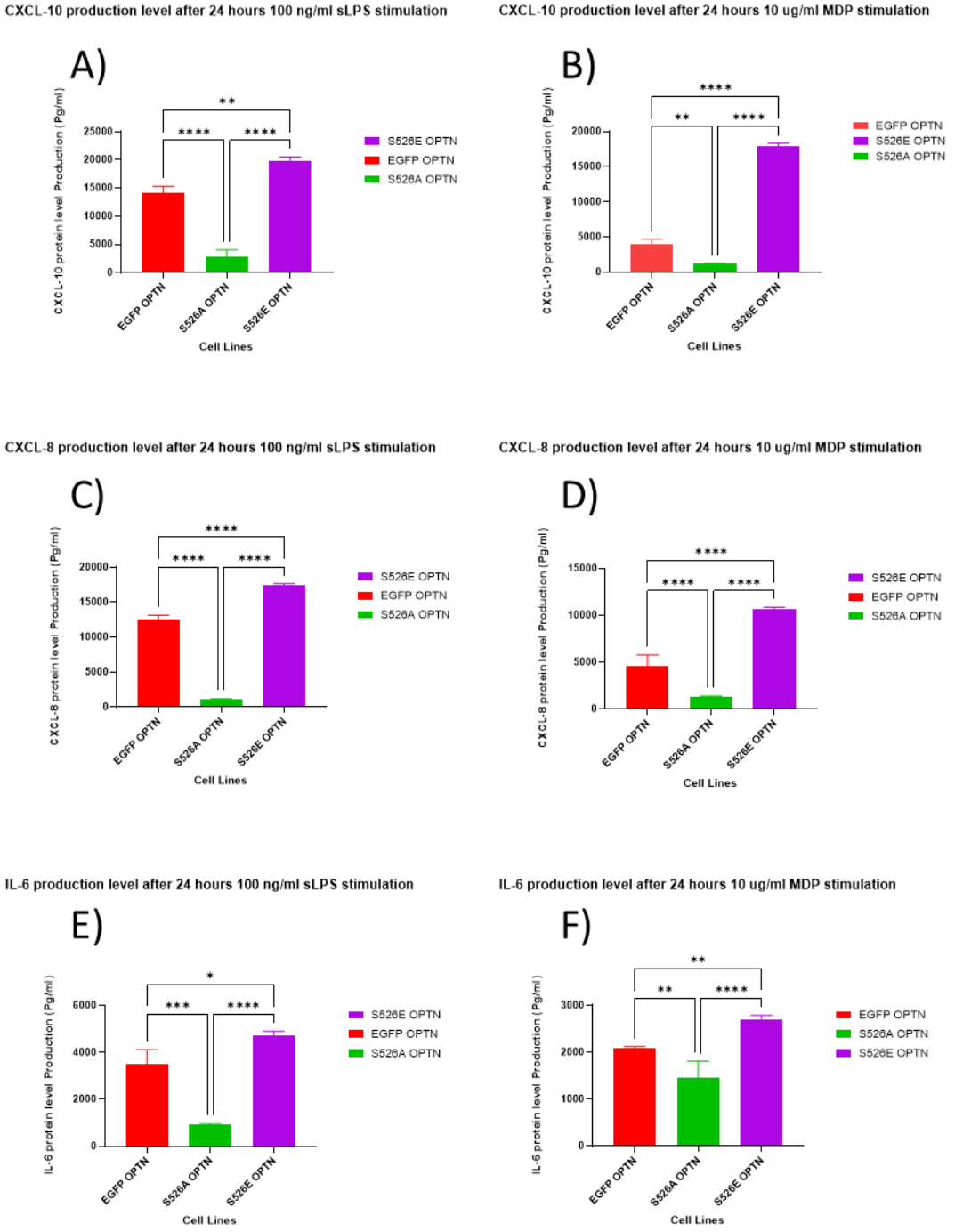

Figure 5. 5 CXCL-8, CXCL-10 and IL-6 secretion levels at 24 hours of EGFP OPTN and its Phospho mutants downstream TLR 4 and NOD2.

Experiments N=3, *P≤0.05, **p≤0.01, ***p≤0.001 ****p≤0.0001. (one-way ANOVA and a Bonferroni posthoc test).

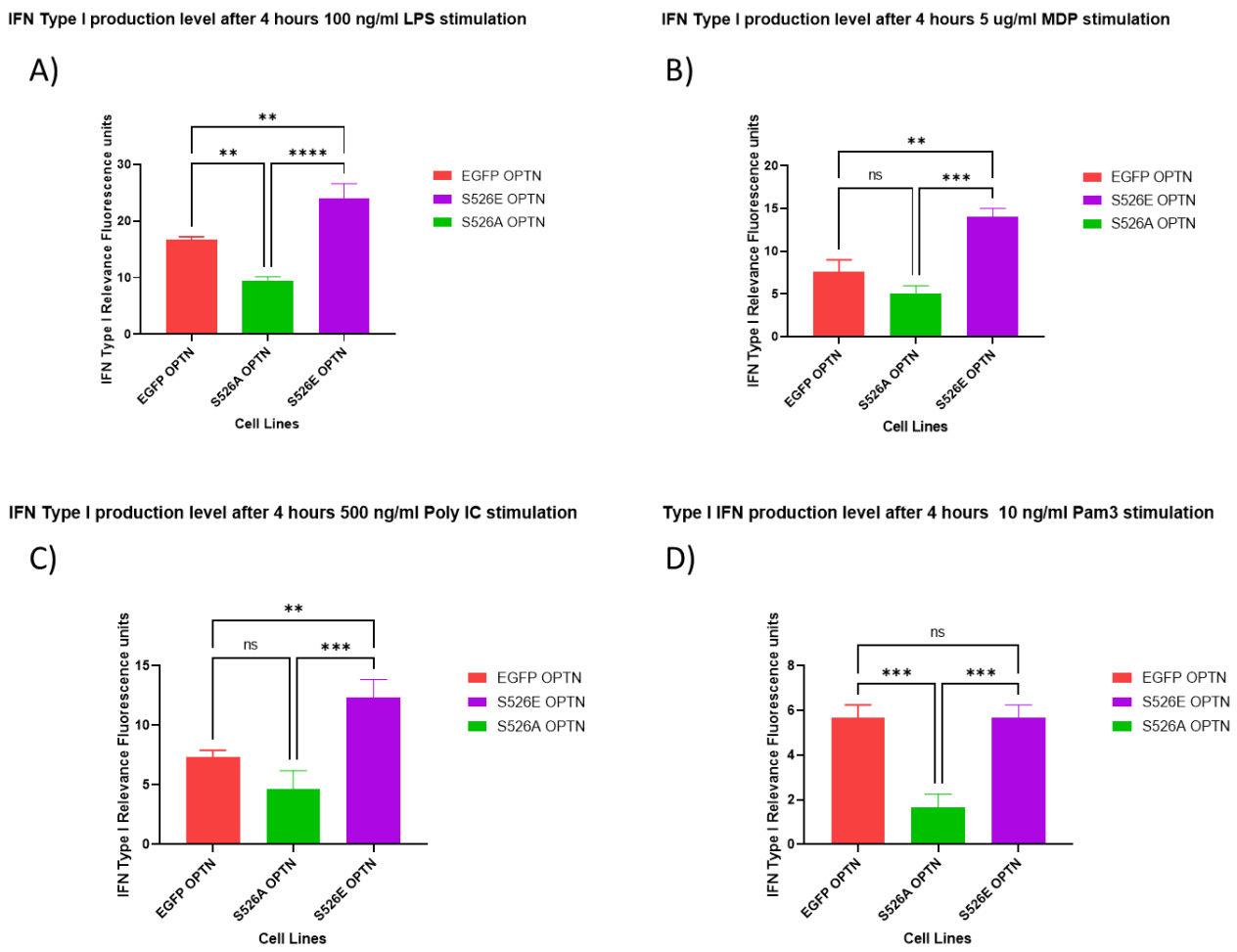

Figure 5. 6 IFNβ secretion levels at 4 hours of EGFP OPTN and its Phospho mutants downstream TLR4, NOD2, TLR3 and TLR2.

Experiments N=3, *P≤0.05, **p≤0.01, ***p≤0.001 ****p≤0.0001. (one-way ANOVA and a Bonferroni posthoc test).

5.4 The impact of the Phospho mutants on NOD2 and TLR4 induced pro-inflammatory chemokine and cytokine gene induction

To determine if the impact of the Ser526 phosphorylation site operates at the level of receptor signalling or the level of protein secretion, cytokine gene induction was determined by qPCR. The mRNA levels of IL-6, CXCL8, CXCL10, IL-1β, IFN-β and TNF-α were mostly found to be elevated at both 4 hours and 24 hours in cells expressing EGFP-OPTN^{S526E}

and diminished in cells expressing EGFP-OPTN^{S526A} (Figures 5.6 and 5.7). This data revealed that OPTN, the phosphorylation at Ser526, is implicated in the signalling downstream of TLR4 and unlikely to be responsible for intracellular cytokine/chemokine trafficking.

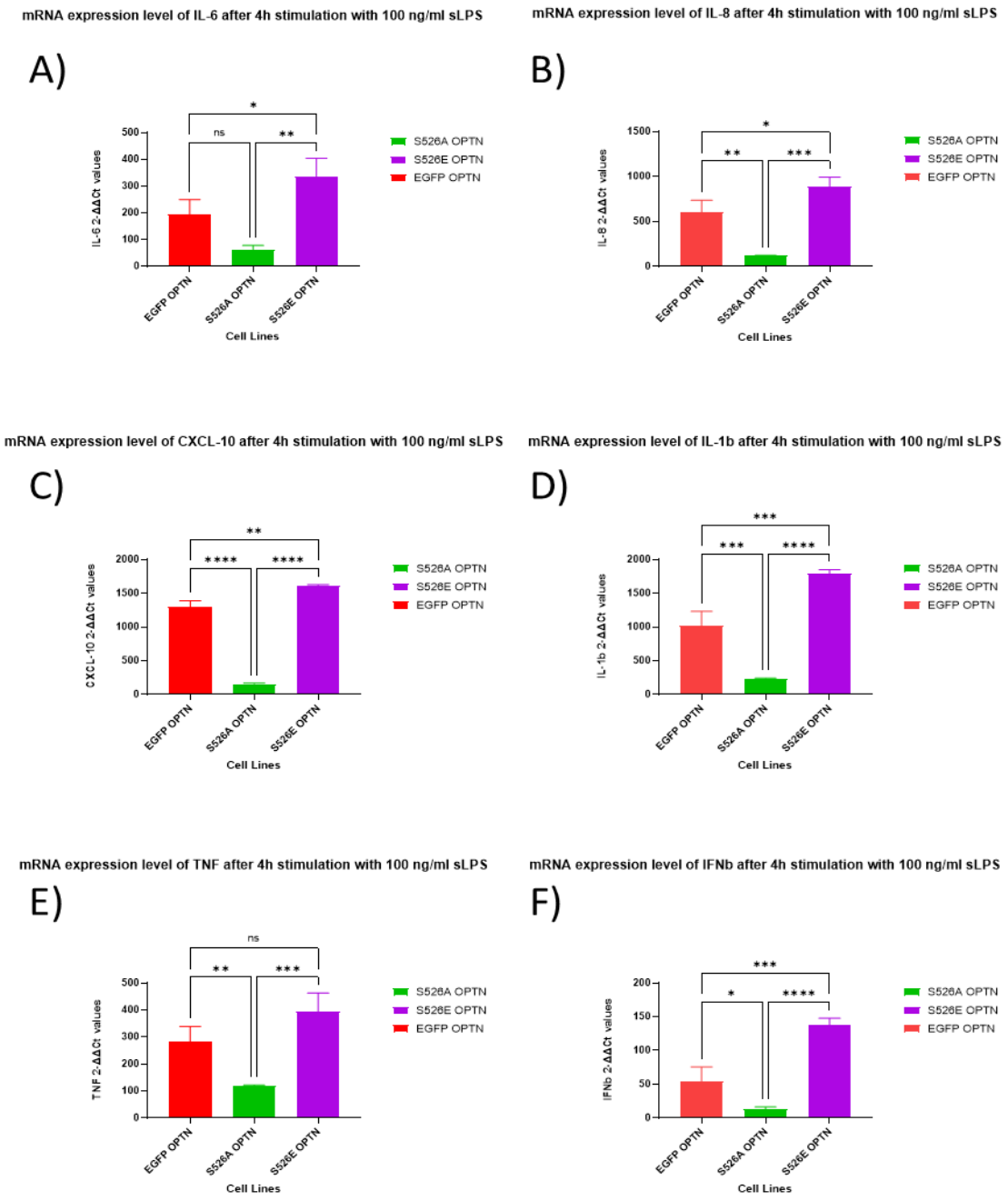

Figure 5. 7 mRNA levels of IL-6, CXCL-8, CXCL-10, IL-1b, TNFα and IFNβ at 4 hours stimulation with sLPS of EGFP OPTN and its phospho mutants.

Experiments N=3, *P≤0.05, **p≤0.01, ***p≤0.001 ****p≤0.0001. (one-way ANOVA and a Bonferroni posthoc test).

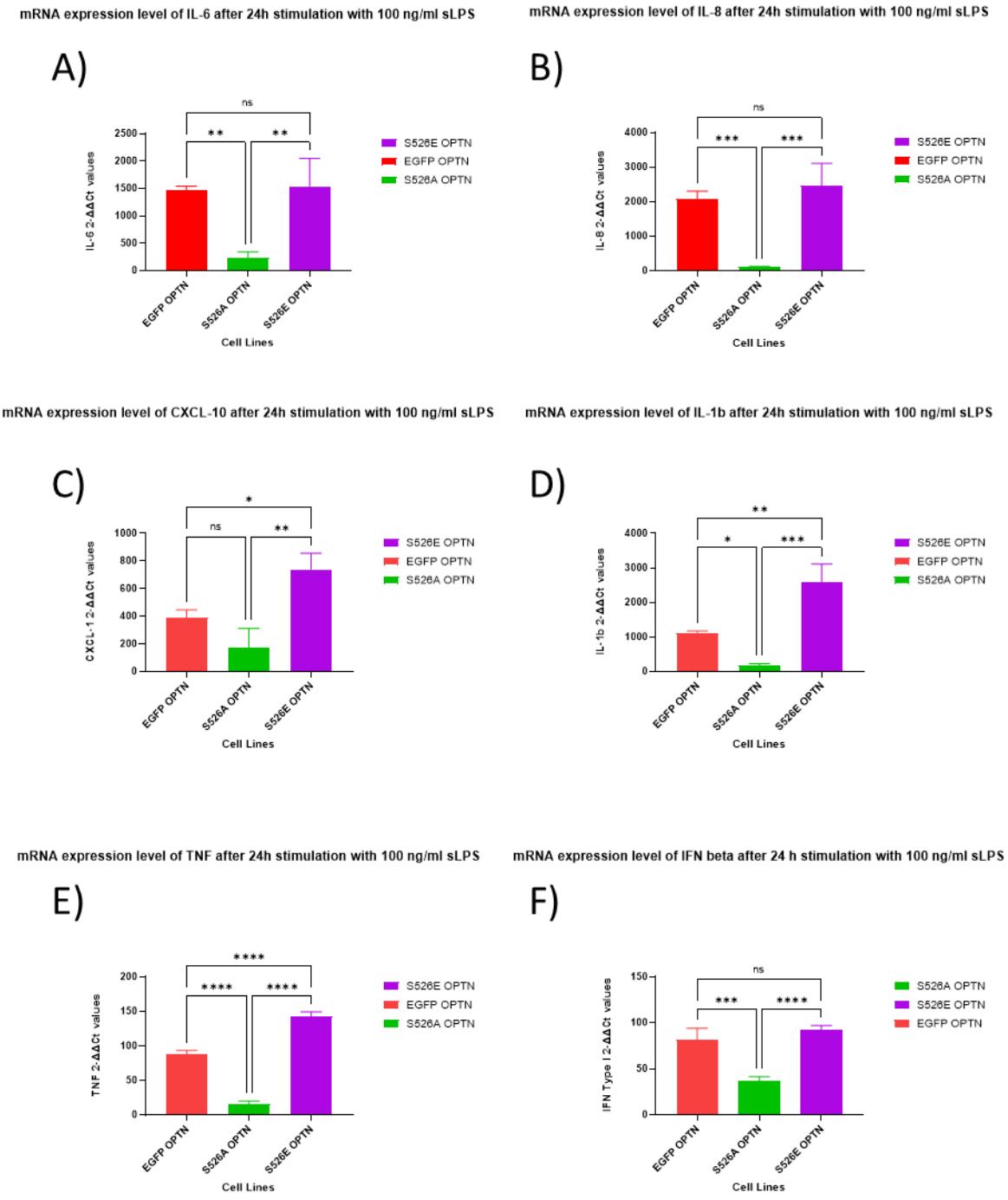

Figure 5. 8 mRNA levels of IL-6, CXCL-8, CXCL-10, IL-1b, TNFα and IFNβ at 24 hours of stimulation with sLPS of EGFP OPTN and its phospho mutants.

Experiments N=3, *P≤0.05, **p≤0.01, ***p≤0.001 ****p≤0.0001. (one-way ANOVA and a Bonferroni posthoc test).

5.5 TBK-1 inhibitor BX795 effect on TLR4 and NOD2 induction of TNFα in WT THP-1.

The kinase TBK-1 is known to phosphorylate OPTN at Ser177 and is also involved in TLR signalling[60]. In addition, there is some evidence of a role for TBK-1 downstream of NOD2[177]. In order to determine if TBK-1 activity is required by THP-1 cells downstream of TLR4 and NOD2, cells were treated with the TBK-1 inhibitor BX795 during stimulation with MDP or LPS. WT THP-1 cells were stimulated for 6 hours with MDP or sLPS ± BX795, and the levels of TNF measured (Figure 5.9)[178]. WT THP-1 cells stimulated with sLPS, or MDP released significant amounts of TNFα at 6 and 24 hours. The inclusion of BX795 almost completely blocked TNFα secretion at both time points and with both ligands. The results demonstrate that TBK-1 activity is required for TNFα release downstream of TLR4 and NOD2.

5.6 TBK-1 inhibitor BX795 effect on TLR4 and NOD2 induction of TNFα in OPTN Phospho mutant cell lines.

Phosphoproteomic analysis of OPTN isolated from THP-1 cells stimulated with LPS or MDP only identified the Ser526 site as phosphorylated. The Ser177 site was not identified in our experiment, and this suggests that the TBK-1 kinase activity identified above may be working differently than expected from previous studies[171]. TBK-1 may phosphorylate OPTN at Ser526 in THP-1 cells; therefore, the effects of BX795 on the OPTN Phospho mutant cell lines were tested. If TBK-1 targets Ser526 then the phospho active mutant may not be as susceptible to BX795 as cells expressing WT OPTN. The release of TNFα at 6 hours post-sLPS or MDP or a combination of the two was diminished in cells expressing EGFP-OPTN^{S526A} and enhanced in EGFP-OPTN^{S526E} cells (Figure 5.10). The inclusion of BX795 almost completely

blocked TNFα in all cell lines stimulated with sLPS or MDP, or a combination of the two (Figure 5.11). The expression of the phospho active Ser526 OPTN was not sufficient to overcome the blockade of TBK-1 by BX795.

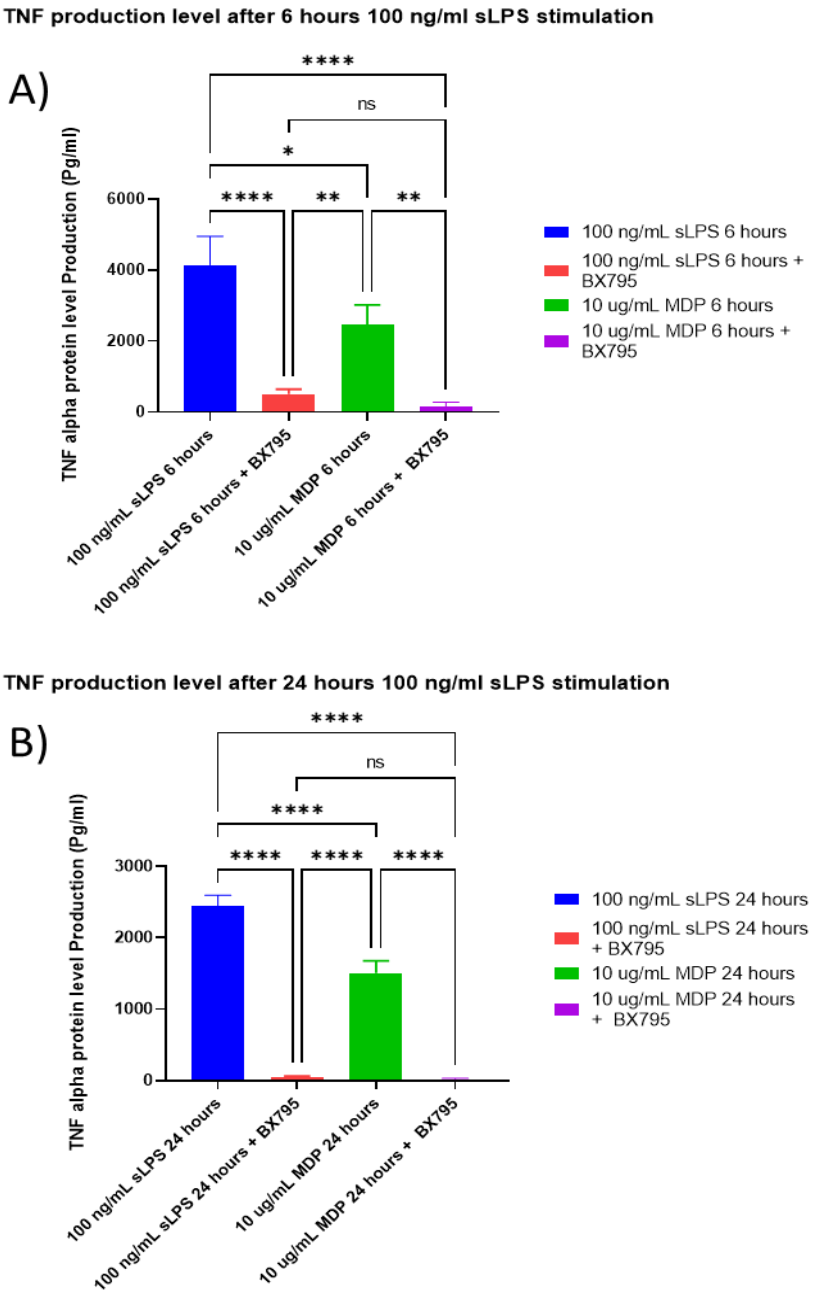

Figure 5. 9 WT THP-1 cells production of TNFα at 6 and 24 hours downstream TLR4 and NOD2.

BX 795 impact on the same stimulation condition was significant, BX 795 diminished TNFα production from both TLR4 and NOD2 signalling cascade. Experiments N=3, *P≤0.05, **p≤0.01, ***p≤0.001 ****p≤0.0001. (one-way ANOVA and a Bonferroni posthoc test).

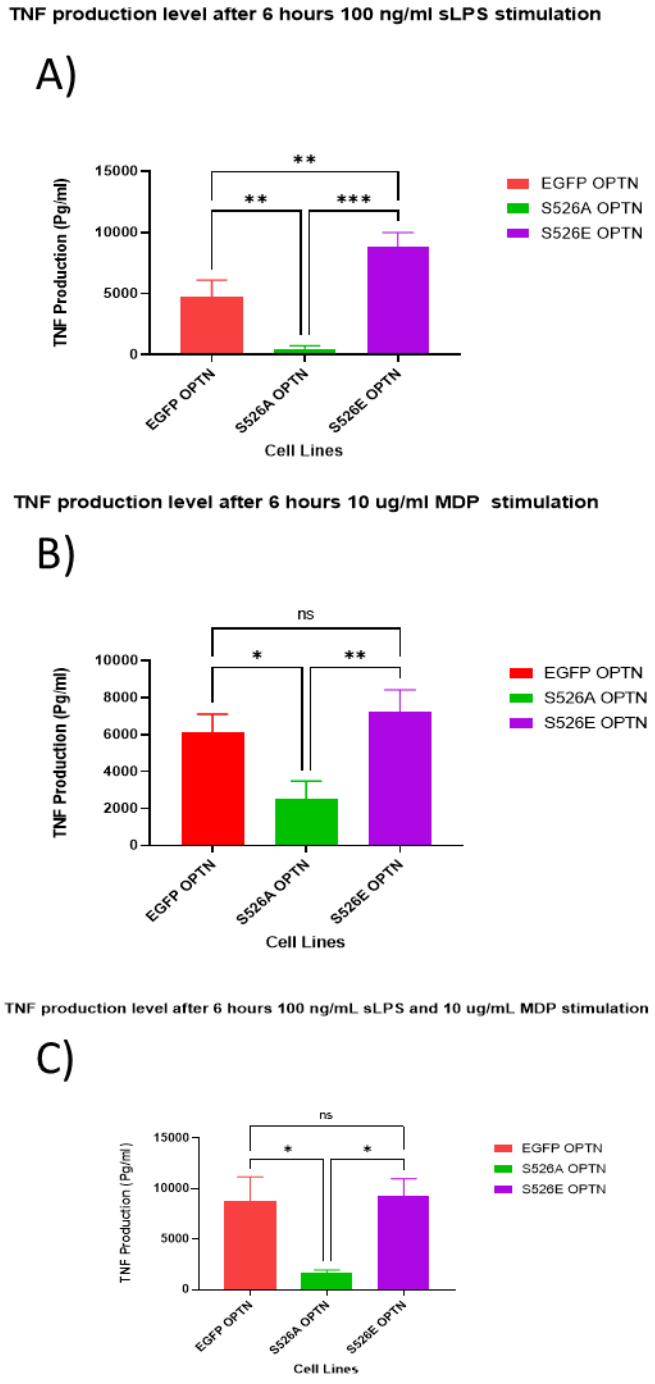

Figure 5. 10 EGFP OPTN THP-1 cells and its Phospho mutants, production of TNFα at 6 hours downstream TLR4 and NOD2 or a combined stimulation.

EGFP OPTN S526A ability to secrete TNFα is significantly lower than EGFP OPTN and EGFP OPTN S526E. Experiments N=3, *P≤0.05, **p≤0.01, ***p≤0.001 ****p≤0.0001. (one-way ANOVA and a Bonferroni posthoc test).

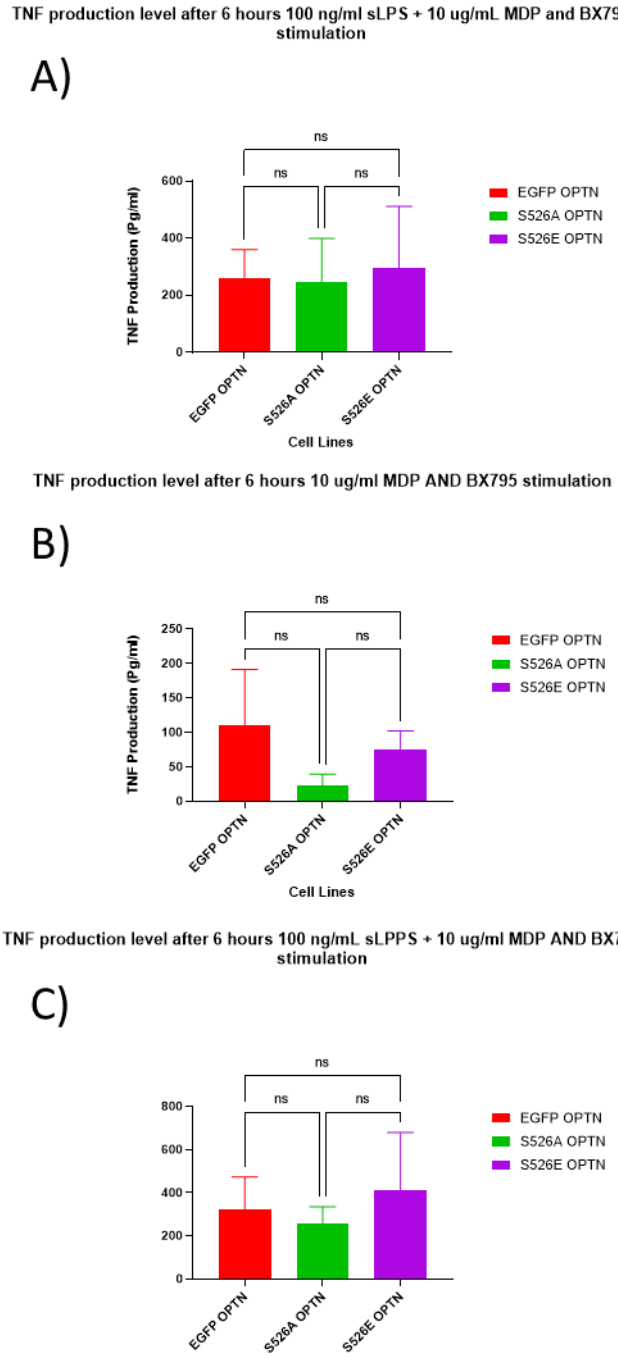

Figure 5. 11 EGFP OPTN THP-1 cells and its Phospho mutants, production of TNFα at 6 hours downstream TLR4 and NOD2 or a combined stimulation.

BX 795 impact on the same stimulation condition was significant, BX 795 diminished TNFα production from both TLR4 and NOD2 signalling cascade from all cell lines. Experiments N=3, *P≤0.05, **p≤0.01, ***p≤0.001 ****p≤0.0001. (one-way ANOVA and a Bonferroni posthoc test).

5.7 Discussion

Results from this chapter indicate that OPTN Ser526 seems to be involved in multiple pathways of the pro-inflammatory process. Elevation in released pro-inflammatory cytokines and chemokines is found in cells that express the OPTN S526E mutant. The impact of constitutive phosphorylation of OPTN at position S526 leads to a significant increase in cytokine release upon TLR/NLR stimulation. This constitutive phosphorylation does not impact the resting state of THP-1 cells, as non-stimulated cell lines did not show any difference in cytokine release.

Although we tested two signalling cascades (TLR4, NOD2), OPTN S526 seems to function at a point downstream of NOD2/TLR4 activation. TBK1 Kinase activity is needed to induce pro-inflammatory cytokines such as TNFα downstream of TLR4 and NOD2 activation. Blocking TBK-1 with the specific inhibitor BX795 revealed that all OPTN phospho mutants responded similarly to WT THP-1 cells, suggesting that the phosphorylation of S526 cannot overcome a loss in TBK-1 signalling. Therefore, it probably places TBK1 activation downstream of OPTN phosphorylation.

THP-1 cells provide a good study model for monocytes behaviour when activated with sLPS and MDP to initialise TLR4 and NOD2 (respectively). It expressed potent pro-inflammatory cytokines and chemokines upon stimulation. It was also genetically modifiable with retroviral transduction to tag and manipulate OPTN structure to facilitate our study of

OPTN's impact on signalling pathways. Also, OPTN impacts a robust immune response when downregulated in monocytes and THP-1 cells[57].

As an adaptor protein OPTN has been studied for its role in impacting innate immunity and has been found as a causative gene in multiple autoimmune conditions like ALS. OPTN ^{E487G} mutation caused hyperreactive intracellular inclusions and excessive activation of NFkB, contributing to ALS pathogenesis[71]. In POAG, OPTN ^{E50K} mutation disrupts OPTN dimerisation and increased TBK-1 interaction, leading to decreased mobility of the OPTN/TBK-1 complex and the formation of numerous peri-nuclear loci that inactivated immune signalling pathways[89].

We discovered that position S526 in OPTN was phosphorylated downstream of NOD2 and, once phosphorylated, had the ability to impact multiple TLRs. The synergy we identified between NOD2 and TLR4 may depend on NOD2's ability to phosphorylate OPTN on Ser526.

A recent study also identified Ser526 as a phosphorylation site on OPTN [63]. The authors described a link between the autophagy-related protein AXL and OPTN phosphorylation at the S526 position. The phosphorylation controlled AXL levels, and the expression of OPTN^{S526A} eliminated this function by changing the OPTN structure. As this publication came out after my PhD ended, I could not verify the findings in the THP-1 cells or determine the autophagy status of my cell lines.

In this chapter, I explored OPTN S526 phosphorylation and its potential effect on the THP-1 cell's ability to affect pro-inflammatory cytokines release downstream of TLR4 and NOD2. Although TLR4 and NOD2 as signalling pathways are not greatly overlapped, OPTN S526 phosphorylation seems to impact both pathways in the THP-1 cell line. Therefore, it is new to discover that OPTN is phosphorylated downstream of NOD2 activation, which I found by MS proteomics in chapter 3. This phosphorylation may also be observed downstream of TLR4, and further investigation is needed to confirm it as an event leading to hypersecretion of pro-inflammatory cytokines releases.

Phosphorylation at this position is needed for a good level of hyper immunity. Looking at EGFP OPTN S526E's constant ability to overexpress pro-inflammatory cytokines and chemokines at a higher level (almost double) than WT THP-1, EGFP OPTN THP-1 or EGFP OPTN S526A confirms the role of such phosphorylation site functional impact on multiple signalling pathways. Similarly, EGFP OPTN ^{S526A} exhibited a lack of hypo immunity to activation of TLR4 and NOD2, which resulted in a functionally significant reduction of pro-inflammatory cytokines response. While both activate distinct signalling pathways, the effect of a lack of phosphorylation at S526 appears universal in reducing the expression of pro-inflammatory cytokines and chemokines.

This effect of OPTN S525 is regulated by a kinase yet to be identified, TBK-1 may play a role in the process, but my experimentation did not find evidence to confirm its involvement. Treating all versions of EGFP OPTN and its Phospho mutants with BX795, an inhibitor of TBK-1, leads to minimal expression of TNFα across all versions of EGFP OPTN.

RIPK2 is another candidate kinase that may be the principal link for such an effect on the immune response. However, further investigation is needed to prove its involvement with OPTN phosphorylation at the S526 position.

Chapter 6. Conclusion

This study discusses the role of NOD2 and OPTN in innate immunity, looking at oral autoimmune and inflammatory diseases. OPTN or NOD2 separately have been found to contribute to a host of diseases through disease causing mutations. Both are impactful on the pro-inflammatory process and autophagy, giving them the status of potential therapeutic targets. Also, the THP-1 cell line provided a valid study model being easily cultured, responsive to multiple PRRs and genetically modifiable to express our protein of interest.

OPTN phosphorylation at the S526 position downstream of NOD2 activation by MDP is established via two different experimental designs. This newly founded novel link between OPTN and NOD2 is an event that may explain hyperinflammation in multiple diseases. OPTN S526 phospho site has emerged as an important site that can impact other aspects of TLRs response. Also, protein manipulation through the introduction of OPTN-containing phosphor-mimetics is achievable, and even though the WT OPTN was still expressed in these cells, a phenotype was identifiable.

Our experimentation shows the involvement of position S526 in OPTN downstream TLR4 and NOD2 signalling cascade. Constituent phosphorylation of S526 in OPTN represented in OPTN ^{S526E} or blockage of this phosphosite did not change proinflammatory cytokines profiles at resting state. Only upon activation of TLR4 or NOD2, do we see a significant

increase in proinflammatory cytokine release in OPTN ^{S526E} mutation. The opposite is founded in OPTN S526A, as a lack of response is founded in the case of TLR4 and NOD2 activation. Regarding the kinase facilitation of this phosphorylation, further investigation is needed to uncover the kinase in question.

Future work

The results from this study present position S526 in OPTN as an impactful modulator of the immune response. Due to its ability to change the profile of proinflammatory cytokine response, it may play a key role in dampening hyperinflammation in diseases where OPTN is involved in the signalling cascade. Further investigation is needed such as:

- Identification of facilitation kinase that phosphorylates OPTN at S526.
- How does phosphorylation at S526 change the function of OPTN during inflammation:
    - Determine the cellular distribution and protein complexes formed during the immune response.
    - Does S526 impact ubiquitin binding, and if so, how?
- Genetic scanning to identify the status of this position in autoimmune diseases.
- Testing drug libraries to find molecules that impact OPTN and its phophosphosites may affect autoimmune disease status favourably.

References

1. Cekici, A., Kantarci, A., Hasturk, H. & Van Dyke, T. E. Inflammatory and immune pathways in the pathogenesis of periodontal disease. *Periodontol. 2000* **64**, 57–80 (2014).

2. Lamkanfi, M. & Dixit, V. M. Inflammasomes and their roles in health and disease. *Annu. Rev. Cell Dev. Biol.* **28**, 137–161 (2012).

3. Deretic, V., Saitoh, T. & Akira, S. Autophagy in infection, inflammation and immunity. *Nat. Rev. Immunol.* **13**, 722–737 (2013).

4. Janeway, C. A. & Medzhitov, R. Innate immune recognition. *Annu. Rev. Immunol.* **20**, 197–216 (2002).

5. Brubaker, S. W., Bonham, K. S., Zanoni, I. & Kagan, J. C. Innate Immune Pattern Recognition: A Cell Biological Perspective. *Annu. Rev. Immunol.* **33**, 257–290 (2015).

6. Cai, X., Chiu, Y. H. & Chen, Z. J. The cGAS-cGAMP-STING pathway of cytosolic DNA sensing and signaling. *Mol. Cell* **54**, 289–296 (2014).

7. Akira, S., Uematsu, S. & Takeuchi, O. Pathogen recognition and innate immunity. *Cell* **124**, 783–801 (2006).

8. Botos, I., Segal, D. M. & Davies, D. R. The structural biology of Toll-like receptors. *Structure* **19**, 447–459 (2011).

9. Kawai, T. & Akira, S. The role of pattern-recognition receptors in innate immunity: Update on toll-like receptors. *Nat. Immunol.* **11**, 373–384 (2010).

10. Lin, Y. *et al.* The lipopolysaccharide-activated Toll-like receptor (TLR)-4 induces synthesis of the closely related receptor TLR-2 in adipocytes. *J. Biol. Chem.* **275**, 24255–24263 (2000).

11. Regan, T. *et al.* Identification of TLR10 as a Key Mediator of the Inflammatory Response to Listeria monocytogenes in Intestinal Epithelial Cells and Macrophages . *J. Immunol.* **191**, 6084–6092 (2013).

12. Lee, S. M. Y. *et al.* Toll-like receptor 10 is involved in induction of innate immune responses to influenza virus infection. *Proc. Natl. Acad. Sci. U. S. A.* **111**, 3793–3798 (2014).

13. Zhang, S. Y. *et al.* TLR3 deficiency in patients with herpes simplex encephalitis. *Science (80-.).* **317**, 1522–1527 (2007).

14. Mancuso, G. *et al.* Bacterial recognition by TLR7 in the lysosomes of conventional dendritic cells. *Nat. Immunol.* **10**, 587–594 (2009).

15. Human TLR7 or TLR8 independently confer responsiveness to the. *Nature* **3**, 2002 (2002).

16. Tian, J. *et al.* Toll-like receptor 9-dependent activation by DNA-containing immune complexes is mediated by HMGB1 and RAGE. *Nat. Immunol.* **8**, 487–496 (2007).

17. Randow, F. & Seed, B. Endoplasmic reticulum chaperone gp96 is required for innate immunity but not cell viability. *Nat. Cell Biol.* **3**, 891–896 (2001).

18. Takahashi, K. *et al.* A protein associated with Toll-like receptor (TLR) 4 (PRAT4A) is required for TLR-dependent immune responses. *J. Exp. Med.* **204**, 2963–2976 (2007).

19. Brinkmann, M. M. *et al.* The interaction between the ER membrane protein UNC93B and TLR3, 7, and 9 is crucial for TLR signaling. *J. Cell Biol.* **177**, 265–275 (2007).

20. Kawasaki, T. & Kawai, T. Toll-like receptor signaling pathways. *Front. Immunol.* **5**, 1–8 (2014).

21. Broz, P. & Monack, D. M. Newly described pattern recognition receptors team up against intracellular pathogens. *Nat. Rev. Immunol.* **13**, 551–565 (2013).

22. Duncan, J. A. *et al.* Cryopyrin/NALP3 binds ATP/dATP, is an ATPase, and requires ATP binding to mediate inflammatory signaling. *Proc. Natl. Acad. Sci. U. S. A.* **104**, 8041–8046 (2007).

23. Koonin, E. V. & Aravind, L. The NACHT family - A new group of predicted NTPases implicated in apoptosis and MHC transcription activation. *Trends Biochem. Sci.* **25**, 223–224 (2000).

24. White, S. R. & Lauring, B. AAA+ ATPases: Achieving diversity of function with conserved machinery. *Traffic* **8**, 1657–1667 (2007).

25. Platnich, J. M. & Muruve, D. A. NOD-like receptors and inflammasomes: A review of their canonical and non-canonical signaling pathways. *Arch. Biochem. Biophys.* **670**, 4–14 (2019).

26. Motta, V., Soares, F., Sun, T. & Philpott, D. J. Nod-like receptors: Versatile cytosolic sentinels. *Physiol. Rev.* **95**, 149–178 (2015).

27. Kofoed, E. M. & Vance, R. E. Innate immune recognition of bacterial ligands by NAIPs determines inflammasome specificity. *Nature* **477**, 592–597 (2011).

28. Ting, J. P. Y. *et al.* The NLR Gene Family: A Standard Nomenclature. *Immunity* **28**, 285–287 (2008).

29. Kim, Y. K., Shin, J. S. & Nahm, M. H. NOD-like receptors in infection, immunity, and diseases. *Yonsei Med. J.* **57**, 5–14 (2016).

30. Hofmann, K., Bucher, P. & Tschopp, J. The CARD domain: a new apoptotic signalling motif. *Trends Biochem. Sci.* **22**, 155–156 (1997).

31. Ogura, Y. *et al.* Nod2, a Nod1/Apaf-1 Family Member That Is Restricted to Monocytes and Activates NF-κB. *J. Biol. Chem.* **276**, 4812–4818 (2001).

32. Conti, B. J. *et al.* CATERPILLER 16.2 (CLR16.2), a novel NBD/LRR family member that negatively regulates T cell function. *J. Biol. Chem.* **280**, 18375–18385 (2005).

33. Cui, J. *et al.* NLRP4 negatively regulates type I interferon signaling by targeting the kinase TBK1 for degradation via the ubiquitin ligase DTX4. *Nat. Immunol.* **13**, 387–395 (2012).

34. Karin, M. The Regulation of AP-1 Activity by Mitogen-activated Protein Kinases *. *J. Biol. Chem.* **270**, 16483–16486 (1995).

35. Kobayashi, K. S. *et al.* Nod2-Dependent Regulation of Innate and Adaptive Immunity in the Intestinal Tract. *Science (80-.).* **307**, 731–734 (2005).

36. Hsu, L.-C. *et al.* A NOD2–NALP1 complex mediates caspase-1-dependent IL-1β secretion in response to Bacillus anthracis infection and muramyl dipeptide. *Proc. Natl. Acad. Sci.* **105**, 7803–7808 (2008).

37. Travassos, L. H. *et al.* Nod1 and Nod2 direct autophagy by recruiting ATG16L1 to the plasma membrane at the site of bacterial entry. *Nat. Immunol.* **11**, 55–62 (2010).

38. Cooney, R. *et al.* NOD2 stimulation induces autophagy in dendritic cells influencing bacterial handling and antigen presentation. *Nat. Med.* **16**, 90–97 (2010).

39. Homer, C. R. *et al.* A Dual Role for Receptor-interacting Protein Kinase 2 (RIP2) Kinase Activity in Nucleotide-binding Oligomerization Domain 2 (NOD2)-dependent Autophagy *. *J. Biol. Chem.* **287**, 25565–25576 (2012).

40. Cadwell, K. Crosstalk between autophagy and inflammatory signalling pathways: balancing defence and homeostasis. *Nat. Rev. Immunol.* **16**, 661–675 (2016).

41. Chu, H. *et al.* Gene-microbiota interactions contribute to the pathogenesis of inflammatory bowel disease. *Science (80-.).* **352**, 1116–1120 (2016).

42. Pattern, P. M. RIG-I-like Receptors Cells of Innate Immunity : Mechanisms of Activation Zebrafish at the Interface of Develop- ment and Disease Research. **5**, (2019).

43. Rehwinkel, J. & Gack, M. U. RIG-I-like receptors: their regulation and roles in RNA sensing. *Nat. Rev. Immunol.* **20**, 537–551 (2020).

44. Oganesyan, G. *et al.* Critical role of TRAF3 in the Toll-like receptor-dependent and -independent antiviral response. *Nature* **439**, 208–211 (2006).

45. Gack, M. U. Mechanisms of RIG-I-Like Receptor Activation and Manipulation by Viral Pathogens. *J. Virol.* **88**, 5213–5216 (2014).

46. Jeong, E. & Lee, J. Y. Intrinsic and extrinsic regulation of innate immune receptors. *Yonsei Med. J.* **52**, 379–392 (2011).

47. Outlioua, A., Pourcelot, M. & Arnoult, D. The Role of Optineurin in Antiviral Type I Interferon Production. *Front. Immunol.* **9**, (2018).

48. Nagabhushana, A., Bansal, M. & Swarup, G. Optineurin Is Required for CYLD-Dependent Inhibition of TNFα-Induced NF-κB Activation. *PLoS One* **6**, e17477 (2011).

49. Tanishima, M. *et al.* Identification of optineurin as an interleukin-1 receptor-associated kinase 1-binding protein and its role in regulation of MyD88-dependent signaling. *J. Biol. Chem.* **292**, 17250–17257 (2017).

50. Nakazawa, S. *et al.* Linear ubiquitination is involved in the pathogenesis of optineurin-associated amyotrophic lateral sclerosis. *Nat. Commun.* **7**, 12547 (2016).

51. Park, B. *et al.* Impairment of Protein Trafficking upon Overexpression and Mutation of Optineurin. *PLoS One* **5**, e11547 (2010).

52. Mankouri, J. *et al.* Optineurin Negatively Regulates the Induction of IFNβ in Response to RNA Virus Infection. *PLOS Pathog.* **6**, e1000778 (2010).

53. Vaibhava, V. *et al.* Optineurin mediates a negative regulation of Rab8 by the GTPase-activating protein TBC1D17. *J. Cell Sci.* **125**, 5026–5039 (2012).

54. Chibalina, M. V, Roberts, R. C., Arden, S. D., Kendrick-Jones, J. & Buss, F. B. T.-M. in E. Rab8-Optineurin-Myosin VI: Analysis of Interactions and Functions in the Secretory Pathway. in *Small GTPases in Disease, Part A* vol. 438 11–24 (Academic Press, 2008).

55. Chew, T. S. *et al.* Optineurin deficiency in mice contributes to impaired cytokine secretion and neutrophil recruitment in bacteria-driven colitis. *Dis. Model. Mech.* **8**, 817–829 (2015).

56. Smith, A. M. *et al.* Disruption of macrophage pro-inflammatory cytokine release in Crohn ' s disease is associated with reduced optineurin expression in a subset of patients. doi:10.1111/imm.12338.

57. Smith, A. M. *et al.* Disordered macrophage cytokine secretion underlies impaired acute inflammation and bacterial clearance in Crohn's disease. *J. Exp. Med.* **206**, 1883–1897 (2009).

58. Smith, A. M. *et al.* Disruption of macrophage pro-inflammatory cytokine release in C rohn's disease is associated with reduced optineurin expression in a subset of patients. *Immunology*

144, 45–55 (2015).

59. Muñoz-Planillo, R. *et al.* K+ Efflux Is the Common Trigger of NLRP3 Inflammasome Activation by Bacterial Toxins and Particulate Matter. *Immunity* **38**, 1142–1153 (2013).

60. Guo, Q., Wang, J. & Weng, Q. The diverse role of optineurin in pathogenesis of disease. *Biochem. Pharmacol.* **180**, 114157 (2020).

61. Levine, B. & Kroemer, G. Autophagy in the Pathogenesis of Disease. *Cell* **132**, 27–42 (2008).

62. Philipp, W. *et al.* Phosphorylation of the Autophagy Receptor Optineurin Restricts Salmonella Growth. *Science (80-.).* **333**, 228–233 (2011).

63. Rao, L. *et al.* p85β regulates autophagic degradation of AXL to activate oncogenic signaling. *Nat. Commun.* **11**, 2291 (2020).

64. Pourcelot, M. *et al.* Optineurin: A Coordinator of Membrane-Associated Cargo Trafficking and Autophagy . *Front. Immunol.* **9**, 1–6 (2018).

65. Wong, Y. C. & Holzbaur, E. L. F. Temporal dynamics of PARK2/parkin and OPTN/optineurin recruitment during the mitophagy of damaged mitochondria. *Autophagy* **11**, 422–424 (2015).

66. Kazlauskaite, A. *et al.* Parkin is activated by PINK1-dependent phosphorylation of ubiquitin at Ser65. *Biochem. J.* **460**, 127–141 (2014).

67. Shiba-fukushima, K., Imai, Y., Yoshida, S., Ishihama, Y. & Kanao, T. PINK1-mediated phosphorylation of the Parkin ubiquitin-like domain primes mitochondrial translocation of Parkin and regulates mitophagy. 1–8 doi:10.1038/srep01002.

68. Richter, B. *et al.* Phosphorylation of OPTN by TBK1 enhances its binding to Ub chains and promotes selective autophagy of damaged mitochondria. *Proc. Natl. Acad. Sci.* **113**, 4039 LP – 4044 (2016).

69. Bansal, M. *et al.* cro Optineurin promotes autophagosome formation by recruiting the autophagy-related Atg12-5-16L1 complex to phagophores containing the Wipi2 protein. *J. Biol. Chem.* **293**, 132–147 (2018).

70. Ryan, T. A. & Tumbarello, D. A. Optineurin: A Coordinator of Membrane-Associated Cargo Trafficking and Autophagy . *Frontiers in Immunology* vol. 9 (2018).

71. Ayaki, T. *et al.* Multiple Proteinopathies in Familial ALS Cases With Optineurin Mutations. *J. Neuropathol. Exp. Neurol.* **77**, 128–138 (2018).

72. Maruyama, H. *et al.* Mutations of optineurin in amyotrophic lateral sclerosis. *Nature* **465**, 223–226 (2010).

73. Lazarou, M. *et al.* The ubiquitin kinase PINK1 recruits autophagy receptors to induce mitophagy. *Nature* **524**, 309–314 (2015).

74. Fifita, J. A. *et al.* A novel amyotrophic lateral sclerosis mutation in OPTN induces ER stress and Golgi fragmentation in vitro. *Amyotroph. Lateral Scler. Front. Degener.* **18**, 126–133 (2017).

75. Belzil, V. V *et al.* Analysis of OPTN as a causative gene for amyotrophic lateral sclerosis. *Neurobiol. Aging* **32**, 555-e13 (2011).

76. Del Bo, R. *et al.* Novel optineurin mutations in patients with familial and sporadic amyotrophic lateral sclerosis. *J. Neurol. Neurosurg. Psychiatry* **82**, 1239–1243 (2011).

77. Turturro, S., Shen, X., Shyam, R., Yue, B. Y. J. T. & Ying, H. Effects of mutations and deletions

in the human optineurin gene. *Springerplus* **3**, 1–16 (2014).

78. Tümer, Z. *et al.* A novel heterozygous nonsense mutation of the OPTN gene segregating in a Danish family with ALS. *Neurobiol. Aging* **33**, 208-e1 (2012).

79. Bury, J. J. *et al.* Oligogenic inheritance of optineurin (OPTN) and C9ORF72 mutations in ALS highlights localisation of OPTN in the TDP-43-negative inclusions of C9ORF72-ALS. *Neuropathology* **36**, 125–134 (2016).

80. Goldstein, O. *et al.* OPTN 691_692insAG is a founder mutation causing recessive ALS and increased risk in heterozygotes. *Neurology* **86**, 446–453 (2016).

81. Ito, H. *et al.* Clinicopathologic study on an ALS family with a heterozygous E478G optineurin mutation. *Acta Neuropathol.* **122**, 223–229 (2011).

82. Markovinovic, A. *et al.* Optineurin in amyotrophic lateral sclerosis: multifunctional adaptor protein at the crossroads of different neuroprotective mechanisms. *Prog. Neurobiol.* **154**, 1–20 (2017).

83. Janssen, S. F. *et al.* The vast complexity of primary open angle glaucoma: Disease genes, risks, molecular mechanisms and pathobiology. *Prog. Retin. Eye Res.* **37**, 31–67 (2013).

84. Rezaie, T. *et al.* Adult-onset primary open-angle glaucoma caused by mutations in optineurin. *Science (80-.).* **295**, 1077–1079 (2002).

85. Ayala-Lugo, R. M. *et al.* Variation in optineurin (OPTN) allele frequencies between and within populations. *Mol. Vis.* **13**, 151 (2007).

86. Willoughby, C. E. *et al.* Defining the pathogenicity of optineurin in juvenile open-angle glaucoma. *Invest. Ophthalmol. Vis. Sci.* **45**, 3122–3130 (2004).

87. Kumar, A. *et al.* Role of CYP1B1, MYOC, OPTN and OPTC genes in adult-onset primary open-angle glaucoma: predominance of CYP1B1 mutations in Indian patients. *Mol. Vis.* **13**, 667 (2007).

88. Funayama, T. *et al.* Variants in Optineurin Gene and Their Association with Tumor Necrosis Factor-α Polymorphisms in Japanese Patients with Glaucoma. *Invest. Ophthalmol. Vis. Sci.* **45**, 4359–4367 (2004).

89. Minegishi, Y. *et al.* Enhanced optineurin E50K–TBK1 interaction evokes protein insolubility and initiates familial primary open-angle glaucoma. *Hum. Mol. Genet.* **22**, 3559–3567 (2013).

90. Chi, Z.-L. *et al.* Overexpression of optineurin E50K disrupts Rab8 interaction and leads to a progressive retinal degeneration in mice. *Hum. Mol. Genet.* **19**, 2606–2615 (2010).

91. Chalasani, M. L. *et al.* A Glaucoma-Associated Mutant of Optineurin Selectively Induces Death of Retinal Ganglion Cells Which Is Inhibited by Antioxidants. *Invest. Ophthalmol. Vis. Sci.* **48**, 1607–1614 (2007).

92. Shen, W.-C., Li, H.-Y., Chen, G.-C., Chern, Y. & Tu, P. Mutations in the ubiquitin-binding domain of OPTN/optineurin interfere with autophagy-mediated degradation of misfolded proteins by a dominant-negative mechanism. *Autophagy* **11**, 685–700 (2015).

93. Sippl, C., Bosserhoff, A. K., Fischer, D. & Tamm, E. R. Depletion of optineurin in RGC-5 cells derived from retinal neurons causes apoptosis and reduces the secretion of neurotrophins. *Exp. Eye Res.* **93**, 669–680 (2011).

94. Smith, B. J. & Eveson, J. W. Paget's disease of bone with particular reference to dentistry.

Journal of Oral Pathology & Medicine vol. 10 233–247 (1981).

95. Welsh, R. A. & Meyer, A. T. Nuclear fragmentations and associated fibrils in giant cell tumor of bone. *Lab. Invest.* **22**, 63–72 (1970).

96. Kanis, J. A. *Pathophysiology and treatment of Paget's disease of bone*. (Taylor & Francis, 1998).

97. Fredrick, R. & Singer, C. H. Paget's disease of bone. *Bone program. St. Monica, Calif. A Publ. Paget Found. Paget's Dis. Bone Relat. Disord.* (2008).

98. Neville, B. W., Damm, D. D., Allen, C. M. & Bouquot, J. E. Paget's disease of bone. Oral and Maxillofacial Pathology. Bone pathology. Chapter 14.

99. Bender, I. B. Paget's disease. *J. Endod.* **29**, 720–723 (2003).

100. Karunakaran, K., Murugesan, P., Rajeshwar, G. & Babu, S. Paget ' s disease of the mandible. **16**, 107–109 (2012).

101. Silva, I. A. L. *et al.* Effect of genetic variants of OPTN in the pathophysiology of Paget's disease of bone. *Biochim. Biophys. Acta - Mol. Basis Dis.* **1864**, 143–151 (2018).

102. Obaid, R. *et al.* Optineurin Negatively Regulates Osteoclast Differentiation by Modulating NF-k B and Interferon Signaling : Implications for Paget ' s Disease Report Optineurin Negatively Regulates Osteoclast Differentiation by Modulating NF- k B and Interferon Signaling. *Cell Rep.* **13**, 1096–1102 (2015).

103. Silva, I. A. L. *et al.* Molecular effect of an OPTN common variant associated to Paget's disease of bone. *PLoS One* **13**, e0197543 (2018).

104. Jin, W. *et al.* Deubiquitinating enzyme CYLD negatively regulates RANK signaling and osteoclastogenesis in mice. *J. Clin. Invest.* **118**, 1858–1866 (2008).

105. Baglama, Š., Trčko, K., Rebol, J. & Miljković, J. Oral manifestations of autoinflammatory and autoimmune diseases. *Acta Dermatovenerologica Alpina, Pannonica Adriat.* **27**, 9–16 (2018).

106. Schifter, M., Yeoh, S. C., Coleman, H. & Georgiou, A. Oral mucosal diseases: the inflammatory dermatoses. *Aust. Dent. J.* **55 Suppl 1**, 23–38 (2010).

107. Eisen, D. Ocular Involvement in Patients With Oral Lichen Planus. *Oral Surg. Oral Med. Oral Pathol.* 431–436 (1999).

108. Al-Hashimi, I. *et al.* Oral lichen planus and oral lichenoid lesions: diagnostic and therapeutic considerations. *Oral Surgery, Oral Med. Oral Pathol. Oral Radiol. Endodontology* **103**, S25.e1-S25.e12 (2007).

109. Ismail, S. B., Kumar, S. K. S. & Zain, R. B. Oral lichen planus and lichenoid reactions: etiopathogenesis, diagnosis, management and malignant transformation. *J. Oral Sci.* **49**, 89–106 (2007).

110. McCartan, B. E. & Healy, C. M. The reported prevalence of oral lichen planus: A review and critique. *J. Oral Pathol. Med.* **37**, 447–453 (2008).

111. Van der Meij, E. H. & Van der Waal, I. Lack of clinicopathologic correlation in the diagnosis of oral lichen planus based on the presently available diagnostic criteria and suggestions for modifications. *J. Oral Pathol. Med.* **32**, 507–512 (2003).

112. Gandolfo, S. *et al.* Risk of oral squamous cell carcinoma in 402 patients with oral lichen planus: A follow-up study in an Italian population. *Oral Oncol.* **40**, 77–83 (2004).

113. Ingafou, M., Leao, J. C., Porter, S. R. & Scully, C. Oral lichen planus: A retrospective study of 690 British patients. *Oral Dis.* **12**, 463–468 (2006).

114. Organization, W. H. *Tobacco or health: a global status report*. (World Health Organization, 1997).

115. Pindborg, J. J., Reichart, P. A., Smith, C. J. & Van der Waal, I. *Histological Typing of Cancer and Precancer of the Oral Mucosa: In Collaboration with LH Sobin and Pathologists in 9 Countries*. (Springer Science & Business Media, 2012).

116. Alrashdan, M. S., Cirillo, N. & McCullough, M. Oral lichen planus: a literature review and update. *Arch. Dermatol. Res.* **308**, 539–551 (2016).

117. Wang, Z., Yao, H., Cui, B., Ning, G. & Tang, G. Y. Genetic linkage analysis of oral lichen planus in a Chinese family. *Genet. Mol. Res.* **10**, 1427–1433 (2011).

118. Tsantoulis, P. K., Kastrinakis, N. G., Tourvas, A. D., Laskaris, G. & Gorgoulis, V. G. Advances in the biology of oral cancer. *Oral Oncol.* **43**, 523–534 (2007).

119. Bergmann, C. *et al.* Toll-like receptor 4 single-nucleotide polymorphisms Asp299Gly and Thr399Ile in head and neck squamous cell carcinomas. *J. Transl. Med.* **9**, 1–9 (2011).

120. Chuang, H. C., Huang, C. C., Chien, C. Y. & Chuang, J. H. Toll-like receptor 3-mediated tumor invasion in head and neck cancer. *Oral Oncol.* **48**, 226–232 (2012).

121. Stanimirovic, D. *et al.* TLR2, TLR3, TLR4 and CD14 gene polymorphisms associated with oral lichen planus risk. *Eur. J. Oral Sci.* **121**, 421–426 (2013).

122. Wang, B. G., Yi, D. H. & Liu, Y. F. TLR3 gene polymorphisms in cancer: A systematic review and meta-analysis. *Chin. J. Cancer* **34**, (2015).

123. Zeljic, K. *et al.* Association of TLR2, TLR3, TLR4 and CD14 genes polymorphisms with oral cancer risk and survival. *Oral Dis.* **20**, 416–424 (2014).

124. Marshall, A., Celentano, A., Cirillo, N., McCullough, M. & Porter, S. Tissue-specific regulation of CXCL9/10/11 chemokines in keratinocytes: Implications for oral inflammatory disease. *PLoS One* **12**, 1–17 (2017).

125. Marlina, E. The clinical and biological effects of the use of probiotic VSL# 3 in patients with oral lichen planus. (2021).

126. Ahn, M.-Y., Kang, J.-K., Kwon, S.-M., Yoon, H.-E. & Yoon, J.-H. Expression of nucleotide-binding oligomerization domain 1 and 2 in oral lichen planus. *J. Dent. Sci.* **15**, 1–8 (2020).

127. Tan, Y.-Q., Wang, F., Ma, R.-J., Zhang, J. & Zhou, G. Interferon-γ activated T-cell IRGM–autophagy axis in oral lichen planus. *Int. Immunopharmacol.* **94**, 107478 (2021).

128. Marchesan, J. *et al.* TLR4, NOD1 and NOD2 mediate immune recognition of putative newly identified periodontal pathogens. *Mol. Oral Microbiol.* **31**, 243–258 (2016).

129. Lalla, E. & Papapanou, P. N. Diabetes mellitus and periodontitis: a tale of two common interrelated diseases. *Nat. Rev. Endocrinol.* **7**, 738–748 (2011).

130. Genco, R. J. & Van Dyke, T. E. Reducing the risk of CVD in patients with periodontitis. *Nat. Rev. Cardiol.* **7**, 479–480 (2010).

131. Lundberg, K., Wegner, N., Yucel-Lindberg, T. & Venables, P. J. Periodontitis in RA—the citrullinated enolase connection. *Nat. Rev. Rheumatol.* **6**, 727–730 (2010).

132. Eke, P. I. *et al.* Periodontitis prevalence in adults≥ 65 years of age, in the USA. *Periodontol. 2000* **72**, 76–95 (2016).

133. Paster, B. J., Olsen, I., Aas, J. A. & Dewhirst, F. E. The breadth of bacterial diversity in the human periodontal pocket and other oral sites. *Periodontol. 2000* **42**, 80–87 (2006).

134. Socransky, S. S., Haffajee, A. D., Cugini, M. A., Smith, C. & Kent Jr, R. L. Microbial complexes in subgingival plaque. *J. Clin. Periodontol.* **25**, 134–144 (1998).

135. Okugawa, T., Kaneko, T., Yoshimura, A., Silverman, N. & Hara, Y. NOD1 and NOD2 mediate sensing of periodontal pathogens. *J. Dent. Res.* **89**, 186–191 (2010).

136. Prates, T. P. *et al.* nod2 contributes to Porphyromonas gingivalis–induced Bone Resorption. *J. Dent. Res.* **93**, 1155–1162 (2014).

137. Souza, J. A. C. *et al.* Role of NOD2 and RIP2 in host–microbe interactions with Gram-negative bacteria: insights from the periodontal disease model. *Innate Immun.* **22**, 598–611 (2016).

138. Llorente, M. A. & Griffiths, G. S. Periodontal status among relatives of aggressive periodontitis patients and reliability of family history report. *J. Clin. Periodontol.* **33**, 121–125 (2006).

139. Jeon, D.-I. *et al.* NOD1 and NOD2 stimulation triggers innate immune responses of human periodontal ligament cells. *Int. J. Mol. Med.* **29**, 699–703 (2012).

140. Sudo, T. *et al.* Association of NOD2 mutations with aggressive periodontitis. *J. Dent. Res.* **96**, 1100–1105 (2017).

141. Mizuno, N. *et al.* Aggressive periodontitis and NOD2 variants. *J. Hum. Genet.* **65**, 841–846 (2020).

142. Zhou, L. *et al.* Palmitoylation restricts SQSTM1/p62-mediated autophagic degradation of NOD2 to modulate inflammation. *Cell Death Differ.* **29**, 1541–1551 (2022).

143. Pereira, M. S. & Munerato, M. C. Oral manifestations of inflammatory bowel diseases: Two case reports. *Clin. Med. Res.* **14**, 46–52 (2016).

144. Chi, A. C., Neville, B. W., Krayer, J. W. & Gonsalves, W. C. Oral manifestations of systemic disease. *Am. Fam. Physician* **82**, 1381–1388 (2010).

145. Gajendran, M., Loganathan, P., Catinella, A. P. & Hashash, J. G. A comprehensive review and update on Crohn's disease. *Disease-a-Month* **64**, 20–57 (2018).

146. Laube, R. *et al.* Oral and upper gastrointestinal Crohn's disease. *J. Gastroenterol. Hepatol.* **33**, 355–364 (2018).

147. Mays, J. W., Sarmadi, M. & Moutsopoulos, N. M. Oral manifestations of systemic autoimmune and inflammatory diseases: Diagnosis and clinical management. *J. Evid. Based. Dent. Pract.* **12**, 265–282 (2012).

148. Grave, B., McCullough, M. & Wiesenfeld, D. Orofacial granulomatosis – a 20-year review. *Oral Dis.* **15**, 46–51 (2009).

149. Sanderson, J. *et al.* Oro-Facial Granulomatosis: Crohn's Disease or a New Inflammatory Bowel Disease? *Inflamm. Bowel Dis.* **11**, 840–846 (2005).

150. Campbell, H. *et al.* Distinguishing orofacial granulomatosis from crohn's disease: Two separate disease entities?1. *Inflamm. Bowel Dis.* **17**, 2109–2115 (2011).

151. Al Johani, K. A., Moles, D. R., Hodgson, T. A., Porter, S. R. & Fedele, S. Orofacial

granulomatosis: Clinical features and long-term outcome of therapy. *J. Am. Acad. Dermatol.* **62**, 611–620 (2010).

152. Gale, G. *et al.* Characterisation of a Swedish cohort with orofacial granulomatosis with or without Crohn's disease. *Oral Dis.* **21**, e98–e104 (2015).

153. Mentzer, A. *et al.* Genetic Association Analysis Reveals Differences in the Contribution of NOD2 Variants to the Clinical Phenotypes of Orofacial Granulomatosis. *Inflamm. Bowel Dis.* **22**, 1552–1558 (2016).

154. Kotzin, B. L. SYSTEMIC_LUPUS_ERYTHEMATOSUS__REVIEW_OF_THE.1.pdf. *Cell* **85**, 303–306 (1996).

155. Finzel, S., Schaffer, S., Rizzi, M. & Voll, R. E. Pathogenesis of systemic lupus erythematosus. *Z. Rheumatol.* **77**, 789–798 (2018).

156. Mustafa, M. B., Porter, S. R., Smoller, B. R. & Sitaru, C. Oral mucosal manifestations of autoimmune skin diseases. *Autoimmun. Rev.* **14**, 930–951 (2015).

157. Bascones-Martínez, A., García-García, V., Meurman, J. H. & Requena-Caballero, L. Immune-mediated diseases: What can be found in the oral cavity? *Int. J. Dermatol.* **54**, 258–270 (2015).

158. Nico, M. M. S., Vilela, M. A. C., Rivitti, E. A. & Lourenço, S. V. Oral lesions in lupus erythematosus: Correlation with cutaneous lesions. *Eur. J. Dermatology* **18**, 376–381 (2008).

159. Pons-Estel, G. J., Alarcón, G. S., Scofield, L., Reinlib, L. & Cooper, G. S. Understanding the Epidemiology and Progression of Systemic Lupus Erythematosus. *Semin. Arthritis Rheum.* **39**, 257–268 (2010).

160. Crowson, A. N. & Magro, C. The cutaneous pathology of lupus erythematosus: A review. *J. Cutan. Pathol.* **28**, 1–23 (2001).

161. Correa, R. G., Milutinovic, S. & Reed, J. C. Roles of NOD1 (NLRC1) and NOD2 (NLRC2) in innate immunity and inflammatory diseases. *Biosci. Rep.* **32**, 597–608 (2012).

162. Gillett, C. D. *et al.* Fine mapping chromosome 16q12 in a collection of 231 systemic lupus erythematosus sibpair and multiplex families. *Genes Immun.* **6**, 19–23 (2005).

163. Hellquist, A. *et al.* Evidence for genetic association and interaction between the TYK2 and IRF5 genes in systemic lupus erythematosus. *J. Rheumatol.* **36**, 1631–1638 (2009).

164. De Jager, P. L. *et al.* The role of inflammatory bowel disease susceptibility loci in multiple sclerosis and systemic lupus erythematosus. *Genes Immun.* **7**, 327–334 (2006).

165. Esmaeilzadeh, E. *et al.* Strong association of common variants in the miRNA-binding site of NOD2 gene with clinicopathological characteristics and disease activity of systemic lupus erythematosus. *Clin. Rheumatol.* **40**, 4559–4567 (2021).

166. Patrick, C. J., M., W. S., C., C. W. & A., K. T. Transient and stable gene expression in mammalian cells transduced with a recombinant baculovirus vector. *Proc. Natl. Acad. Sci.* **96**, 127–132 (1999).

167. Lee, J. S., Hmama, Z., Mui, A. & Reiner, N. E. Stable Gene Silencing in Human Monocytic Cell Lines Using Lentiviral-delivered Small Interference RNA: SILENCING OF THE p110α ISOFORM OF PHOSPHOINOSITIDE 3-KINASE REVEALS DIFFERENTIAL REGULATION OF ADHERENCE INDUCED BY 1α,25-DIHYDROXYCHOLECALC. *J. Biol. Chem.* **279**, 9379–9388 (2004).

168. Benjamin, R. *et al.* Phosphorylation of OPTN by TBK1 enhances its binding to Ub chains and promotes selective autophagy of damaged mitochondria. *Proc. Natl. Acad. Sci.* **113**, 4039–4044 (2016).

169. Chen, Y. *et al.* Relation between NOD2 genotype and changes in innate signaling in Crohn's disease on mRNA and miRNA levels. *npj Genomic Med.* **2**, 3 (2017).

170. Stafford, C. A. *et al.* IAPs Regulate Distinct Innate Immune Pathways to Co-ordinate the Response to Bacterial Peptidoglycans. *Cell Rep.* **22**, 1496–1508 (2018).

171. Gleason, C. E., Ordureau, A., Gourlay, R., Arthur, J. S. C. & Cohen, P. Polyubiquitin Binding to Optineurin Is Required for Optimal Activation of TANK-binding Kinase 1 and Production of Interferon β *. *J. Biol. Chem.* **286**, 35663–35674 (2011).

172. Matsuoka, M. & Jeang, K.-T. Human T-cell leukemia virus type 1 (HTLV-1) and leukemic transformation: viral infectivity, Tax, HBZ and therapy. *Oncogene* **30**, 1379–1389 (2011).

173. Klingseisen, L. *et al.* E3-14.7K Is Recruited to TNF-Receptor 1 and Blocks TNF Cytolysis Independent from Interaction with Optineurin. *PLoS One* **7**, e38348 (2012).

174. Sirohi, K., Kumari, A., Radha, V. & Swarup, G. A Glaucoma-Associated Variant of Optineurin, M98K, Activates Tbk1 to Enhance Autophagosome Formation and Retinal Cell Death Dependent on Ser177 Phosphorylation of Optineurin. *PLoS One* **10**, e0138289 (2015).

175. Forman, H. J. & Torres, M. Redox signaling in macrophages. *Mol. Aspects Med.* **22**, 189–216 (2001).

176. Pashenkov, M. V, Murugina, N. E., Budikhina, A. S. & Pinegin, B. V. Synergistic interactions between NOD receptors and TLRs: Mechanisms and clinical implications. *J. Leukoc. Biol.* **105**, 669–680 (2019).

177. Corridoni, D. *et al.* NOD2 and TLR2 Signal via TBK1 and PI31 to Direct Cross-Presentation and CD8 T Cell Responses . *Frontiers in Immunology* vol. 10 (2019).

178. He, L., Chen, L. & Li, L. The TBK1-OPTN Axis Mediates Crosstalk Between Mitophagy and the Innate Immune Response: A Potential Therapeutic Target for Neurodegenerative Diseases. *Neurosci. Bull.* **33**, 354–356 (2017).

Appendix 1

Oral presentation

PhD Research symposium – Eastman Dental Institute

London, United Kingdom, 2017

Poster presentation

2nd prize for poster presentation at Eastman Research Away Day

London, United Kingdom, 2019

Publication

O'Loughlin, Thomas, Antonina J. Kruppa, Andre LR Ribeiro, James R. Edgar, Abdulaziz Ghannam, Andrew M. Smith, and Folma Buss. "OPTN recruitment to a Golgi-proximal compartment regulates immune signalling and cytokine secretion." *Journal of cell science* 133, no. 12 (2020): jcs239822.